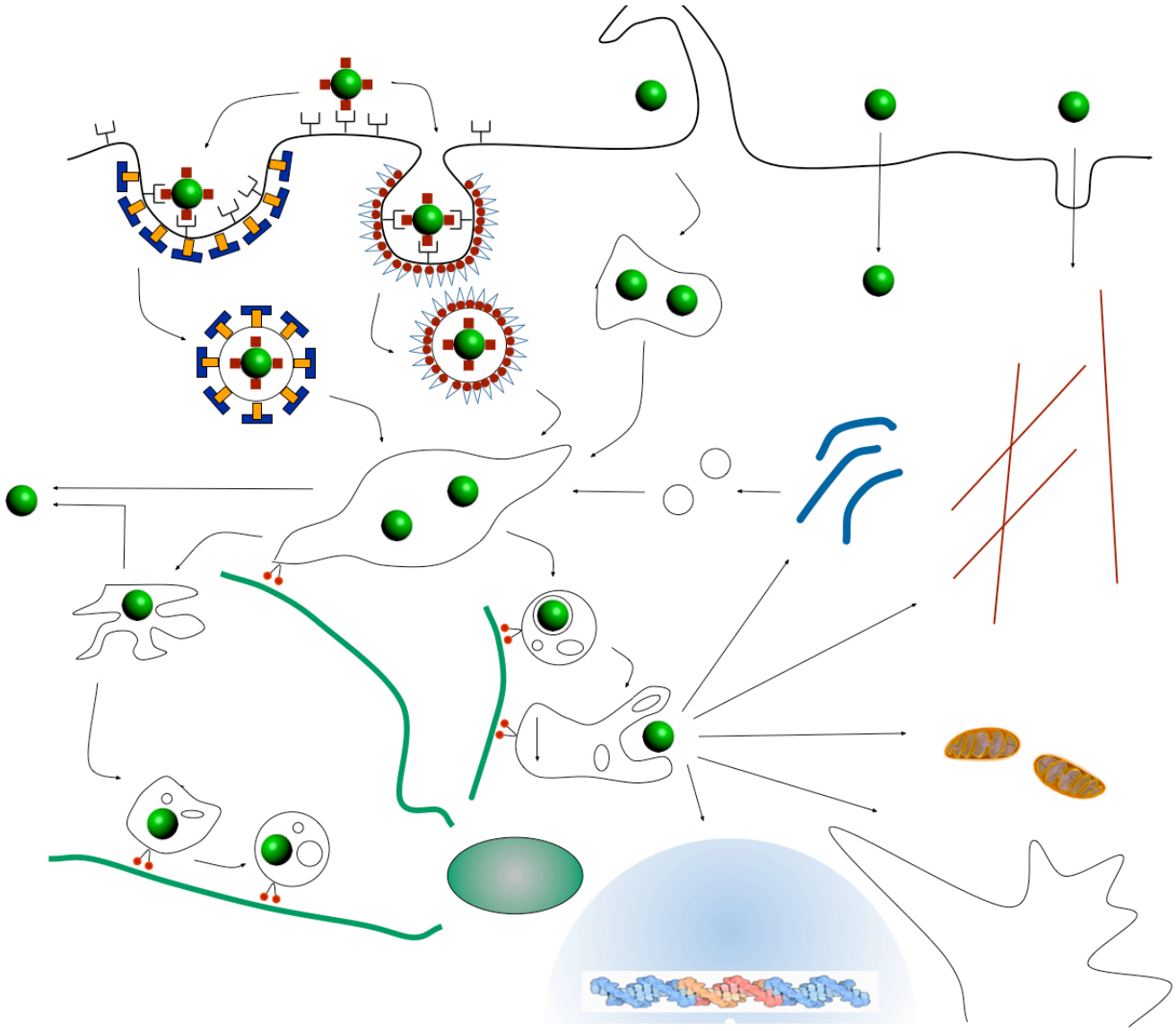

Carlos Samuel Marques Boto

LEUKEMIA CELLS MODULATION BY LIGHT-ACTIVATABLE NANOPARTICLES

Doctoral Thesis in the scientific area of Chemical Engineering, specialty of Biotechnology, supervised by Doctor Lino Ferreira and Doctor Jorge Rocha and submitted to the Department of Chemical Engineering, Faculty of Science and Technology, University of Coimbra

2014

· U C ·

Carlos Samuel Marques Boto

LEUKEMIA CELLS MODULATION BY LIGHT-ACTIVATABLE NANOPARTICLES

Doctoral Thesis submitted to the DEPARTMENT OF CHEMICAL ENGINEERING from the FACULTY OF SCIENCE AND TECNOLOGY of the UNIVERSITY OF COIMBRA in partial fulfilment of the requirements for the degree of DOCTOR OF PHYLOSOPHY in CHEMICAL ENGINEERING, area of BIOTECNOLOGY

Supervisor:
Doctor Lino da Silva Ferreira

Host Institutions:
Biomaterials & Stem Cell-Based Therapeutics Laboratory,
Center for Neuroscience and Cell Biology (CNC), University of Coimbra, Portugal
Experimental and Translational Oncology Laboratory: Stem Cells, Cancer Stem Cells and Cancer, Instituto de Biologia Molecular y Celular del Cancer (IBMCC), CSIC/Universidad de Salamanca, Spain
Stem Cell Laboratory, UCL Cancer Institute, University College London, United Kingdom
Key Laboratory of Cell Differentiation and Apoptosis of National Ministry of Education, Shanghai Jiao Tong University School of Medicine (SJTU-SM), China

Funding:
FCT – Portuguese Foundation for Science and Technology: doctoral degree grant SFRH/BD/62419/2009
ERC – European Research Council: ERC fellowship ERC-2012-StG_20111012
FCT project- PTDC/CTM-NAN/120552/2010

Coimbra
2014

· U C ·

UNIVERSIDADE DE COIMBRA

I gratefully acknowledge the financial support from:

Portuguese Foundation for Science and Technology (FCT)

FCT Fellowship SFRH/BD/62419/2009

FCT R&D Grant PTDC/CTM-NAN/120552/2010

European Research Council (ERC)

ERC Fellowship ERC-2012-StG_20111012

NanoTrigger – Triggerable Nanomaterials to Modulate Cell Activity

I gratefully acknowledge the resources and knowledge support from:

Lino da Silva Ferreira

Biomaterials and Stem Cell-Based Therapeutics Laboratory

Center for Neuroscience and Cell Biology (CNC), University of Coimbra, Portugal

Isidro Sánchez-García

Experimental and Translational Oncology Laboratory: Stem Cells, Cancer Stem Cells and Cancer

Instituto de Biologia Molecular y Celular del Cancer (IBMCC), CSIC/Universidad de Salamanca, Spain

Tariq Enver

Stem Cell Laboratory

UCL Cancer Institute, University College London, United Kingdom

Dengli Hong

Department of Pathophysiology, Ruijin Hospital

Key Laboratory of Cell Differentiation and Apoptosis of National Ministry of Education

Shanghai Jiao Tong University School of Medicine (SJTU-SM), China

To my Father, that will always be with me.
And Vânia… you light up my life.

Para o meu Pai, que sempre estará comigo.
E para ti, Vânia, que iluminas a minha existência.

For all the small things that give meaning to life.
Por todas as pequenas coisas que dão sentido à vida.

To my Family and Friends

Para a minha Família e Amigos

For all the support and patience.

Por todo o apoio e paciência.

ACKNOWLEDGEMENTS

I'd like to thank the many talented and devoted people who assisted me with this complex project:

My supervisor, Lino Ferreira, who provided leadership, enthusiasm and resources, but also confidence and friendship during the entire PhD; Ricardo Neves that follow my work daily and shared with me the dedication to turn this project into reality and Jorge Rocha, who never fail to provided strong support and guidance.

Isidro Sánchez-García for his hospitality, availability and cooperation during the initial *in vivo* animal studies; to Alberto, Begonã, Isabel and all other members of the Grupo de Oncología Experimental y Translacional of the Instituto de Biologia Molecular y Celular del Cancer (IBMCC) of the Universidad de Salamanca for their generosity towards me and my work. Tariq Enver and Rajeev Gupta, for all the guidance, resources and valuable insights; Dengli Hong and Caiwen Duan that join forces with us and provide important contribution in the *in vivo* studies.

Rui Carvalho and Emeric Wasielewski for the availability and guidance in the NMR studies. Luís Carvalho and Francisco Gil for the help during the initial laser irradiation assays. Sandra Pinto, for the invaluable assistance with gene expression analysis by PCR

Maria Filomena Botelho, Ana Abrantes and Salomé Lourenço of the Biophysics and Biomathematics Institute (IBILI) and Attila Kofalvi of the Laboratory of Neuromodulation and Metabolism (CNC) of the University of Coimbra, for providing the facilities and equipment's in the quantification assays of tritium-labeled Retinoic Acid.

NanoTrigger Team (Adrián, Sónia, Josephine, Emanuel, Miguel and Sandra) for helping me to develop my ideas through scientific discussions; Renata Gomes and Ana Lima for the good times in London and all the friendship that encourage me to work, and all my Biomaterials and Stem Cell-Based Therapeutics Laboratory colleges for the excellent work environment that I experience at Biocant and UC Biotech.

I'd like to express my deepest love to the memory of my father, José, for his life, for the shear inspiration and support that he offer to all my ideas and dreams, which gave me the confidence and freedom to learn and grow. My family, that had an essential role in overcoming the difficulties during this long period, and my love, Vânia, that gives my life meaning and motivation.

AGRADECIMENTOS

Gostaria de expressar o meu agradecimento ao grande número de pessoas talentosas e devotadas que me assistiram na realização deste projecto complexo:

O meu supervisor, Lino Ferreira, pela liderança, entusiasmo e recursos, mas também pela confiança e amizade durante todo o doutoramento; Ricardo Neves, que acompanhou o meu trabalho diariamente e partilhou comigo a dedicação para tornar este projecto realidade; e Jorge Rocha, que em nenhum momento falhou na oferta de apoio e orientação.

Isidro Sánchez-García pela sua hospitalidade, disponibilidade e cooperação na realização dos estudos animais; Alberto, Begonã, Isabel e todos os outros membros do Grupo de Oncología Experimental y Translacional do Instituto de Biologia Molecular y Celular del Cancer (IBMCC) da Universidad de Salamanca pela sua generosidade em relação a mim e ao meu trabalho. Tariq Enver e Rajeev Gupta, por toda a orientação, recursos e observações; Dengli Hong e Caiwen Duan pela colaboração e importante contribuição nos estudos animais.

Rui Carvalho e Emeric Wasielewski pela disponibilidade e ajuda na realização dos estudos de NMR. Luís Carvalho e Francisco Gil pela colaboração nos ensaios iniciais de irradiação com laser. Sandra Pinto, pela assistência na análise de expressão génica por PCR.

Maria Filomena Botelho, Ana Abrantes e Salomé Lourenço do Instituto de Biofísica e Biomatemática (IBILI) e Attila Kofalvi do Laboratório de Neuromodulação e Metabolismo (CNC) da Universidade de Coimbra, pelas instalações e equipamentos para os ensaios de quantificação de ácido retinóico radioactivo.

A equipa NanoTrigger (Adrián, Sónia, Josephine, Emanuel, Miguel and Sandra) pela ajuda no desenvolvimento de novas ideias através de discussões científicas; Renata Gomes e Ana Lima pelos bons tempos em Londres e toda a amizade que me encorajou a trabalhar; e todos os meus colegas do Laboratório de Biomateriais e Terapias Baseadas em Células Estaminais pelo excelente ambiente de trabalho que tive no Biocant e no UC Biotech.

Gostaria de expressar o meu mais profundo amor à memória do meu Pai, José, pela sua vida, pelo exemplo e apoio basilar que deu a todos os meus sonhos e ideias, criando em mim a confiança e liberdade para aprender e crescer. Ao meu amor, Vânia, por dares motivação e sentido à minha vida.

"We can easily forgive a child who is afraid of the dark;
the real tragedy of life is when men are afraid of the light."

Plato

Abstract

Acute myeloid leukemia (AML) is a group of heterogeneous diseases defined morphologically by an abnormal increase in myeloblasts in the bone marrow (BM). Current therapies include the use of *all trans* retinoic acid (RA) to induce the differentiation of leukemic cells. Unfortunately, the efficiency of the process is limited, even if coupled with chemotherapy, since patients can relapse after remission (25% of the patients actually die) [1]. This relapse is likely related to an induction of RA-binding protein and increased RA metabolism by cytochrome P-450-mediated reactions. In addition, one-third of patients develop the so-called "RA syndrome" characterized by dyspnea, fever, weight gain and hypotension. In the last years, RA delivery formulations have been proposed to overcome these unwanted effects and some of them evaluated in human clinical trials. A lipossomic RA delivery system has been shown to improve the pharmacokinetic profile of RA as compared to a non-lipossomal formulation and maintained higher and sustained plasma drug concentrations. Further, the liposomal formulation decreased the probability of relapse after remission but not eliminate it. The main goal of this project was to develop a light-activatable nanoparticle system to improve the intracellular delivery of RA in leukemic cells. The possibility of remotely activating the drug delivery system opens new therapeutic opportunities due to the possibility of activating the differentiation of the cells at the bone marrow niche and potentially interfering with the leukemic stem cell niche. The light-activatable NPs have approximately 140 nm in diameter, positive net charge, and disassemble when exposed to UV light (365 nm) or blue light (405 nm) releasing RA. These NPs can be taken up rapidly (below 4 h) by acute myeloid leukemia cells (K562, NB4, U937 and AML stem cells). Importantly, our results show that the light activation of NPs contribute for the differentiation of these cells at levels not observed using formulations that release passively RA or by conventional chemotherapy. Light-activated RA^+ NPs induce 1.92 (± 0.17) times higher levels of erythroid differentiation in K562, 1.19 (± 0.01) times of myelocytic differentiation in NB4 and 1.45 (± 0.03) times of myelocytic differentiation in U937 cells as compared to non-activated NPs. In addition, light-activated RA^+ NPs induce 1.83 (± 0.17) times higher levels of erythroid differentiation in K562, 1.12 (± 0.01) times of myelocytic differentiation in NB4 and 1.44 (± 0.04) times of myelocytic differentiation in

U937 cells as compared to 1 μM RA in solution. It should be noted that RA^+ NPs contain ~10 times less RA than the one used in solution. This experimental result is particularly important in the RA-low sensitive cell line U937-PLZF/RARA where the high RA intracellular release is able to overcome the low sensitivity of the cell. Finally, AML stem cells treated with light-activated RA^+ NPs showed 69.6 ± 9.2 % and 61.8 ± 10.1 % less colonies, in CFC and LTC-IC colony assays, respectively. Consistent with the *in vitro* data, CD11b expression was statistical higher in NB4 cells treated with *ex vivo* and *in vivo* light-activated RA^+ NPs than in cells treated with RA^+ NPs without light activation in the animal experiments. These results indicate that the enhanced intracellular release and the kinetic control mediated by the light triggered-NPs may be an effective strategy to treat leukemia. In summary, we have established an opto-nanomedicine approach for the treatment and study of leukemic stem cells either *in vitro* or *in vivo*. This approach allows remote control in the release of biomolecules with spatio-temporal resolution. These light-activatable NPs might be suitable for general therapeutic and regenerative medicine applications.

Resumo

Leucemia mielóide aguda (AML) é um grupo de doenças heterogéneas definidas morfologicamente por um crescimento anormal do número de mieloblastos na medula óssea (BM). As presentes terapias incluem o uso de ácido retinóico (RA) para induzir a diferenciação de células de leucemia. Infelizmente, a eficiência do processo é limitada, mesmo quando em conjunto com quimioterapia convencional, uma vez que os pacientes sofrem do retorno da doença após remissão (na realidade 25% dos pacientes morrem) [1]. Esta recaída esta provavelmente relacionada com a indução de proteínas de ligação de RA e pelo aumento do metabolismo de RA por reacções mediadas pelo citocromo P-450. Além disso, um terço dos pacientes desenvolvem o designado "síndrome de RA" caracterizado por dispneia, febre, aumento de peso e hipotensão. Nos últimos anos, sistemas de libertação de RA foram propostos para ultrapassar estes efeitos indesejáveis, encontrando-se alguns em ensaios clínicos em humanos. Um sistema de libertação de RA baseado em liposomas demonstrou uma melhoria no perfil farmacológico de RA, em comparação com uma formulação não-liposómica e mostrou ser capaz de manter concentrações de elevadas e sustentadas de droga. Além disso, a formulação liposómica demonstrou a capacidade de diminuir a probabilidade de ocorrência de recaídas, sem no entanto as eliminar. O principal objectivo deste projecto foi o desenvolvimento de uma nanoformulação polimérica fotodissociável para aumentar a entrega intracelular de RA em células de leucemia. A possibilidade de activar de forma remota a libertação controlada de drogas abre novas oportunidades terapêuticas pela possibilidade de activação da diferenciação celular no nicho da medula óssea e potencialmente interferir com o nicho de células estaminais de leucemia. A nanoformulação polimérica fotodissociável tem aproximadamente 140 nm de diâmetro, carga superficial positiva e capacidade de dissociação quando exposta a luz UV (365 nm) ou luz azul (405 nm) libertando RA. Estas NPs são rapidamente internalizadas (períodos inferiores a 4 h) por células de leucemia mielóide aguda (K562, NB4, U937 e células estaminais de AML). Os nossos resultados demonstram que a fotoactivação das nanopartículas contribui para a diferenciação destas células em níveis não observados utilizando nanoformulações que libertam RA de forma passiva ou através de quimioterapia convencional. A activação através de luz das RA^{+} NPs induz 1.92 (± 0.17) vezes maior

diferenciação eritróide em células K562, 1.19 (± 0.01) vezes diferenciação mielóide em células NB4 e 1.45 (± 0.03) vezes diferenciação mielóide em células U937, quando comparadas com as condições de NPs não activadas com recurso a luz. De igual modo RA^+ NPs activadas com luz induzem 1.83 (± 0.17) vezes maior diferenciação eritróide em células K562, 1.12 (± 0.01) vezes diferenciação mielóide em células NB4 e 1.44 (± 0.04) vezes diferenciação mielóide em células U937, quando comparadas com a utilização de 1 μM de RA na solução de cultura. Deve ser salientado que RA^+ NPs contêm ~10 vezes menor quantidade de RA do que o utilizado em solução na cultura celular. Estes resultados experimentais são especialmente relevantes no tratamento da linha cellular resistente à acção de RA U937-PLZF/RARA na qual a elevada concentração intracelular de RA consegue induzir diferenciação celular com sucesso. Finalmente, células estaminais de AML tratadas com RA^+ NPs activadas com luz apresentam 69.6 ± 9.2 % e 61.8 ± 10.1 % menor número de colónias, na contagem de unidades formadoras de colónias (CFC e LTC-IC), respectivamente. A informação colectada nos ensaios animais demonstrou estar de acordo com a obtida nos ensaios *in vitro*. A expressão de CD11b foi superior de forma consistente (com relevância estatística) para células NB4 tratadas com RA^+ NPs activadas com luz tanto para as condições nas quais a activação pela luz foi realizada *ex vivo*, como na condição em que esta activação se realizou *in vivo*. Isto, comparativamente às condições nas quais as células tratadas com RA^+ NPs não foram alvo de activação. Estes resultados indiciam que o controlo conferido pela nanoformulação sensível à acção da luz na cinética de libertação intracelular pode ser uma estratégia efectiva para o tratamento de leucemia. Em resumo, foi estabelecida uma abordagem baseada em opto-nanomedicina para o tratamento e estudo de células estaminais de leucemia tanto *in vitro* como *in vivo*. Esta estratégia permite o controlo remoto sobre a libertação de biomoléculas com resolução espaço-temporal. Esta formulação fotossensível apresenta grande potencial para aplicação em terapias médicas e medicina regenerativa.

Table of Contents

List of Symbols and Acronyms

ϕ	Quantum yield
ε	Absorption coefficient
^{1}H	Proton NMR
[^{3}H]	Tritium
3-IC	3-indenecarboxylic acid
6-MP	6-mercaptopurine
$_{\gamma}$H2AX	Phosphorylated H2A histone on serine 139
ABC	ATP-binding cassette
AbVF	VEGF antibody
Ac-Dex	Acetal-modified dextran
AgNPs	Silver nanoparticles
ALL	Acute lymphocytic leukemia
AML	Acute myeloid leukemia
AMML	Acute myelomonocytic leukemia
AMkL	Acute megakaryoblastic leukemia
AmoL	Acute monocytic leukemia
APL	Acute promyelocytic leukemia
Ara-C	Cytarabine
ASXL1	Additional sex combs like 1
ATO	Arsenic trioxide
ATP	Adenosine-5'-triphosphate
ATRA	All-trans retinoic acid
AuNP	Gold nanoparticle
AuNR	Gold nanorod
BCP	Block copolymers
BM	Bone marrow
BSA	Bovine Serum Albumin
C18	Octadecyltrimethoxysilane
CAV-1	Caveolin-1

CBL	Casitas B-lineage lymphoma
CD	Cluster of differentiation
CD11b	Cluster of differentiation molecule 11B
CDC42	Cell division control protein 42
cDNA	Complementary DNA
CEBPA	CCAAT/enhancer-binding protein alpha
CFC	Colony-forming cell
CLIC/GEEC	Clathrin-independent carriers / GPI-enriched early endosomal compartments
CLL	Chronic lymphocytic leukemia
CLL-1	C-type lectin-like molecule-1
CLTC	Clathrin heavy chain 1
CM	Conditioned medium
CME	Clathrin-mediated endocytosis
CML	Chronic myelogenous leukemia
CR	Complete remission
CR1	First remission
CSC	Cancer stem cells
CO_2	Carbon dioxide
CPC	Cancer-propagating cells
CTBP1	C-terminal-binding protein 1
CW	Continuous-wave
CXCL12	CX chemokine ligand 12
CXCR4	C-X-C chemokine receptor type 4
Cy3	Cyanine dye yellow-green
DAPI	4',6-diamidino-2-phenylindole
DDACMM	[7-(didodecylamino) coumarin-4-yl] methyl methacrylate
DEACM	[7-(diethylamino) coumarin-4-yl] methyl
Dex	Dextran
DIC	Disseminated intravascular coagulation
DMNA	4,5-dimethoxy-2-nitrobenzyl alcohol
DMNB	4,5-dimethoxy-2-nitrobenzyl
DMNC	4,5-dimethoxy-2-nitrobenzyl chloroformate

DMSO	Dimethylsulfoxide
DMSO-d6	Deuterated dimethylsulfoxide
D*n*	Generation *n*
DNA	Deoxyribonucleic acid
DNMT3A	DNA (cytosine-5-)-methyltransferase 3 alpha
DNQ	2-diazo-1,2-naphthoquinone
DOX	Doxorubicin
DPPC	Dipalmitoylphosphatidylcholine
DR	Daunorubicin
DS	Dextran sulphate
DS_n	Degree of substitution
Dtxl	Docetaxel
EBM	Endothelial basal medium
EDC	1-ethyl-3-(3-dimethyllaminopropyl)carbodiimide hydrochloride
EEA1	Early Endosome Antigen 1
EGM	Endothelial growth medium
EIPA	5-(N-Ethyl-N-isopropyl)amiloride
ETV6	E-twenty-six translocation variant 6
EZH2	Histone-lysine N-methyltransferase 2
FA	Folic Acid
FAB	French-American-British
FACS	Fluorescence activated cell sorting
FBS	Fetal Bovine Serum
FDA	US Food and Drug Administration
FITC	Fluorescein isothiocyanate
FLT3	FMS-like tyrosine kinase-3
Flt-3L	FMS-like tyrosine kinase-3 ligand
FRET	Fluorescence resonance energy transfer
G_0	Quiescent state
G_1	First gap phase
G_2	Second gap phase
GA	Gambogic acid

Gd	Gadolinium
GMP	Granulocyte-monocyte progenitor
Gy	Gray (unit)
HDAC	Histone deacetylase
HEA	Hydroxyethylacrylate
HMS	Hollow mesoporous silica
HSC	Hematopoietic stem cell
HUVECs	Human umbilical vein endothelial cells
ICP-MS	Inductive coupled plasma mass spectrometry
IDA	Idarubicin
IDH1 / 2	Isocitrate dehydrogenase 1 / 2
IgG	Immunoglobulin G
IL	Interleukin
IL-3	Interleukin-3
JAK2	Janus kinase 2
K562	Human chronic myelogenous cell line K562
KCl	Potassium chloride
Lac	Lactose
LC	Liquid crystalline
LCP	Liquid crystalline polymer
LDLR	Low-Density Lipoprotein Receptor
LMPP	Lymphoid-primed multipotent progenitor
LSC	Leukemia stem cell
LTC-IC	Long-term culture-initiating cell
M	Mitosis
mAb	Monoclonal antibody
MACS	Magnetic activated cell sorting
MC	Merocyanine
MDS	Myelodysplastic syndromes
MDR	Multi-drug resistance
MLL	Murine lymphocytic leukemia
MPN	Myeloproliferative neoplasms
MR	Magnetic resonance

MRI	Magnetic resonance imaging
MSC	Mesenchymal Stem Cell
MSN	Mesoporous silica nanoparticles
MTX	Methotrexate
MWCO	Molecular weight cut off
NB	Theo-nitrobenzyl
NB4	Human acute promyelocytic t(15;17) cell line NB4
NBA	*o*-nitrobenzyl acrylate
NCOR	Nuclear co-repressor
NHL	Non-Hodgkin's lymphoma
NIPAM	*N*-isopropylacrylamide
NIR	Near infrared
NK	Natural killer
NMR	Nuclear magnetic resonance
NOD/SCID	Non-obese diabetic / severe combined immunodeficiency
NOS	Not otherwise specified
NPM1	Nucleophosmin
NPs	Nanoparticles
NR	Nile Red
ONB / *o*-NB	*o*-nitrobenzyl
OPN	Osteopontin
OS	Overall survival
OEGMA	Oligo(ethylene glycol) methyl ether methacrylate
PAG	Photoacids generator
PAMAM	Poly(amido amine)
PBS	Phosphate buffered saline
PCS	Photon correlation spectroscopy
PCR	Polymerase chain reaction
PDMS	Poly(dimethylsiloxane)
PE	Phycoerythrin
PEG	Poly(ethylene glycol)
PEI	Poly(ethyleneimine)
PEI-DMNC	Poly(ethyleneimine) conjugated with 4,5-dimethoxy-2-

	nitrobenzyl chloroformate
PEO	Poly(ethylene oxide)
Pgp	P-glycoprotein
pH	Potential of hydrogen
Ph-	Philadelphia chromosome-negative
PLA	Poly(lactic acid)
PLGA	Poly(lactic-*co*-glycolic acid)
PLZF	Promyelocytic leukemia zinc finger
PMA	Poly(methacrylate)
PMAA	Poly(methacrylic acid)
PML	Promyelocytic leukemia
PMMA	Poly(methyl methacrylate)
PNBA	Poly(2-nitrobenzyl acrylate)
PNBC	Poly(*S*-(*o*-nitrobenzyl)-*L*-cysteine)
POEGMA	Poly[oligo(ethylene glycol) methyl ether methacrylate]
PPG	Photolabile protective groups
PVP	Polyvinylpyrrolidone
Qdot	Quantum dot
RA	Retinoic acid
RAB5	Ras-related protein Rab-5
RAB7	Ras-related protein Rab-7
RAC1	Ras-related C3 botulinum toxin substrate 1
RAFT	Reversible addition-fragmentation chain transfer
RARα	Retinoic acid receptor α
RARE	Retinoic acid response element
RARs	Retinoic acid receptors
RAS	Retinoic acid syndrome
RNA	Ribonucleic acid
ROS	Reactive Oxygen Species
RPMI	Roswell Park Memorial Institute
RUNX1	Runt-related transcription factor 1
RXRs	Retinoid X receptors
S	Synthetic phase

SCF	Stem cell factor
SDF1	Stromal-derived factor 1
SEM	Scanning electron microscope
SFEM	Serum-free expansion medium
siRNA	Small interfering RNA
SIRPα	Signal regulatory protein α
SP	Spiropyran
STEM	Scanning transmission electron microscopy
SUZ12	Suppressor of zeste 12
SWNT	Single-walled nanotubes
TET2	Ten-eleven translocation methylcytosine dioxygenase 2
TIM3	T-cell immunoglobulin mucin-3
TP53	Tumor protein p53
TPO	Thrombopoietin
TRITC	Tetramethylrhodamine-5-(and-6-)-isothiocyanate
U937	Human myelomonoblastic cell line U937
U937-B412	Human myelomonoblastic cell line U937, containing PLZF/RARα cDNA under the control of the zinc inducible human-metallothionein promoter
U937-MT	Human myelomonoblastic cell line U937, empty vector control (PML/RARα expression)
UCL	University College London
UCNP	Up-converting nanoparticles
UTX	Ubiquitously transcribed tetratricopeptide repeat on chromosome X
UV	Ultraviolet
VCAM-1	Vascular cell adhesion molecule-1
VLA-4	Very late antigen-4
WBC	White blood cells
WHO	World Health Organization
$ZnSO_4$	Zinc sulfate

List of Figures

by the expression of CD11b. (C) Effect of multiple light activation in CD11b expression in Zn-induced U937-B412 cells. Cells were cultured with RA^+ NPs (10 μg/mL) for 4 h, washed with PBS, resuspended in cell culture media, exposed to multiple 5 min-cycles of UV light (365 nm, 100 Watts) during the 72 h of culture. Myelocytic differentiation ($CD11b^+$ cells) of human leukemia Zn-induced U923-B412 cells was determined by FACS. Results are expressed as Mean ± SEM (n = 3).

Figure 3.13 Effect of RA^+ NPs on human leukemia cells. In the case of cells treated with NPs, cells were treated with RA^+ NPs for 4 h, washed, activated or not with UV light (365 nm, 100 Watts) for 5 min, and then cultured for a certain period of time. In case of cells treated with soluble RA, cells were cultured in media containing soluble RA for the entire period of culture. (A.1) Erythroid differentiation of human leukemia K562 cells cultured with light-activated NPs or soluble RA. K562 cells were cultured for 6 days. (A.2) Percentage of $benzidine^+$ cells in K562 cells after 6 days of culture. (B.1) Myelocytic differentiation ($CD11b^+$ cells) of human leukemia NB4 cells cultured with light-activated NPs or soluble RA. NB4 cells were cultured for 3 days. (B.2) Percentage of $CD11b^+$ cells in NB4 cell cultures after 1 and 3 days of culture. (C.1) Myelocytic differentiation ($CD11b^+$ cells) of human Zn-induced U937-B412 cells cultured with light-activated NPs or soluble RA. Zn-induced U937-B412 cells were cultured for 3 days. (C.2 and C.3) Percentage of $CD11b^+$ cells in Zn-induced U937-B412 cell cultures after 1 day (C.2) or 3 days (C.3) of culture. Cells cultured with 10^{-7} M of vitamin D3 for 1 or 3 days were used as positive controls. (D.1 and D.2) Differentiation of AML stem cells cultured with light-activated NPs or soluble RA. Cell differentiation was evaluated by a colony forming unit assay at day 14. (D.2) AML stem cells were cultured for 14 days with RA in medium (10^2 – 10^5 nM) or RA^+ NPs (0.01 – 10 μg/mL) or blank NPs (10 μg/mL), exposed or not to UV light. Cell differentiation was evaluated by a colony forming unit assay at 73

List of Schemes

List of Tables

CHAPTER 1 – INTRODUCTION

1.1 – Aims and contributions

Cancer is a leading cause of death worldwide. An estimated 200 000 cases of leukemia occur annually which result in 145 000 deaths [2]. Acute myeloid leukemia (AML) is a severe, life threatening malignancy characterized by a clonal expansion of immature myeloid cells in the bone marrow, resulting in severe infections and bleedings and represents 37% of all leukemia cases. Current therapies include chemotherapy followed or not by stem cell transplantation [3-5]. Chemotherapy main objective is to kill the cancer cells, mainly through the capacity to halt cell division. High dose chemotherapy is able to normalize the blood cell cycle and bone marrow morphology (complete remission, CR) in a majority of treated patients, but even with these treatments people died in a 5 years period of time. In other cases, when the treatment is successful, there are considerable side effects such as growth, neurocognitive and reproductive abnormalities in survivors of childhood AML [6], fatigue, lower resistance to infection and damage to hearth, lungs, thyroid gland and eyes in both adult and child survivors [7], among other long-term complications. Since further intensification of chemotherapeutic regimens is usually ineffective in relapse patients and is accompanied by excess toxicity, there is the need of new strategies for the treatment of this hematopoietic malignancy.

The results described in this thesis show for the first time the development of an opto-nanomedicine platform to induce the differentiation of leukemia cells and thus a potential alternative for the treatment of leukemia patients. The opto-nanomedicine platform consists on nanoparticles (NPs) that are able to release retinoic acid (RA) after exposure to UV/blue laser light. Indeed, the NPs are (i) non-cytotoxic upon concentrations up to 100 μg/mL, (ii) are rapidly internalized by cancer cells and escape endolysomal compartment and (iii) can rapidly deliver the payload after exposure to UV/blue laser. The controlled delivery improves the therapeutic effect of the RA to levels that cannot be achieved by either soluble RA or NPs releasing RA by passive diffusion. The nanoformulation developed in this work opens new research opportunities regarding non-invasive modulation of stem cells, offering a powerful tool for research study and clinical therapy.

The development of the platform involved: (i) the development of light-activatable polymeric NPs capable of efficiently loading RA and being internalised by leukemia (stem)

cells; (ii) the evaluation of the impact of light-activatable polymeric NPs (with and without RA) on leukemia stem cells differentiation; and (iii) the demonstration that is possible to remotely activate the polymeric nanoformulation *in vivo*.

1.2 – Thesis outline

The PhD thesis is divided in four chapters. Chapter 1 provides a general overview of the present work, providing information about the problem, motivation and contributions to advance the state of the art.

Chapter 2 reviews the state-of-the-art relative to hematopoietic malignancies and opto-nanomedicine. This section also describes the design principles of existing micro- and nano light-triggered drug delivery systems and their current applications.

Chapter 3 provides all information regarding the development of a NP system possessing a trigger to allow precise control of the timing, duration and magnitude of drug release. It describes light-activatable polymeric NPs that rapidly release RA when exposed to a blue laser/UV light. These NPs reduce the clonogenicity of bone marrow tumor cells from patients with acute myeloid leukemia bone marrow and induce the differentiation of RA-low sensitive leukemia cells expressing the chimeric promyelocytic leukemia zinc finger/RARα fusion protein. RA released from light-activated NPs was superior at inducing leukemia cell differentiation compared to RA released by passive diffusion. Further, we demonstrate the importance of temporal activation of the nanoformulation during the intracellular trafficking to maximize RA effect and show *in vivo* that leukemic cells loaded with NPs can be light-activated to release RA, thereby allowing greater spatio-temporal control of drug delivery.

Chapter 4 summarizes the major findings and conclusions of this work. This chapter also describes future research avenues that should be explored.

CHAPTER 2 – STATE OF THE ART

2.1 – Cancer biology

Cancer describes a large and heterogeneous group of diseases characterized by the uncontrolled multiplication and spread of abnormal forms of the body's own cells [8-10]. Carcinogenesis is a multistep process where normal cells acquire accumulated mutations over time. Hallmarks of cancer include uncontrolled proliferation and unlimited replicative potential as well as evasion of apoptosis. Furthermore, cancer cells loose the spatial boundaries of the surrounding tissues that healthy cells maintain to enable normal continuous growth, thereby making cancer invasive and prone to metastasize [11]. Additionally, epigenetic modulation of gene expression, i.e. modifications occurring without alterations in the DNA sequence itself, is another key characteristic of cancer [12].

Another problem associated with cancer cells is the malfunctioning cell cycle control. The irreversible, ordered sets of events that characterize the cell cycle are not only critical for regulation of cell division and growth in general, but also for cell division after DNA damage [13]. Most cells in adults are not in process of cell division, but rest in a quiescent state (G_0) outside the division machinery. Mitogens or growth factors can release the cells from G_0, thereby introducing them into the first gap phase (G_1) during which the cell prepare for DNA replication. However, before this passage, cells must pass through the G_1 restriction point, but once they do so, cells are irreversibly committed to progress through the cell cycle. G_1 is followed by the synthetic phase (S), in turn succeeded by the second gap phase (G_2) and subsequent mitosis (M), the latter two with their own checkpoints aiming to maintain the integrity of the genome. After the completed cell division, the two new daughter cells have the option of either become inactive in G_0, or to re-enter the cell cycle through G_1 [14]. Deregulation of this intricate system and mutations in its regulators are common features in human malignancies [15].

Two models have been proposed to explain tumor[1] heterogeneity: the stochastic and the cancer stem cell (CSC) models (**Fig. 2.1**) [16]. Both models predict that only a small number of cells within a tumor have the capacity to initiate and sustain tumor growth. However, the stochastic model proposed that all cells within a tumor are biologically

[1] Tumor: An abnormal new growth of tissue that grows more rapidly than normal cells and will continue to grow if not treated. These growths will compete with normal cells for nutrients. This is a non-specific term that can refer to benign or malignant growths.

[2] The term "blast cells" refers to myeloblasts or myeloid blasts. These are the very earliest and most immature

homogenous and therefore have equal capacity to regenerate the tumor [17]. The stochastic events that govern tumor-initiating capacity can be intrinsic, such as a requirement for appropriate levels of critical transcription factors, or extrinsic, such as a requirement for the appropriate microenvironment and immune response. In contrast, the cancer stem cell model suggested that only a subset of tumor cells possess the capacity to regenerate the tumor [17]. According to the cancer stem cell model, it should be possible to isolate tumor cells into fractions that are tumor initiating and non-tumor initiating, where only tumor initiating cells are capable of sustaining tumor growth. The tumor-initiating cells, also referred to as CSCs, are defined by their capacity for self-renewal, the potential to develop into any cells in the tumor, and proliferative capacity to drive continued expansion of the tumor population [18]. The stochastic model states that all cells within a tumor possess equal potential to drive tumor growth, making it impossible to prospectively isolate the tumor-initiating fraction.

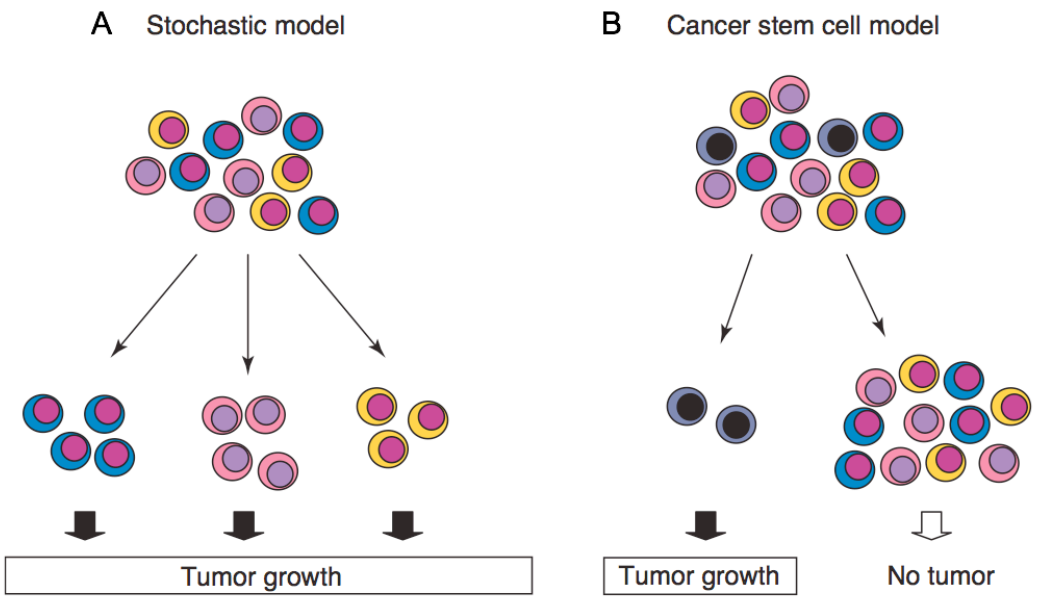

Figure 2.1 – Models of tumor cell proliferation. (A) Tumor cells are heterogeneous, and every cell has a low but equal probability of proliferating extensively and forming new tumors. Therefore, subpopulations enriched for tumor-initiating activity cannot be consistently isolated. According to this model, the genetic changes leading to development and progression of malignancy are operative in all cells within the tumor. Existing therapeutic and research approaches aimed at the bulk cells of the tumor are largely based on this model. (B) Tumor cell are heterogeneous, but most cells have only limited proliferative potential and only a small subset of cancer cells has the ability to initiate new tumor growth. According to this model, these cancer stem cells (CSCs) are biologically and functionally distinct from the bulk of tumor cells and must be specifically targeted by cancer treatments to achieve permanent cure (taken from Ref. [16]).

2.2 – Leukemic stem cells

The CSC theory arises from the poor probability of short-lived differentiated progenitors or terminally differentiated cells to accumulate mutations that become cancer. On the other side, the normal tissue stem cells or early progenitors that already possess the most important characteristics of cancer are an easy target for the accumulation of genetic aberrations that lead to cancer formation. The idea of stem cells in leukemia was put forward by John Dick and coworkers by a series of pioneering investigations to understand whether the functional hierarchy observed in normal hematopoiesis was conserved in blood tumors [19, 20]. These studies showed that leukemia stem cells (LSCs) were exclusively found in acute myeloid leukemia (AML) cells with hematopoietic stem cells (HSC) ($CD34^+/CD38^-$) phenotype, completely independent of the phenotype of the total AML sample, AML cell morphology or classification of the AML samples. Since LSCs were not detected in the $CD38^+$ fraction, which is highly enriched for committed myeloid progenitors, Bonnet and Dick concluded that in AML, LSCs originate from HSCs and not from committed progenitors [20]. Largely owing to improved mouse models compared to the ones available in the first studies, more and more evidence has been published that LSCs can be found in phenotypic subpopulations of AML cells that initially were not believed to contain any LSC activity [21].

The proof of the existence of cancer stem cells in AML has implications with respect to prognosis and therapy of AML. Treatment of AML patients with chemotherapeutics regularly leads to quick improvements up to complete remission, where no residual disease is detectable anymore. However, remission is unfortunately very often short-lived and commonly results in relapse. The cancer stem cell theory offers an elegant explanation for this clinical observation. While the rapidly dividing leukemic blasts which represent the majority of the leukemic population are killed efficiently by chemotherapy, the long-lived and quiescent LSCs are spared and can reinitiate the disease. It is believed that leukemic stem cells, compared to the bulk of leukemic cells, possess extraordinary resistance to chemo- and radiotherapy, the mechanisms of which are still under investigation but probably depend on the interaction with the bone marrow microenvironment [22]. Therefore it is vital to also target LSCs for therapy to completely eradicate the disease.

2.2.1 – Characterization of leukemic stem cells

The first evidence for the concept of cancer stem cells was reported in patients with acute myeloid leukemia (AML) and on xenogenic transplant models that have demonstrated that a very small number of leukemic blast cells can engraft and restore a leukemic clone, fuelling the hypothesis of leukemia stem cells (LSC) [20, 23].

Classification of cells can be made by detection of cell surface markers. LSCs, like its normal stem cell counterpart, is usually found in the $CD34^{+}/CD38^{-}$ marker compartment, although LSCs have been also found in the $CD34^{-}$ sub-population [24]. The original hypothesis defended the thesis that LSCs have its origin in a primitive stem cell compartment undergoing malignant transformation through a series of mutations [20]. Alternative theories suggested that LSC could also arise from more committed progenitors due to changes in gene expression, leading to enhanced self-renewal capacity [25]. Importantly, normal $CD34^{+}CD38^{+}$ progenitor cells are only able to transiently reconstitute NOD/SCID mice and cannot repopulate secondary recipients [26]. In fact, studies in ALL may suggest an even greater degree of plasticity within the LSC compartment. In these studies, LSC potential was also demonstrated in populations with phenotypic characteristics of progenitors ($CD19^{+}$ and $CD34^{-}$) [27]. However, not only were these populations able to transfer leukemia to recipient mice, but $CD34^{-}$ populations were also able to regenerate $CD34^{+}$ progeny within the transplanted leukemia. Similar results within a recently described murine model of AML suggest that AML LSC may also have a comparable developmental plasticity [28].

A more detailed comparison of the LSC phenotype with normal myeloid stem and progenitor ontogeny has revealed that in the vast majority of $CD34^{+}$ AML patients, $CD34^{+}CD38^{-}CD90^{-}CD45RA^{+}$ and $CD34^{+}CD38^{+}CD123^{+}CD45RA^{+}$ LSC compartments coexist. These respective populations resemble the normal lymphoid-primed multipotent progenitor (LMPP) and granuloctye-monocyte progenitor (GMP) populations at both the phenotypic and molecular level [29]. Although the majority of AML cases express the CD34 marker, in some patients, including those with Nucleophosmin (NPM1) mutations, the $CD34^{+}$ percentage is very low. In patients with less than 0.5 % $CD34^{+}$ cells, LSC activity was exclusively restricted to the $CD34^{-}$ population, whereas in other patients LSC were present in both the $CD34^{+}$ and $CD34^{-}$ populations [30]. Together, these studies confirm that the LSC population is phenotypically diverse and can vary markedly between patient subgroups, and even between individual patients within these subgroups. However, how this

might reflect the heterogeneity of the initial target cell transformed or the combinations of collaborating mutations is, as yet, unknown.

Table 1 – Summary of cell marker expression on HSCs and AML LSCs described in this work.

Marker	Expression on HSC	Expression on LSC	Reference
CD34	+	+/-	[19, 20, 30]
CD38	-	+/-	[19, 20, 29]
CD90	+	-/+	[29]
CD123	+	++	[29, 31]
CD45RA	-	+	[29]
CD33	++	++	[31]
CD13	+	++	[31]
CLL-1	-	+	[32, 33]
CD96	+	++	[34]
TIM3	+	++	[35]
CD47	+	++	[36]
CD32	-	+	[37]
CD25	-	+	[37]

+ indicates expression of the marker on some or all of the cells; ++ indicates that the marker is expressed at high levels; and – indicates that the marker is not expressed in this compartment.

In addition to CD34 and CD38, LSC have been shown to express a variety of other markers including the myeloid antigens CD33, CD123 and CD13 [31]. More recently several novel markers that are more highly expressed on $CD34^+CD38^-$ LSC than normal $CD34^+CD38^-$ HSC have been described. These include CLL-1, CD96, TIM3, CD47, CD32 and CD25 (**Table 1**). C-type lectin-like molecule-1 (CLL-1) was expressed by leukemic blasts at diagnosis from 92% of AML patients analyzed [32]. Moreover, although this antigen was expressed on normal $CD34^+CD38^+$ myeloid progenitors, it was absent on normal HSC. However, as with many LSC selective antigens, it is not expressed on every LSC. Within the $CD34^+CD38^-$ LSC compartment, a median expression of 33 % $CLL\text{-}1^+$ cells was observed when the data from 29 AML patients were combined [33]. CD96 (also known as Tactile) is a member of the Ig gene family. It is also expressed at higher levels in normal progenitors than HSC. Expression was elevated in the $CD34^+CD38^-$ LSC compartment when compared to normal HSC in 65 % of AML patients [34]. TIM3 is a negative regulator of Th-1-T cell immunity. In addition, the low level of TIM3 expression by

HSC compared to LSC enabled the prospective separation of LSC in a variety of AML patients [35]. The transmembrane protein CD47 is the ligand for signal regulatory protein α (SIRPα). SIRPα is expressed on phagocytic cells and its interaction with CD47 results in inhibition of phagocytosis. Expression of CD47 by LSC was found to protect them from being phagocytozed by macrophages and dendritic cells and its presence contributed to poor overall survival in patients [36]. Although CD47 was consistently more highly expressed by LSC than HSC, there was a large degree of variation across patients in terms of the percentage of LSC that expressed CD47 [36]. This was also true for the recently identified LSC-specific markers CD25 and CD32, which were found on 34.4 % and 24.6 %, respectively, of LSC from 61 AML patients analyzed [37]. Thus, despite the identification of novel LSC-specific markers, there is a large degree of heterogeneity in expression of these markers among patients. Thus, patient-specific targeting of LSC surface antigens may be necessary.

Another important aspect to consider is that like normal stem cells, LSCs are often quiescent, which decreases the efficiency of standard chemoterapies that target cells actively proliferating [38]. Recent gene expression analysis of AML subpopulations with LSC activity, revealed a LSC-associated signature highly predictive for poor clinical outcome, a finding possibly useful in defining patients with increased risk of relapse [21, 23]. It is also under consideration the exploration of the properties conferred by the stem cell niche that induces stem cells to a status of dormancy that many researchers account as reason for the resistance of normal HSCs and leukemia stem cells to chemotherapy [39]. The modulation of stem cells in the niche to leave their quiescence state would make it possible to change their sensitivity to chemotherapy action.

2.2.2 – Leukemic stem cell niche

The stem cell niche is important to maintain both HSCs and LSCs [40]. The HSC niche, a term first coined by Schofield [41], comprises supportive bone marrow microenvironment structures that are essential for the long-term maintenance of a stable HSC pool [42]. The niche integrates the function of multiple participants. The HSC niche remains incompletely defined and many competing models are under study [43, 44]. The niche is anatomically and functionally defined, and has an endosteal and perivascular compartment within the bone marrow [40]. The perivascular compartment, created partly by mesenchymal stromal cells and endothelial cells is often located near trabecular bone (**Fig. 2.2**). The most

primitive and quiescent HSCs are maintained by a perivascular niche [44]. Whether there are functionally distinct perivascular niches in different regions of the bone marrow remains an open question [44]. Within the niche, there are critical bidirectional signals that ensure the regulation of normal HSC numbers [45, 46] and maintenance of the quiescent long-term HSC pool [47] (**Table 2**). Osteopontin (OPN) [46, 48], calcium ions that signal through the calcium sensing receptor [49] or inputs from the sympathetic nervous system [50] have all been shown to affect HSC function [40]. Osteoclasts also play a role in regulating HSC niche and are important in stem cell mobilization [51]. Perivascular structures, defined by proximity to sinusoidal vascular endothelium, and surrounding supportive structures such as stromal cells, also have essential roles in bone marrow niche [40]. The axis CXCR4 expressed by HSCs and CXCL12 (SDF-1) expressed by cells of the bone marrow niche is important for the localization and retention of HSCs and progenitor cells [52]. CXCL12 has a critical role in colonization of the bone marrow by HSCs during early development, as CXCL12-deficient embryos have severely reduced HSC numbers and function [40, 53]. In addition, cells expressing CXCL12 can recapitulate the hematopoietic microenvironment [54]. For example, mesenchymal cells located adjacent to blood vessels and expressing CXCL12 can recapitulate a hematopoietic microenvironment [54].

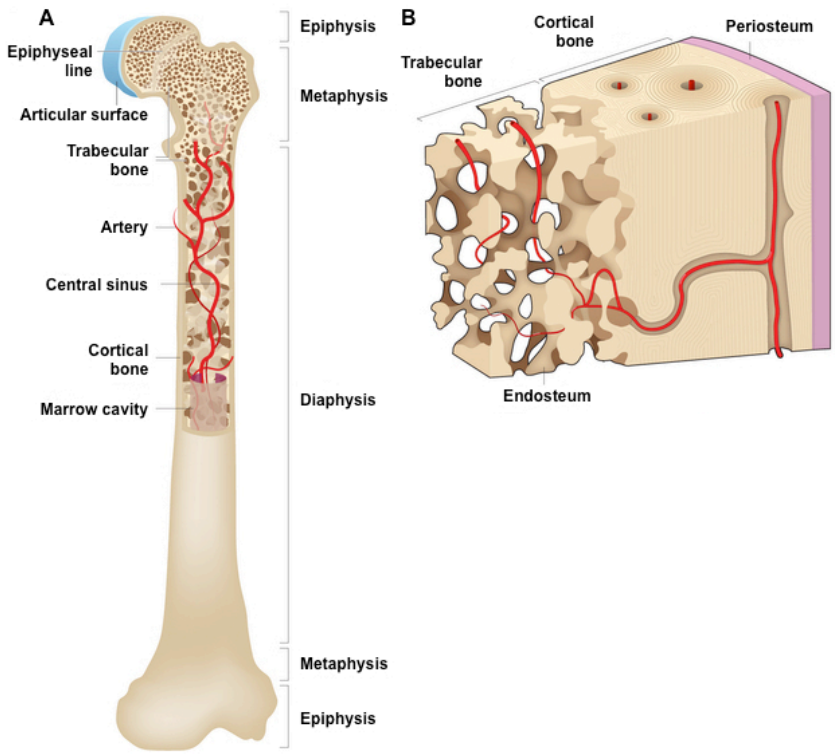

Figure 2.2 – HSCs reside mainly within bone marrow during adulthood. Bone marrow is a complex organ, containing many different hematopoietic and non-hematopoietic cell types, that is surrounded by a shell of

vascularized and innervated bone. **A**: Minute projections of bone (trabeculae) are found throughout the metaphysis such that many cells in this region are close to the bone surface. **B**: The interface of bone and bone marrow is known as the endosteum, which is covered by bone-lining cells that include bone-forming osteoblasts and bone-resorbing osteoclasts. Arteries carry oxygen, nutrients and growth factors into the bone marrow, before feeding into sinusoids, which coalesce as a central sinus to form the venous circulation. Sinusoids are specialized venules that form a reticular network of fenestrated vessels that allow cells to pass in and out of circulation. There is a particularly rich supply of arterioles, as well as sinusoids, near the endosteum (adapted from [44]).

Table 2 – Molecular pathways implicated in HSC-niche interactions (taken from Ref. [40]).

Molecular pathway	Reference
Calcium-sensing receptor	[49]
Parathyroid hormone receptor (potentially as a function of increased osteoblast numbers)	[45]
Bone morphogenic protein receptor 1A (also potentially as a function of increased osteoblast numbers)	[55]
Osteopontin	[46, 48]
CX chemokine ligand 12 (also known as stromal-derived factor-1)-CX chemokine receptor 4 interactions	[52, 56]
Angiopoietin-Tie2 interactions	[57]
Canonical Wnt signaling	[47]
Notch activation (with osteoblast parathyroid hormone receptor activation)	[45]
Mpl receptor, thrombopoietin	[58]
cKit receptor, stem cell factor (SCF)	[51]
Cdc42 and Rac proteins	[59, 60]
Insulin-like growth factor 2	[61]
N-cadherin (conflicting data exist)	[55, 62, 63]
VLA-4	[64]
VCAM-1	[52]

Experimental evidences suggest that LSCs receive important signals from the niche that support self-renewal and may exploit the normal homeostatic mechanisms that preserve long-term HSCs [40]. Leukemic cells reside and engraft in normal endosteal niches that are quiescent and resistant to chemotherapy [37, 65]. Yet, other studies have observed that the

growth of leukemic cells alters bone marrow environments and interferes with normal hematopoiesis [66-68]. For example, leukemia cells are able to directly modulate the niche at the expense of normal hematopoietic stem and progenitor cells [66] by down-regulating CXCL12 levels in areas of leukemia infiltration. Stem cell factor, a niche regulator, might be secreted by leukemia cells leading to abnormal retention and engraftment of normal HSC, and progenitor cells in the tumor-infiltrated microenvironment.

The development of methodologies to modulate the LSC niche could open new research avenues to disrupt cancer stem cell resistance, a crucial step towards the long-term cure of cancers [69]. Niche-targeted approaches have been suggested in the context of regenerative medicine [70] to enhance HSC engraftment; however, the use of niche-targeted approaches to treat leukemia patients remains elusive. There is emerging evidence that the complex interactions between LSCs and their niche could be targeted *in situ* to selectively deplete the repopulation (or regenerative) ability of LSCs as opposed to their normal HSC counterparts. Experimental evidence also suggests that the incorporation of LSCs in facultative niches promotes the chemoresistance and regeneration of leukemia following induction and consolidation therapy [71]. Niche-targeted therapy could successfully overcome cell intrinsic mechanisms of resistance such as increased expression of MDR [69, 72]. The hypothesis in this thesis is that leukemic cells might act as carriers to transport NPs to the bone marrow. Once the cells are at the bone marrow, NPs inside the cells can be activated by light and release RA to induce the differentiation of the transporting cells. This differentiation process will impact the homeostasis of the niche and might block the resistance observed after conventional therapy.

2.2.3 – Hematological malignancies

Hematological malignancies are types of cancer that affect blood, bone marrow and lymph nodes. Hematological malignancies are divided into myeloid or lymphoid depending on the origin of the cell type primarily affected. These groups are traditionally subdivided into chronic and acute depending on the stage of maturity of the malignant cells and their clinical outcome. The six hallmark properties that traditionally define malignant populations include: (i) self-sufficiency in growth signals, (ii) insensitivity to growth inhibitory (antigrowth) signals, (iii) evasion of programmed cell death (apoptosis), (iv) limitless replicative potential, (v) sustained angiogenesis, and (vi) tissue invasion and metastasis [8]. Conceptual progress recently added two emerging hallmarks of potential generality to the

list: (vii) reprograming of energy metabolism, and (viii) evading immune destruction [9]. The type and frequency of specific events necessary to result in these cell regulatory changes varies among different malignancies and among different patients with the same malignancy [8, 9].

2.2.3.1 – Myeloid malignancies

Myeloid malignancies are a group of disorders that manifest themselves as malignant dysregulation of the myeloid lineage such as myelodysplastic syndromes (MDS), myeloproliferative neoplasms (MPN) including chronic myeloid leukemia (CML), myelodysplastic/myelomonocytic neoplasms and AML [73]. There are clonal diseases that arise in hematopoietic stem or progenitor cells, mainly due to mutations in genes involved in signaling pathways (e.g. *CBL, FLT3, JAK2, RAS*), epigenetic regulators (e.g. *DNMT3A, ASXL1, EZH2, IDH1, IDH2, SUZ12, TET2, UTX*), transcription factors (e.g. *CEBPA, ETV6, RUNX1*), and tumor suppressors (e.g. *TP53*) [74].

Despite the advances in the therapy of AML, the majority of patients will die from their disease [75]. AML describes a group of different malignant disorders that originate in the hematopoietic system and are characterized by a rapid expansion of undifferentiated myeloid cells disturbing normal hematopoiesis. AML disease accounts for ~80% of adult acute leukemias [76]. In AML, myeloid progenitor cells of the bone marrow undergo a malignant transformation resulting in accelerated production of poorly differentiated myeloblasts that are not able to mature into more differentiated cell types but remain as immature cells. AML patients present with symptoms resulting from bone marrow failure (i.e. anaemia, neutropenia and thrombocytopenia), and/or symptoms resulting from organ infiltration and/or proliferation of leukemic cells (i.e. splenomegaly, hepatomegaly, swollen bleeding gums, bone and joint pain, respiratory distress and alterations in mental state as well as disseminated intravascular coagulation (DIC) [1].

During the last decades and until recently, AML has been classified according to the French-American-British (FAB) classification that divides AML into 8 subtypes (M0 to M7) defined by morphologic and cytochemical characteristics [77]. The different subclasses represent different states of maturation of the leukemia blast cells[2] and what lineage that is

[2] The term "blast cells" refers to myeloblasts or myeloid blasts. These are the very earliest and most immature cells of the myeloid cell line.

engaged (**Table 3**). Healthy individuals do not present values of blast cells in bone marrow superior to 5%. However, in patients with AML, these values are above 30%.

Table 3 – FAB classification of AML (adapted from [78]).

FAB subtype	Name
M0	Undifferentiated acute myeloblastic leukemia
M1	Acute myeloblastic leukemia with minimal maturation
M2	Acute myeloblastic leukemia with maturation
M3	Acute promyelocytic leukemia (APL)
M4	Acute myelomonocytic leukemia (AMML)
M4 eos	Acute myelomonocytic leukemia with dysplastic eosinophilia
M5	Acute monocytic leukemia (AMoL)
M6	Acute erytroid leukemia
M7	Acute megakaryoblastic leukemia (AMkL)

In recent years, the new WHO classification replaced more and more the FAB classification. The WHO classification is based on the fact that an increasing number of acute leukemias should be categorized based upon their underlying genetic abnormalities and/or their pathophysiologic characteristics (**Table 4**) [79]. For AML, the WHO classification requires information on the chromosomal aberrations, about the mutational status, a previous exposure to chemotherapy or radiation therapy or to the presence of an antecedent myelodysplastic syndrome.

Table 4 – AML and related precursor neoplasms, and AMLs of ambiguous lineage. WHO 2008 categories, (adapted from [79]).

Acute myeloid leukemia with recurrent genetic abnormalities
AML with t(8:21)(q22;22); RUNX1-RUNX1T1
AML with inv(16)(p13.1q22) or t(16;16)(p13.1;q22); CBFB-MYH11
APL with t(15;17)(q22;q12); PML-RARA
AML with t(9;11)(p22;q23); MLLT3-MLL
AML with t(6;9)(p23;q34); DEK-NUP214
AML with inv(3)(q21q26.2) or t(3;3)(q21;q26.2); RPN1-EVI1
AML (megakaryoblastic) with t(1;22)(p13;q13); RBM15-MKL1
Provisional entity: AML with mutated NPM1
Provisional entity: AML with mutated CEBPA

Table 4 – AML and related precursor neoplasms, and AMLs of ambiguous lineage. WHO 2008 categories, (adapted from [79]) (cont.).

Acute myeloid leukemia with recurrent genetic abnormalities
AML with t(8:21)(q22;22); RUNX1-RUNX1T1
AML with inv(16)(p13.1q22) or t(16;16)(p13.1;q22); CBFB-MYH11
APL with t(15;17)(q22;q12); PML-RARA
AML with t(9;11)(p22;q23); MLLT3-MLL
AML with t(6;9)(p23;q34); DEK-NUP214
AML with inv(3)(q21q26.2) or t(3;3)(q21;q26.2); RPN1-EVI1
AML (megakaryoblastic) with t(1;22)(p13;q13); RBM15-MKL1
Provisional entity: AML with mutated NPM1
Provisional entity: AML with mutated CEBPA
Acute myeloid leukemia with myelodysplasia-related changes
Therapy-related myeloid neoplasms
Acute myeloid leukemia, not otherwise specified (NOS)
Acute myeloid leukemia with minimal differentiation
Acute myeloid leukemia without maturation
Acute myeloid leukemia with maturation
Acute myelomonocytic leukemia
Acute monoblastic/monocytic leukemia
Acute erythroid leukemia
Pure erythroid leukemia
Erythroleukemia, erythroid/myeloid
Acute megakaryoblastic leukemia
Acute basophilic leukemia
Acute panmyelosis with myelofibrosis (acute myelofibrosis)
Myeloid sarcoma (extramedullary myeloid tumor; granulocytic sarcoma)
Myeloid proliferations related to Down syndrome
Transient abnormal myelopoiesis (transient myeloproliferative disorder)
Myeloid leukemia associated with Down syndrome
Blastic plasmacytoid dendritic cell neoplasm
Acute leukemias of ambiguous lineage
Acute undifferentiated leukemia
Mixed phenotype acute leukemia with t(9;22)(q34;q11.2); BCR-ABL1
Mixed phenotype acute leukemia with t(v;11q23); mixed lineage leukemia
Mixed phenotype acute leukemia, B/myeloid, NOS
Mixed phenotype acute leukemia, T/myeloid, NOS
Provisional entity: Natural killer (NK)–cell lymphoblastic leukemia/lymphoma

2.2.4 – Treatment of AML

Existing treatment protocols involve the combined use of chemotherapeutics administered at maximum tolerated doses. The use of such combinatorial regimens is far more effective than using single drugs in achieving complete or long-term remission. With single agents, only 60% of patients achieved completed remission, whereas the remainder did not respond or relapse within 6-9 months [80]. Despite great effort to stratify patients, AML first line treatment is still very uniform, with the exception of acute promyelocytic leukemia (APL). APL has a specific morphology and is clinically characterized by disseminated intravascular coagulopathy and high incidence of early fatal hemorrhages [81]. The introduction of retinoic acid (RA) has revolutionized the treatment for APL patients. In 95% of cases of APL, RA receptor alpha (RARA) gene on chromosome 17 is involved in a reciprocal translocation with the promyelocytic leukemia gene (PML) on chromosome 15, a translocation denoted as t(15;17)(q22;q21) [81]. The RA receptor (RAR) is dependent on RA for regulation of transcription. The fusion of PML and RARA results in expression of a hybrid protein with altered functions. This fusion protein binds with enhanced affinity to sites on the cell's DNA, blocking transcription and differentiation of granulocytes. It does so by enhancing interaction of nuclear co-repressor (NCOR) molecule and histone deacetylase (HDAC). Treatment with RA dissociates the NCOR-HDAC complex from RAR and allows DNA transcription and differentiation of the immature leukemic promyelocytes into mature granulocytes by targeting the oncogenic transcription factor and its aberrant action [81]. Unlike other chemotherapies, RA does not directly kill the malignant cells [81]. RA induces the terminal differentiation of the leukemic promyelocytes, after which these differentiated malignant cells undergo spontaneous apoptosis on their own. When RA therapy is combined with conventional chemotherapy, a complete remission (CR) rate of 90-95% can be achieved, thereby shifting the prognosis from highly fatal to strikingly curable [82]. Standard treatment of acute myeloid leukemia is based on induction therapy and consolidation therapy.

2.2.4.1 – Induction therapy

Induction therapy aims to achieve a CR, which is defined as less than 5% leukemic blasts in the bone marrow and recovery of neutrophil count $>1.0 \times 10^9$ L^{-1} and platelet count $>100 \times 10^9$ L^{-1}. Conventional induction therapy in adults consists of a combination regimen

of the deoxycytidine analogue cytarabine and an anthracycline antibiotic (daunorubicin or idarubicin) or the anthracenedione mitoxantrone, an inhibitor of the topoisomerase IIa enzyme [83]. Anthracyclines attack cancer cells by multiple mechanisms, inhibiting replication and damaging cells in ways that promote cell death [84]. They work primarily by DNA intercalation[3]. Approximately 50% to 75% of adults with AML achieve CR with that regimen. The most commonly used standard induction therapy for the last 4 decades consists of daunorubicin intravenously for 3 days and cytarabine 100 or 200 mg/m^2 (the use of body surface area (mg/m^2) in dose normalization is a standard practice for anticancer agents [85]) by continuous infusion for 7 days [83]. With this standard regimen 60% to 80% of young adults and 40% to 60% of older adults can achieve a CR. Many studies have compared the standard regimen with different doses of daunorubicin and the conclusion is that 45 mg/m^2 (the previous standard dose) should no longer be considered as the standard of care as the higher dose between 60 and 90 mg/m^2 for 3 days has proven to be safe and yield either higher CR and prolonged overall survival (OS) rates [86]. Some elderly patients tolerate and benefit from intensive induction approaches, while others are best managed with less aggressive strategies. In order to maximize the therapeutic benefit and minimize toxicity for those patients, a strategy to stratify them based on host-related and biological features is of paramount importance [76].

2.2.4.2 – Consolidation therapy

Consolidation and maintenance therapy, also known as post-remission treatments are given after achieving the first remission (CR1) aiming to maintain the CR and to eradicate remaining leukemic cells. Consolidation therapy often includes repeated courses with intermediate/high-dose cytarabine (Ara-C) with or without an anthracycline, or arsenic trioxide (ATO). It is difficult to determine whether re-induction therapy should be attempted or hematopoietic cell transplantation should be directly performed in relapsed patients with histocompatible donors. Consolidation with allogeneic stem cell transplantation in CR1 after relapse is an often-preferred treatment option for younger patients [87]. Though, contradictory results showed that patients transplanted shortly after achieving CR appeared to have a worse prognosis than those transplanted further into remission [88], but overall

[3] DNA intercalation is a process by which another molecule (called a "ligand") binds between base pairs of DNA. DNA intercalators are used to inhibit DNA replication in order to inhibit cell division, particularly in rapidly dividing cells such as cancer cells.

intensive consolidation therapy contributes to improving survival. The addition of targeted therapy with gemtuzumab ozogamicin (exploring the CD33 or CD123 target, a myeloid differentiation antigen found on AML blasts in most patients) to standard therapy has not improved on these outcomes. New agents that target specific molecular abnormalities or survival mechanisms in the leukemic cell are being studied as alternative therapies [89, 90].

Conventional chemotherapeutics induce cytotoxicity in rapidly dividing cells (a characteristic trait of cancer). However, such agents also affect cellular division and viability of normal cells and tissues. Side effects, such as myelosuppression (reduced blood cells and platelets), immunosuppression (reduced efficacy of the immune system), mucositis (inflammation of mucous membranes that line the digestive tract), and alopecia (hair loss), are observed among many other side effects [81, 91]. The development of new treatment strategies and innovative controlled drug delivery systems is of critical importance to increase therapeutic efficacy and patient quality of life.

2.2.4.3 – Retinoid acid therapy

One of the reasons for the failure of AML therapies is that normal hematopoiesis is compromised during the eradication of leukemia cells, with patients requiring blood and platelet transfusion. To overcome this pressing concern, there is a growing need for new therapeutic strategies able to induce more effective AML cells differentiation, presenting lower hematological toxicity, comparing to standard therapies [92].

Retinoids serve as intracellular messengers or activating ligands for the RAR and retinoid X receptors (RXR) [93]. Because of their potential to inhibit growth and promote differentiation, retinoids hold therapeutic promise in treating cancer, especially when used in combination with other chemotherapeutic agents [94]. The introduction of RA as differentiation inducing agent to treat acute APL (that accounts for around 5-10% of AML cases) pioneered a new approach to obtain remission. Differentiation therapy also offers the prospect of a less aggressive treatment by virtue of attenuated growth of leukemic cells coupled to limited damage to normal cells.

Although RA is generally well tolerated, the development of RA syndrome (RAS) in some patients is recognized as a complication and a potential life-threatening adverse reaction. The incidence of RAS has been reported to range from 2 to 27% in clinical trials and case reports [95]. The onset of the syndrome ranges from 2 to 21 days (median period of 10 days) after initiating RA therapy. RAS is characterized by unexplained fever, weight gain,

elevated numbers of white blood cells (WBCs), respiratory distress, interstitial pulmonary infiltrates, pleural and pericardial effusion, dyspnea, episodic hypotension and acute renal failure. The most common manifestations include respiratory distress and fever in >80% of patients. Mortality from RAS has been reported to be about 2% of patients treated with RA [81].

Therapies using RA were shown to be successful in the treatment of APL, but the promise of extending the efficacy of RA-based differentiation therapy to other types of AML, and other leukemias and cancers, has still to be fulfilled [96]. The development of drug delivery systems able to efficiently encapsulate, transport and release RA in a controlled fashion could be the key to extend and improve differentiation therapy for AML.

2.3 – Nanotechnology

Richard Feynman established the principles of contemporary nanotechnology, in a visionary lecture at the annual meeting of the American Physical Society, at Caltech, on 1959. The lecture entitled "There is Plenty of Room at the Bottom" [97], Feynman speculated about what it would take to carry miniaturization all the way through to the atomic level, and about "what would happen if we could arrange the atoms one by one the way we want them" [97]. Many of the principles and goals of nanotechnology – such as miniaturization and convergence of physical, chemical and biological processes at the molecular level – were already explicited in Feynman's lecture, and several of his predictions indicated a great deal of foresight. However, Feynman's lecture had virtually no impact on scientific development at that time. This changed with Drexler 1986 publication of *Engines of Creation*, where nanotechnology is presented not only as a panacea for all kinds of technological problems but also as the inevitable outcome of a deterministic evolution from a simple tool use to highly complex technology with the power to transform the world around us. Drexler´s book caused controversy and led many researchers to take an active interest in nanotechnology [98]. The growing impact of nanotechnology made it the first major worldwide research initiative of the 21st century. Nanotechnology has matured over the past 20 years from a field focused on understanding miniaturization and its consequences to a research area defined by the rational design, synthesis and manipulation of nanoscale objects. The advantage of operating in this range is that materials can be engineered to interact with cell features and substrates at a scale that was hitherto impossible to achieve or

to reach, promising new therapeutic interventions with greater safety and security, along many other industrial and societal applications.

By definition, nanotechnology deals with materials that range from 1 to 100 nm in size in at least one of the three dimensions. The application of such materials in the field of medicine is termed "nanomedicine". The final biomedical application, route of administration and the type of drug to administer determines the optimal size range of the carrier [99]. The high surface area/volume ratio of nanomaterials enables the accommodation of multiple functional elements to modulate biomaterial properties. Advantages can be achieved towards (i) a tailored drug loading, (ii) the incorporation of drug combinations, (iii) a targeted delivery of clinical agents, (iv) reduced dosage, (v) reduced frequency of dosing, (vi) improved drug solubility, (vii) controlled drug delivery, (viii) reduced immunogenicity, and (ix) superior half-life of clinical agents *in vivo* for clinical therapy.

2.3.1 – Type of nanocarriers

The majority of nanomaterial-based drug delivery systems that have advanced to clinical development are based on liposomes or polymers [91]. Liposomes are artificial vesicles composed of amphiphilic lipid bilayers, mimicking bio-membranes that can encapsulate water-soluble agents within the central polar cavity and oil-soluble agents within the lipid bilayer. Polymeric formulations are derived from polymers that form polymer-drug conjugates or micelles that self-assemble from amphiphilic block copolymers in aqueous solution. The third class of polymeric nanocarriers are dendrimers which are composed of highly branched (symmetrical) structures that rise from a central core to form particles of nanosized dimensions. Therapeutic payloads can be integrated into such engineered nanostructures via covalent bonds that are stable or that degrade in response to internal or external stimuli [100].

Nanotherapeutics have evolved through three generations to date [91]. The first generation of nanocarriers were evaluated for their ability to encapsulate and release drugs, their biocompatibility and cell uptake rates. Despite enhancing the solubility of hydrophobic drugs incorporated within, clinical advancement of first-generation NPs was hindered by drawbacks, such as instability and lack of prolonged circulation half-lives. These limitations were overcomed by modifying the nanomaterial composition in order to improve stability and surface chemistry and to enhance by that the *in vivo* circulation rates, giving rise to the second generation of nanotherapeutics. However, new limitations of second-generation

nanocarriers were identified such as lack of control over drug release, poor cell uptake and targeting efficiency. Controlled drug delivery is essential to avoid premature drug release from the carrier and excessive levels of free drug in the blood. This causes drug accumulation at nonspecific sites, undermining the very significance of developing drug delivery strategies to treat any form of disease [101]. These drawbacks led to the development of NPs with increased cellular and subcellular targeting capabilities. Such particles can be retained at active sites while possessing long circulating half-lives in the blood and reduced clearance rates, giving raise to a third generation of NP-mediated therapeutic carriers. Targeted nanocarriers use ligands (e.g. mAbs, peptides and aptamers, among others), generally located on the surface of the carrier for a selective cell surface targeting. Due to the presence of these ligands, NPs readily interact with biomolecules or receptors overexpressed on the target cell surface and undergo receptor-mediated endocytosis [91, 102].

Growing research efforts are being employed in the development of nanocarriers able to incorporate multiple features providing simultaneous targeting, enhanced delivery, and tracking capabilities from a single biomaterial (**Fig. 2.3**).

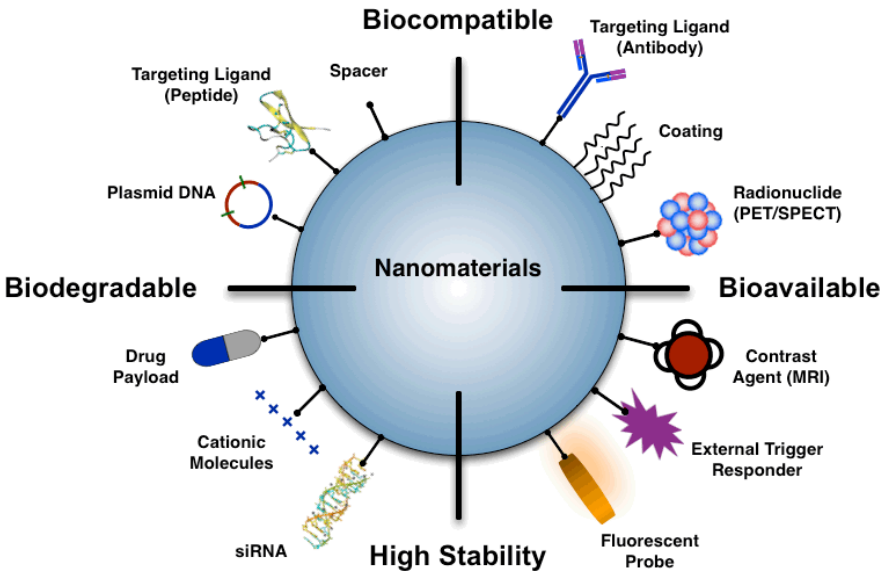

Figure 2.3 – Multifunctional NPs for cell targeting, tracking, labeling, imaging and modulation.

Nanomedicine platforms have improved significantly the therapeutic properties of anticancer drugs (**Table 5**) and support the growing efforts to use these therapeutic strategies in the clinic. Hopefully, in the near future, current research efforts can lead to personalization of chemotherapy and improve dramatically patient outcomes [103].

Table 5 – Examples of micro- and nanocarriers clinically approved or advanced to clinical trials

Formulation	Size	Drug	Cancer Type	Current Status	Reference
Non-PEGylated Liposome	45 nm	Daunorubicin (DaunoXome)	AML	FDA approved	[104]
Non-PEGylated Liposome	115 nm	Vincristine sulphate liposome (Marquibo)	ALL, NHL	FDA approved (Ph-adult ALL) Phase II (NHL) Phase I (pediatric ALL)	[105]
Non-PEGylated Liposome	100 nm	Cytarabine/Daunorubicin (CPX-351)	AML	Phase III	[106]
PEGylated Liposomes	88 nm	Doxorubicin (Caelyx or Doxil)	Variety of cancers	FDA approved	[107]
PEGylated Liposomes	180 m	Oxaliplatin (MBP-426)	Advanced/metastatic solid tumors	Phase I/II	[108]
Polymeric Micelles	85 nm	Paclitaxel (NK911)	Gastrointestinal cancer	Phase III	[109]
Polymeric Micelles	10-150 nm	Paclitaxel poliglumex (Opaxio)	Ovarian cancer	Phase III	[110]
Polymeric Micelles	100 nm	Docetaxel (BIND-014)	Solid tumors	Phase I Completed	[111]
Protein-drug Conjugates	130 nm	Paclitaxel (Abraxane)	Metastatic breast cancer	FDA approved	[112]

ALL, acute lymphocytic leukemia; AML, acute myeloid leukemia; FDA, US Food and Drug Administration; NHL, non-Hodgkin's lymphoma; PEG, polyethylene glycol; Ph-, Philadelphia chromosome-negative.

2.3.2 – Endocytosis and intracellular fate of nanoparticles

Nanoparticles (NPs) must be capable of reaching their biological targets with high efficiency and specificity (**Fig. 2.4**). The intracellular milieu is physically segregated from the environment by the plasma membrane, an elastic lipid bilayer embedded with domains of lipids, carbohydrates, and membrane proteins. In order to deliver NPs into cells and to their subcellular targets, NPs must first cross the plasma membrane. NPs placed in the external milieu of a cell can interact with the exterior of the plasma membrane, which can lead to the carrier's entry inside the cell (**Fig. 2.4C**).

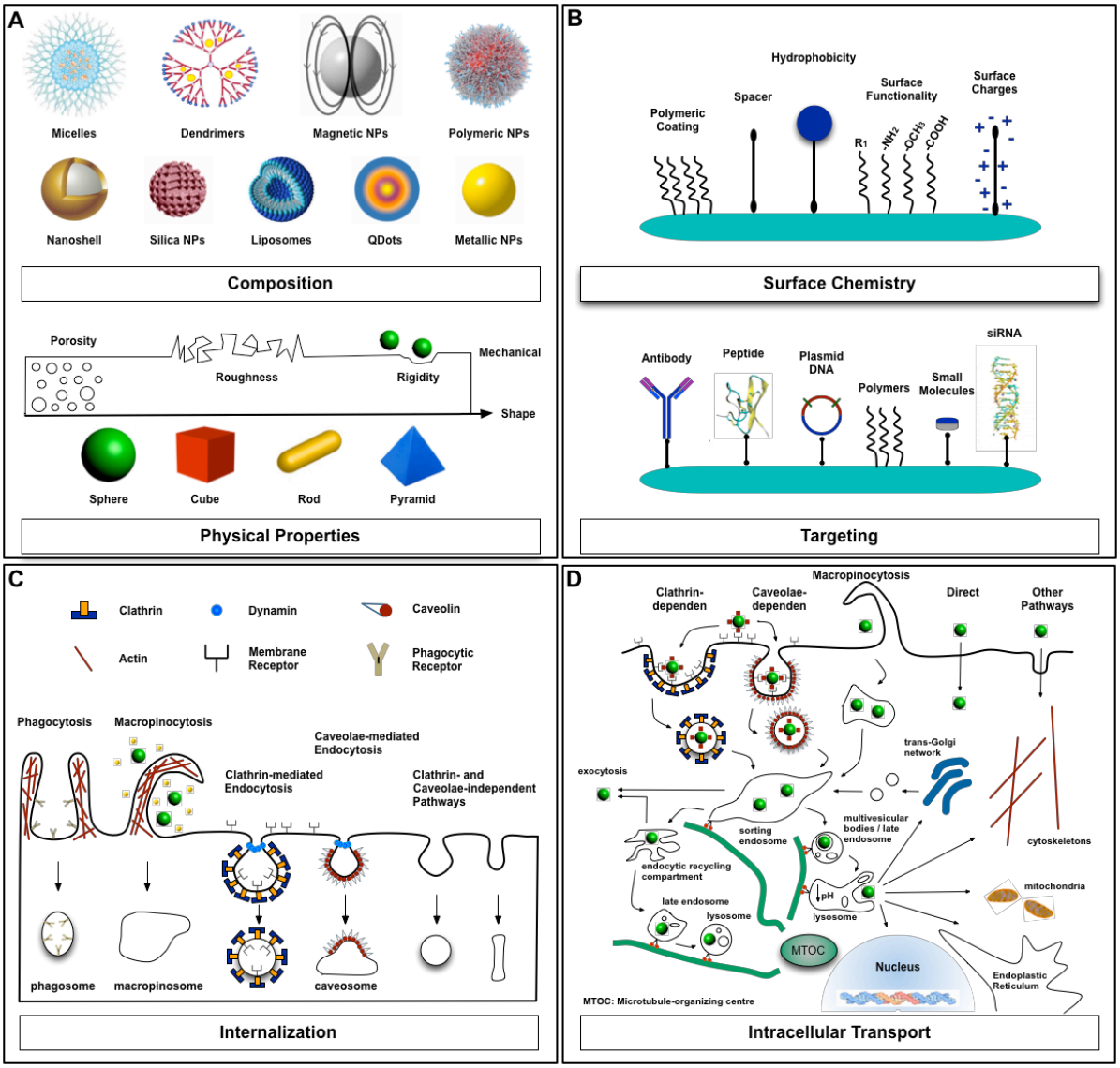

Figure 2.4 – Designing NPs for intracellular applications. NPs can be: (A) modularly assembled from distinct materials composition with different physical and chemical properties, and (B) functionalized with a myriad of

ligands for biological interaction and targeting. (C) Pathways of entry into the cell. An increasing number of endocytic pathways are being defined, each mechanistically distinct and highly regulated at the molecular level. These pathways facilitate cellular signalling and cargo transport. Controlling the route of NP uptake is important for both mediating their intracellular fate as well as their biological response. (D) Intracellular transport of NPs. After internalization *via* one or more of the endocytic pathways, NPs are trafficked along the endolysosomal network within vesicles with the help of motor proteins and cytoskeletal structures. Vesicles can transport their contents into sorting endosomes, or excrete/recycle them back to the cell surface by fusing with the plasma membrane. Alternatively, endosomes can mature into lysosomes via luminal acidification and recruitment of degradative enzymes, which target the vesicle contents for degradation. In order to access cytoplasmic or nuclear targets, NPs must be capable of escaping from the endolysosomal network as well as traverse through the crowded cytoplasm (adapted from [102]).

The process is termed endocytosis and can occur by the following pathways: (i) receptor mediated endocytosis, (ii) non-specific endocytosis, and (iii) internalization under endocytosis-inhibiting conditions [113]. Generally, endocytosis can be divided into two broad categories - phagocytosis (the uptake of large particles) and pinocytosis (the uptake of fluids and solutes) [114]. The endocytosis process involves multiple stages. First, the cargo is engulfed in membrane invaginations that are pinched off to form membrane-bound vesicles, also known as endosomes (or phagosomes in case of phagocytosis). Cells contain heterogeneous populations of endosomes equipped with distinct endocytic machineries, which originate at different sites of the cell membrane. Second, the endosomes deliver the cargo to various specialized vesicular structures, which enables the sorting of a cargo towards different destinations. Finally, the cargo is delivered to various intracellular compartments, recycled to the extracellular milieu or delivered across cells (a process known as "transcytosis" in polarized cells) (**Fig. 2.4D**). Once in the endosomes, NPs are then trafficked to acidic and oxidative environments of lysosomes and peroxisomes. At this stage they have three possible fates: (i) degradation by enzymes or the acidic pH, (ii) exocytosis, (iii) escape from the endo-lysosomal compartment and travel to other intracellular locations including cell nucleus [113].

It has been reported that cellular uptake is dependent on the charge of the nanocarrier. The majority of reports suggest that positively charged nanomaterials are predominantly internalized through clathrin-mediated endocytosis (CME) and a minor fraction using macropinocytosis [114]. Some cationic polymers are powerful transfection agents due to their pH-buffering properties. In this case they activate the proton pumps increasing the osmotic pressure inside the endosome, which in turn leads to the swelling/bursting of the

endosome and subsequent escape of the carrier (**Fig. 2.5**) [115]. This mechanism is called "proton sponge effect". Alternatively, it has been suggested that cationic components of nanocarriers interact with the anionic lipids of the endosome, causing a destabilization of the endosomal membrane which leads of the escape of the nanocarrier [116-118]. Among the cationic polymers used as transfection agents, polyethyleneimine is one of the best studied [119].

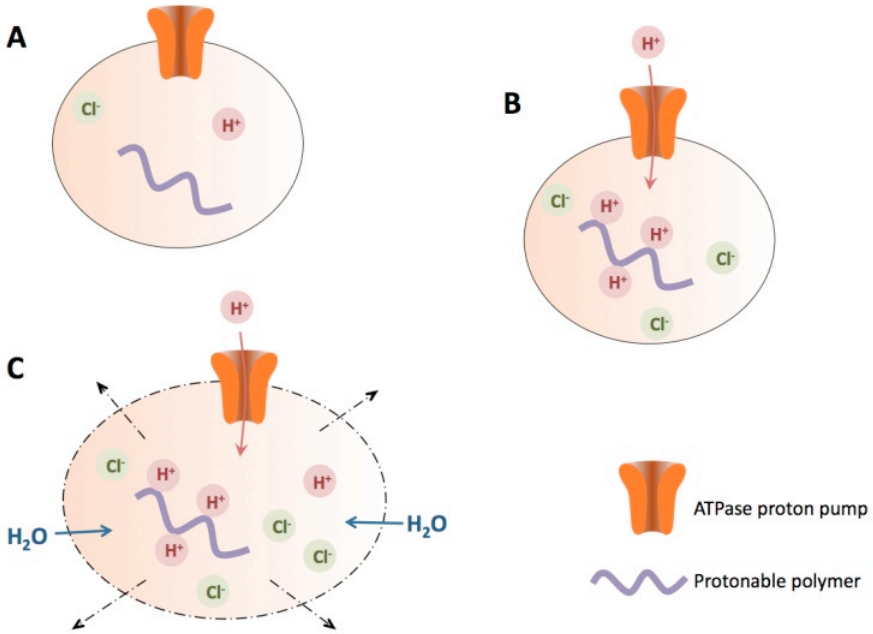

Figure 2.5 – The 'proton sponge' hypotheses (pH-buffering effect). (A) Polyplexes (complexes of nucleic acids with polycations) enter the cell via endocytosis and are trapped in endosomes. (B) The membrane bound ATPase proton pumps actively translocate protons into endosomes. Polymers become protonated and resist the acidification of endosomes. Hence more protons will be pumped into the endosomes continuously to lower the pH. (C) The proton pumping action is followed by passive chloride ions entry, increasing ionic concentration and hence water influx. High osmotic pressure causes the swelling and rupture of endosomes, releasing their contents to cytosol (adapted from [117]).

2.3.3 – Polyethyleneimine

Polyethyleneimine (PEI), a commercially available cationic polyamine is a synthetic polymer prepared from aziridine by cationic polymerization. Its structure contains primary, secondary, and tertiary amino groups due to chain transfer reactions. The amino group ratio is 1 : 2 : 1 (i.e., 25 % of primary amines, 50 % of secondary amines, and 25 % of tertiary

amines). The amino groups of PEI are chemically reactive and consequently enable a wide variety of chemical modifications, which provide PEI with appropriate physicochemical properties for *in vitro* and *in vivo* cargo delivery [120, 121]. Since 1995 has been used for the intracellular DNA delivery in many pre-clinical studies [119]. With protonable amino groups in every third position, PEI has a high positive charge density that allows the spontaneous formation of non-covalent polyelectrolyte complexes. With a positive surface charge (zeta-potential) the interaction with negatively charged components of the cell membrane is promoted, namely the heparin sulfate proteoglycans, facilitating cellular uptake by endo-, pino-, or phagocytosis [122]. In addition, the PEI buffers low pH values in the endosomal/lysosomal system, decreasing protease activity, and facilitating endolysosomal escape [123].

The effect of PEI molecular weight and structural configuration on transfection activity and cytotoxicity has been study *in vitro* and *in vivo*. Both enhancement and reduction in PEI activity has been observed with increasing PEI molecular weight. High *in vitro* [124] and *in vivo* [125] transfection efficiency has been documented for increasing molecular weight of PEI (*in vitro*: 70 kDa > 10 kDa >>> 1.8 kDa; *in vivo*: 25 kDa > 50 kDa > 800 kDa). However, high transfection efficiency and reduced toxicity has been reported for low-molecular-weight PEI (5 kDa) in several different cell lines [126].

A systematic study has been conducted to evaluate how chemical modifications can enhance PEI transfection efficiency [127]. The resultant structure/activity relationship has both provided mechanistic insights and led to PEI derivatives with markedly enhanced performance. For example, N-acylation of PEI with a molecular weight of 25 kDa (PEI25) with alanine nearly doubles its transfection efficiency in the presence of serum and also lowers its toxicity. Furthermore, dodecylation of primary amino groups of 2 kDa PEI yields a nontoxic polycation whose transfection efficiency in the presence of serum is 400 times higher than the parent's and which exceeds 5-fold even that of PEI25 [127].

The structure and molecular weight of PEI are also major determinants for the biological activity and biocompatibility. In general, PEI polymers with higher molecular weight show higher transfection efficiency as well as higher cytotoxicity [124, 128, 129]. Cross-linked PEI is typically less efficient than linear PEI, but substantially less cytotoxic. These PEI derivatives are designed to degrade in the cytoplasm in low molecular weight blocks and, as a consequence, exhibit reduced cytotoxicity. The degradation mechanisms and kinetics inside the cell of PEI is highly pH dependent and the degradation rate increases with increasing pH value [130]. Other studies discuss the role of the type of amines for toxicity

and conclude that the presence of primary amines has a significant toxic effect on cells, comparing with tertiary amine groups that exhibit a lower toxicity. Therefore, not only the type of amino function but also the charge density resulting from the number and three-dimensional arrangement of the cationic residues of PEI is an important factor for cytotoxicity. Despite this knowledge, the mechanism of cytotoxicity of PEI is still poorly understood. One hypothesis is that PEI aggregates on the cell surface and impairs important membrane functions [131]. Another possibility is that PEI interferes with critical intracellular processes, and that intra- rather than extracellular effects of PEI on the health of target cells are a factor to address. For these reasons, modifications of PEI have been introduced that aim at the alteration of the physicochemical properties of PEI. Among these modifications is the development of PEI-based copolymers, such as coacervates formed by electrostatic interaction between PEI and the polyanion dextran sulfate (DS) that became a viable strategy to reduce positive surface charge of these nanocarriers as well as complex aggregation, nonspecific interactions and opsonization, leading to an overall reduction of the toxic side effects [132]. These nanocarriers have gained attention as drug delivery systems due to their relatively high drug loading capacity, easy of fabrication, limited immunogenicity, and versatility for chemical modifications [133]. DS is among the best-studied substances in pharmaceutical technology and biopharmacy. Due to its high biocompatibility, the FDA has approved DS as vehicle or additive in food, cosmetics, and drugs [134, 135].

These polyelectrolyte-based NPs, composed by polyethylenimine and DS have been used successfully in the delivery of small hydrophobic therapeutics to modulate the activity/differentiation of stem cells [133, 136]. In this thesis, we have explored PEI:DS NPs for the delivery of RA in leukemia cells.

2.4 – Drug delivery systems for leukemic cells

In recent years, scientists and engineers have been exploring different drug delivery approaches to treat cancer, including leukemia [137, 138]. Nanotechnology has emerged as a powerful platform to enhance pharmacokinetics, biodistribution and membrane transport properties, as well as higher therapeutic efficacy and target selectivity [91, 100, 139] (**Table 6**). Several NP formulations have been proposed in the last years including liposomes [72, 104-106, 140-144], polymeric [145-148] and inorganic NPs [149-157]. The majority of drug

delivery systems using NPs have prolonged release of drugs, but through a passive manner. In this case, the pattern of drug release is beyond the control of the patient or physician and severely hindered by issues related to poor drug selectively, including side effects, and the emergence of drug resistance [137, 144, 145, 158]. This resistance may be mediated by multiple multi-drug resistance (MDR) proteins, with 48 ATP-binding cassette (ABC) transporters having been identified as facilitating the efflux of various substrates, including anticancer drugs, from cells [138, 159]. For these, P-glycoprotein (Pgp) has been identified as the most relevant ABC transporter associated with drug resistance [160].

Table 6 – Examples of nanocarriers for leukemia therapy.

Nanocarrier System	Agents	Indication | Status	Ref
Non-PEGylated Liposome	DR (DaunoXome)	AML | FDA approved	[104]
Non-PEGylated Liposome	Vincristine sulphate (Marquibo)	Pediatric ALL | Phase I	[105]
Non-PEGylated Liposome	Cytarabine/DR (CPX-351)	AML | Phase III	[106]
Non-PEGylated Liposome	6-MP/DR	ALL | *in vitro*	[142]
Non-PEGylated Liposome	DOX/Verapamil	CML | *in vitro*	[144]
Non-PEGylated Liposome	RA	APL/AML | clinical trials	[140, 141]
PEGylated Liposome	Topotecan/Amlodipine	CML/APL | *in vitro*	[143]
PEGylated Liposome	Vincristine/Quinacrine	CML | *in vitro*	[72]
Polymeric Micelles	Dexamethasone	ALL | *in vitro* and *in vivo*	[148]
Polymeric Micelles	DOX/P85 (Pluronic P85)	MLL | *in vitro* and *in vivo*	[145]
PEGylated Polymeric NPs	RA	APL | *in vitro*	[146]
PEGylated Polymeric NPs	Cytarabine	MLL | *in vitro* and *in vivo*	[147]
Dendrimer	MTX/RA	AML | *in vitro*	[161, 162]
Solid Lipid NPs	DOX/IDA	APL | *in vitro* and *in vivo*	[163]
Protein-drug Conjugates	Gemcitabine (SQdFdC NA)	ALL | *in vitro* and *in vivo*	[164, 165]
Carbon Nanotubes	DOX/Ap-SWNTs	CML | *in vitro*	[166]
PEGylated Inorganic NPs	PEG-AuNPs	CML | *in vitro*	[167]
PEGylated Inorganic NPs	ROS / glutathione depletion	AML | *in vitro*	[168]

6-MP, 6-mercaptopurine; ALL, acute lymphoblastic leukemia; AML, acute myeloid leukemia; APL, acute promyelocytic leukemia; AuNPs, gold nanoparticles; CML, chronic myeloid leukemia; DOX, doxorubicin; DR, daunorubicin; FDA, US Food and Drug Administration; IDA, idarubicin; MLL, murine lymphocytic leukemia; MTX, methotrexate; PEG, polyethylene glycol; RA, retinoic acid; ROS, reactive oxygen species; SWNT, single-walled nanotubes.

Table 6 – Examples of nanocarriers for leukemia therapy (cont.).

Nanocarrier System	Agents	Indication | Status	Ref
Inorganic NPs	AuNPs-AbVF	CLL | *in vitro*	[149]
Inorganic NPs	AuNPs/6-MP	CML | *in vitro*	[150]
Inorganic NPs	Zn-DR	CML | *in vitro*	[151]
Inorganic NPs	AuNR thermolysis	APL/CML | *in vitro*	[157]
Inorganic Magnetic NPs	Fe_3O_4-DR	CML | *in vitro* and *in vivo*	[153]
Inorganic Magnetic NPs	Fe_3O_4-GA	CML | *in vitro*	[152]
Inorganic Magnetic NPs	Paclitaxel	CML | *in vitro* and *in vivo*	[154]
Inorganic Magnetic NPs	DR/5-bromotetrandrin	CML | *in vitro*	[155, 156]
Nanocomposites	PLA/Au-DR	CML | *in vitro*	[169]
Nanocomposites	PVP-coated AgNPs ROS	AML | *in vitro*	[170]

6-MP, 6-mercaptopurine; AbVF, VEGF antibody; AgNPs, silver nanoparticles; AML, acute myeloid leukemia; APL, acute promyelocytic leukemia; AuNPs, gold nanoparticles; AuNR, gold nanorods; CLL, chronic lymphocytic leukemia; CML, chronic myeloid leukemia; DR, daunorubicin; GA, gambogic acid; PLA, poly(lactic acid); PVP, polyvinylpyrrolidone; ROS, reactive oxygen species.

Current strategies to overcome MDR arising from drug efflux are based on the inhibition of Pgp and other MDR proteins by agents such as verapamil, quinidine, amiodarone and cyclosporine A [72]. However, clinical trials using these drugs were not successful mainly because low concentration of the drugs cannot exert a completely reversing MDR effect [158], while high concentrations of these drugs cause toxicity [171, 172]. On the other hand, current combination chemotherapies are far from perfect. Varying pharmacokinetics, biodistribution and membrane transport properties among different drug molecules make dosing and scheduling optimization extremely difficult [139]. Higher therapeutic efficacy and target selectivity is requested, especially to avoid the existing therapy-associated side effects. These challenges are driven researchers and clinicians to investigate advanced approaches for drug delivery in leukemia cells.

2.5 – Remotely triggered particulate drug delivery systems

Particles (micro- and nanoparticles) offer many advantages in drug delivery over conventional formulation approaches [91, 173]. Particles are able to (i) protect the drug from the harsh internalization pathway environment; (ii) minimize drug degradation upon

administration on the target site; (iii) enhance drug efficiency by delivering higher concentrations; (iv) maintain drugs activity for a longer window of time; and (v) may prevent undesirable side effects [174]. Recently, the development of particle systems that respond to external stimuli such as ultrasound [175], light [176-178], radiowaves [179] or magnetism [180] offer an extra level of control for spatial and time drug release [181, 182]. The most important advantages of light relatively to the other triggers are: (i) possibility of activating multiple drug delivery systems that respond at specific wavelengths (light can penetrate human body from ~1 mm for 440 nm wavelength up to more than 4 mm for wavelengths above 650 nm) [183, 184]; (ii) possibility of activating specific areas of the human body being the resolution determined by the spot of the laser, making the activation process very selective and precise; and (iii) user friendly, since the operator can change many parameters such as the intensity and the wavelength of light and thus having an extraordinary control over the process [185, 186].

2.5.1 – Light as trigger

Near infrared (NIR) and ultraviolet (UV) light are typically used to trigger the release in drug delivery systems [174, 182, 187]. The selection of a wavelength to trigger the release in a drug delivery system should be based in the ability to penetrate tissue and the capacity to manipulate the drug delivery system. NIR has been used for *in vivo* clinical applications [188] for more than 30 years [189, 190]. NIR penetrates deep in the body [191, 192], and safe limits of NIR exposure have been established [193]. Unfortunately, NIR is a low-energy radiation. UV light, on the other hand, is a high-energy radiation, able to break chemical bonds, such as between a drug molecule and a carrier or NP. In contrast to NIR, UV light has a low penetration level in biological tissues [183]; however, UV light may be used within the human body though optical fibers and endoscopic apparatus [191, 194, 195].

Long-time exposure of cells and tissues to UV light may induce cell damage at the nuclear level [196-199]. For example, long exposure of cell lines to UV irradiation may induce overexpression of near-UV-absorbing proteins, production of active oxygen species and direct destruction of UV-absorbing macromolecules [199, 200], among other effects. The conjugation of these factors may lead to cell cycle arrest and apoptosis [198, 201]. However, UV light has been successfully used in the clinic to treat various diseases, including skin disorders (e.g., psoriasis, atopic dermatitis, among others) [202] by taking advantage of slow growth of affected skin cells promoted by UV light, dermatological

applications such as wrinkles, acne scars, hypertrophic scars [202] and healing of burns through UV light activation of electron transport, adenosine triphosphate nitric oxide release, blood flow and diverse signalling pathways activation [202]. Also ocular conditions [203] use the potential of UV light to cross-link tissues in the presence of non-toxic photosensitizing agents to strengthen the corneal stroma [203]. Therefore, short exposure of cells and tissues to 365 nm lights is a methodology of relatively low risk. We should also consider that most of radiation treatments routinely performed nowadays involve forms of radiation much more harmful to the human body (i.e., radiation therapy) than UV radiation [204].

2.5.2 – Light-triggered mechanisms

There are two main approaches for the development of light-triggered drug delivery systems: (i) photolabile molecules [205, 206]; or (ii) photoswitches for reversible switching [207, 208].

2.5.2.1 – Photolabile protective groups

Recent developments in light sources and technologies are promoting a photolabile (also called photoactivatable, light-triggered, photoremovable, or even photocleavable) protective groups (PPGs) renaissance in recent years by their capability to control spatial and temporal delivery of drugs. The design process of any photoremovable protecting group for biological application showed consider the following criteria: (i) the photoreaction should be clean and occur with high *quantum yield* ϕ; (ii) the chromophore should have high *absorption coefficients* ε at wavelengths above 300 nm, where irradiation is less likely to be absorbed by (and possibly cause damage to) the biological environment; however, low absorption coefficients may be required to achieve deep penetration when higher concentrations are used; (iii) the *photochemical by-products* accompanying the released bioactive reagent should be biocompatible and not interfere with the photoreaction and ideally be transparent at the irradiation wavelength in order to avoid competitive absorption of the photolysing light; (iv) for time-resolved work the *release rate of the bioagent* must exceed that of the response investigated; (v) the protected compounds should be soluble in the targeted biological (mostly aqueous) media, and it may be required that they pass biological barriers or show affinity to specific sites [206, 209]. No single system will excel in

all of these requirements. The variety of applications is such that it is desirable to have a range of photo-responsive groups with different characteristics to choose from. *O*-nitrobenzyl and coumarin-based photolabile protecting groups are the most commonly used.

2.5.2.1.1 – *O*-nitrobenzyl-based photolabile protecting groups

Among the many photolabile protective groups that have been studied, *o*-nitrobenzyl-based (*o*-NB) compounds and their dimethoxy derivatives (nitroveratryl) are by far the most commonly used photolabeled protecting groups (**Scheme 2.1**). Linkers and protecting groups based on *o*-NB chemistry can usually be cleaved in minutes when exposed to 300−365 nm light. This process is based on the photoisomerization of an *o*-nitrobenzyl alcohol derivative into a corresponding o-nitrosobenzaldehyde upon irradiation with UV light, simultaneously releasing a free carboxylic acid. Studies have demonstrated that including substituents on the aromatic ring or at the benzyl position of the linker can shift the photocleavage wavelength or prevent the formation of photodimerized by-products [210].

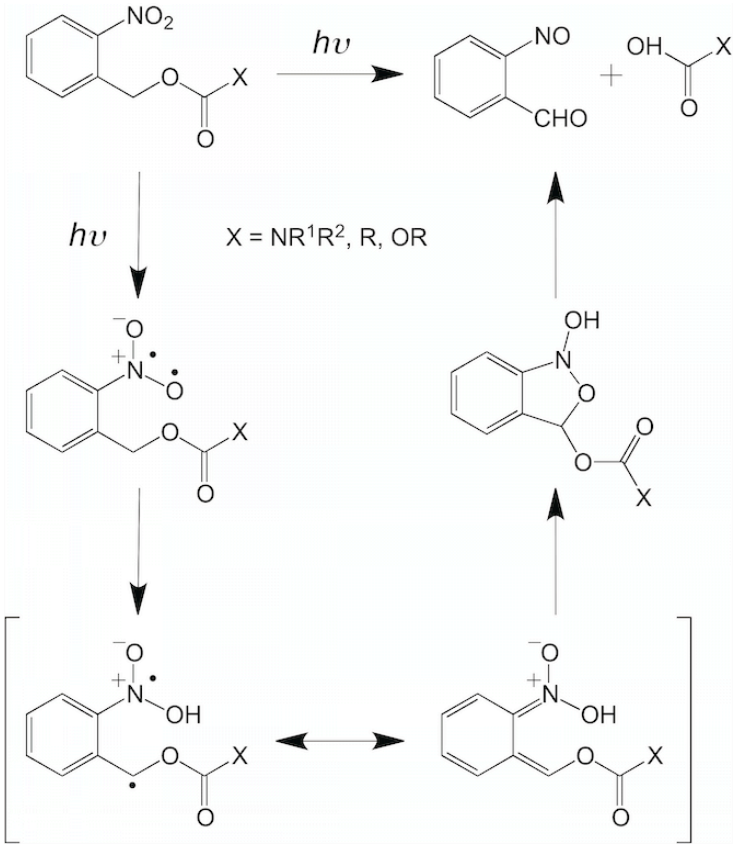

Scheme 2.1 – Photochemically-induced photoisomerization of *o*-nitrobenzyl alcohol derivatives into *o*-nitrobenzaldehyde.

2.5.2.1.2 – Coumarin-based photolabile protecting groups

Among the developed phototriggers, coumarin-based phototriggers arouse much interest and have been applied to cage multiple compounds [206]. Compared with the more popular *o*-nitrobenzyl phototriggers with absorbance normally located around UV light wavelengths and low uncaging cross-section in the NIR range, coumarin-based phototriggers have longer wavelength absorption, bigger responsivity in the NIR range of excitation, are able to provide fast release rates and present high stability and fluorescent properties that could be employed as a tag for convenient monitoring of the reaction process (**Scheme 2.2**). Coumarin groups suffer from self-quenching and have a low fluorescence emission when confined. After photolysis and release into aqueous medium, the fluorescence intensity of coumarin increases dramatically, creating a fluorescence contrast between irradiated and nonirradiated compound. The mechanism for the photorelease has been extensively investigated; coumarin derivatives are members of arylalkyl-type photoremovable protecting groups, and the photolysis upon cleavage of a C–O bond produces a leaving group and a solvent-trapped coumarin as a photo-by-product [206].

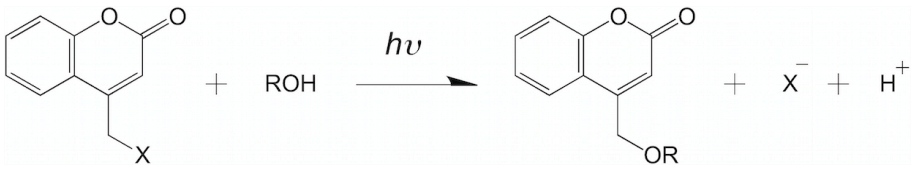

Scheme 2.2 – Photochemically-induced cleavage reaction of Coumarin-4-ylmethyl derivatives.

2.5.2.2 – Photoswitchable compounds

Controlling the conformation and activity of biomolecules in a reversible manner is a fascinating challenge that has an outstanding potential to modulate the spatial and temporal release of drug delivery carriers [211]. One of the most widely used methods for the introduction of light-sensitivity into particles is through functionalization with bistable photoswitchable compounds. A variety of synthetic photoswitches, that undergo a reversible change in their structure upon irradiation with light, have been designed (**Scheme 2.3**). The chromophores switch upon irradiation between the *cis* and *trans* isomers (azobenzenes) or interconvert between closed and open forms (spiropyrans). This results in a change in geometry, which can be especially large in the cases of azobenzenes. Besides this change,

photoisomerization may also alter the polarity and charge distribution of the compound [206].

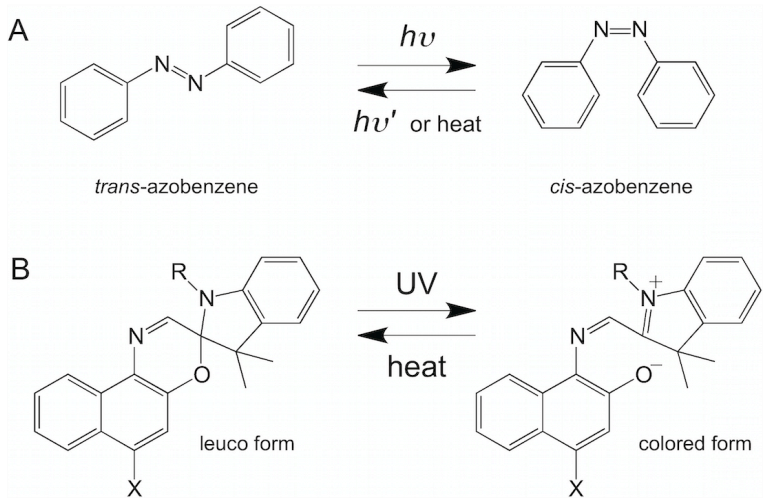

Scheme 2.3 – Examples of photo-isomerizable groups for reversible light-induced drug release: (A) azobenzene and (B) spiropyran.

A photoswitchable compound must fulfil a set of requirements for biomedical applications: (i) the change in concentration of the more active isomer upon irradiation must be sufficient to provide a large difference in response; (ii) the isomerization should preferably be achieved using deep-penetrating light of low cellular toxicity; (iii) the thermal re-isomerization to the thermodynamically stable form should proceed on the time scale relevant for the intended application; (iv) the photoswitchable compound should be metabolically stable enough to reach its intended target, and non-toxic [185, 206, 207].

2.5.2.2.1 – Azobenzene-based compounds

Among the different molecules able to modify their hydrophobic or hydrophilic character upon irradiation, azobenzenes and their derivatives constitute the most studied reversible photo-responsive molecules. They undergo a photochemically induced *cis/trans* isomerization of the N=N bond. This results in a change from the more stable and planar *trans*-azobenzene to *cis*-azobenzene, in which the two parts of the molecule are tilted by about 55º [207]. The isomerization from *trans* to *cis* is typically accomplished at 350 nm, while *cis* to *trans* conversion can be achieved at 450 nm or thermally. As there is a distinct overlap in the UV/Vis spectra of both isomers, complete *trans* to *cis* conversion is not possible photochemically, and irradiation generally produces photostationary states

composed of 80% *cis* at best. Conversely, photoisomerization of *cis* to *trans* can only produce up to 95% of the *trans* isomer [185].

2.5.2.2.2 – Spiropyran-based compounds

Spiropyran-type switches, as well as azobenzenes, are mostly used in biological applications. Although the photochemical behaviour of spiropyran-type switches is more difficult to predict and more environment-dependent than azobenzenes, the changes in their geometry and polarity through photoswitching are more pronounced. The photochromic behaviour of spiropyrans stems from the fact that the C_{spiro}-O bond undergoes heterolytic cleavage upon UV irradiation (360 – 370 nm), leading through ring opening of the bulky colourless spiro state to the planar and colourful merocyanine state [208, 212]. This isomerization is accompanied by a very large change in polarity and is reversible both thermally and photochemically, by irradiation with visible light (>460 nm). The well separated absorption bands of spiro and merocyanine state enables clean switching between the two isomers to be performed and the importance of spiropyrans as regulatory elements stems mainly from the large change in polarity upon photoisomerization, which is reflected by changes in hydrophilicity/hydrophobicity [185].

2.5.3 – Light-triggered drug delivery systems

Light-responsive particles can release their cargo by several distinct mechanisms: changes in hydrophobicity [178, 213, 214], photo-degradation effects [176, 215, 216], photothermal effects [217-219], and photoisomerization [177, 212, 220]. **Table 7** present several light-responsive particles having multiple mechanisms for drug delivery. For biological applications, photolabile and photoswitchable compounds should respond to wavelengths that have low scattering and do not induce photodamage. Since most photolabile compounds are responsive only to UV light due to its high energy, a requirement for most relevant chemical changes, and NIR generally lacks the energy required to initiate a chemical change, new photolabile compounds have been developed that absorb two photons of low energy NIR light to undergo the same photoinduced change as with the absorption of one higher energy UV photon [174, 206, 209].

Table 7 – Examples of light-triggered particle formulations.

Principle	NPs	Photo-responsive compound	Light source	Drug	Cells	Concentration or Molarity	Time Exposure	Ref.
Hydrophobicity change	POEGMA-*b*-P(NIPAM-*co*-NBA-*co*-*Gd*) diblock copolymer covalently labeled with Gd^{3+} complex (50 nm)	*o*-nitrobenzyl acrylate (NBA)	UV (λ = 365 nm)	DOX	HepG2	3 mg/mL	30 min	[221]
Hydrophobicity change	Amphiphilic AuNPs carrying hydrophilic PEG and photo-responsive hydrophobic PNBA assembled into plasmonic vesicles Au@PEG/PMMA (210 nm)	Poly(2-nitrobenzyl acrylate) (PNBA)	UV (λ = 365 nm) (2.3 mW/cm^2)	DOX	MDA-MB-435	0.5 nM	15 min	[222]
Hydrophobicity change	Dextran-graft-(2-diazo-1,2-naphthoquinone) amphiphilic copolymers micelles (230 nm)	2-diazo-1,2-naphthoquinone (DNQ)	UV (λ = 365 nm) (125 W) NIR (λ = 808 nm) (500 mW)	DOX	HeLa	500 μg/mL	30 min	[223]
Hydrophobicity change	Dextran-graft-(2-diazo-1,2-naphthoquinone) amphiphilic copolymers micelles (180 nm)	2-diazo-1,2-naphthoquinone (DNQ)	UV (λ = 365 nm) NIR (λ = 808 nm) (300 mW)	Nile Red Coumarin 102 DOX	HepG2	250 μg/mL	5 min	[224]
Hydrophobicity change	Spiropyran initiated hyperbranched polyglycerols micelles (40 nm)	Spiropyran (SP)	UV (λ = 254 nm / 365 nm)	Pyrene	WI-38 HeLa	1000 μg/mL	30 min	[225]
Photocleavage	Polymers with a 2-nitrophenylethylene glycol moiety and diamines nanocarriers (217−358 nm)	2-nitrophenylethylene glycol moiety	UV (λ = 365 nm)	Nile Red Tagalsin G	RAW 264.7	150 μg/mL	15 min	[216]
Photocleavage	Mesoporous silica NPs-coumarin based system (130 nm)	7-amino-coumarin	Two-Photon (λ = 800 nm) (10 mW/cm^2) Visible Light (λ = 400 nm) (120 mW/cm^2)	Chlorambucil	MCF-7 HeLa	20 - 160 μg/mL	180 min 15 min	[226]

DOX, doxorubicin; Hydrophobicity change, photo-disassembly of drug delivery systems by changes in the hydrophobicity/hydrophilicity balance; Photocleavage, photo-disassembly of drug delivery systems by photo-degradation of nanoparticle components.

Table 7 – Examples of light-triggered particle formulations (cont.).

Principle	NPs	Photo-Responsive Element	Light Source	Drug	Cells	Concentration	Time Exposure	Ref.
Photocleavage	Octadecyltrimethoxysilane (C18) - modified hollow mesoporous silica nanoparticles (HMS@C18) - Copolymer-coumarin based system (130 nm)	[7-(diethylamino) coumarin-4-yl] methyl (DEACM)	Two-photon (λ = 800 nm) (2.3 - 2.7 W)	DOX	KB A549	1000 μg/mL	60 min	[227]
Photocleavage	Acetal-modified dextran (Ac-Dex) with caged photoacids generator (PAG) (520 - 620 nm)	2-(4-methoxystyryl)-4,6-bis(trichloromethyl) -1,3,5-triazine (PAG)	UV (λ = 365 nm)	Irinotecan	HT-29	200 μg/mL	20 min	[228]
Photocleavage	Upconverting NPs coated with mesoporous silica functionalized with crosslinked photosensitive theo-nitrobenzyl (NB) (UCNP@mSiO2-NB) (170 nm)	Lanthanide-doped UCNPs / 1-(2-nitrophenyl) ethyl caged oligo (ethylene) glycol (NB)	NIR (λ = 980 nm)	DOX	A-498 HeLa NIH/3T3	5 μM	120 min	[229]
Photothermal	Aptamer/hairpin DNA-gold NPs (13 - 23 nm)	Resonant wavelength of AuNPs	Green Light (532 nm) (2 W/cm^2)	DOX	CCRF-CEM Ramos	12.6 nM	20 min	[217]
Photothermal	Upconverting NPs coated with mesoporous silica functionalized with specific platinum prodrug and an apoptosis sensing peptide (UCNPs@mSiO2) (50 nm)	Lanthanide-doped UCNPs	NIR (λ = 980 nm) (1.5 W/cm^2)	Platinum(IV)	A2780 A2780cis	10 μM	60 min	[230]

DOX, doxorubicin; Photocleavage, photo-disassembly of drug delivery systems by photo-degradation of nanoparticle components; Photothermal, photo-disassemble of drug delivery systems based on photothermal effects.

Table 7 – Examples of light-triggered particle formulations (cont.).

Principle	NPs	Photo-Responsive Element	Light Source	Drug	Cells	Concentration	Time Exposure	Ref.
Photothermal	Polyester particles (0.5 - 1.0 μm)	Confined H_2O	NIR (λ = 980 nm) (0.5 - 1 W)	Fluorescein / Nile Blue & Red / IR780 Fluorescein diacetate	MV-4-11	100 μg/mL	30 min	[231]
Photoisomerization	Upconverting NPs coated with mesoporous silica functionalized with azobenzene groups (UCNP@mSiO2-azo) (54 nm)	Lanthanide-doped UCNPs associated with azobenzene	NIR (λ = 980 nm) (2.4 - 8.9 W/cm^2)	DOX	HeLa	1000 μg/mL	20 min	[220]
Photoisomerization	Mesoporous silica NPs-azobenzene based system (100 nm)	Azobenzene-modified nucleic acids	UV (λ = 365 nm)	Rhodamine 6G DOX	CEM A549	150 μg/mL	30 min	[232]
Photoisomerization	Mesoporous silica NPs-azobenzene based system (100 nm)	Silylated Fluorophore and FRET to photoisomerize azobenzene	Two-Photon (λ = 760 nm) (3 W)	Camptothecin	MCF-7	20 - 80 μg/mL	5 s	[233]
Photoisomerization	Hybrid NPs [spiropyran (SP) and lipid-polyethylene glycol (PEG)] (40 - 150 nm)	Hydrophobic spiropyran	UV (λ = 365 nm)	Docetaxel (Dtxl)	HT-1080	1 mg/mL	20 s	[234]
Photoisomerization	Spyropyran functionalized UCNPs (190 nm)	Lanthanide-doped UCNPs / Spiropyran	NIR (λ = 980 nm) (0.5 W/cm^2)	FITC-labeled β-gal	HeLa	1000 μg/mL	20 min	[235]
Photo-targeting	Carboxylated polystyrene NPs functionalized with amino acid YIGSR caged with DMNB (330 nm)	4,5-dimethoxy-2-nitrobenzyl (DMNB)	UV (λ = 365 nm)	Blank	HUVECs MSCs	200 μg/mL 20 μg/mL	1 min	[236]

DOX, doxorubicin; Photothermal, photo-disassemble of drug delivery systems based on photothermal effects; Photoisomerization, induction of drug release by light-activated conformational change; Photo-targeting, target drug delivery systems binding to cells selectively through light-activation.

2.5.3.1 – Photo-disassembly of drug delivery systems by changes in the hydrophobicity/hydrophilicity balance

The formation and stability of micelles and other vesicles rely on the hydrophilicity/ hydrophobicity balance. When this balance is disrupted, the micellar system disintegrates, releasing the cargo. The disruption of this balance can be triggered by light, in case the micelles or vesicles incorporate light-sensitive chromophores. The general strategy is to incorporate a chromophore into the structure of the hydrophobic block, whose photoreaction can result in a conformational or structural change that shifts the hydrophilicity/hydrophobicity balance toward the destabilization of the nanocarrier [178].

Several strategies have been reported to induce the disruption of aqueous polymer micelles by light [213, 214, 237]. Briefly, they synthesized diblock copolymers containing one hydrophilic poly(ethylene oxide) (PEO) sequence linked to a hydrophobic poly(methacrylate) (PMA) block containing a photolabile chromophore as a pendent group. Different types of photocleavable blocks have been tested, including pyrenylmethyl esters [213], *o*-nitrobenzyl esters [214] and esters of (diaethylamino)methylcoumarinyl [237]. Those block copolymers (BCP) form micelles in water with a PEO corona and a PMA core that can be further loaded with hydrophilic molecules. Micelle integrity is lost after UV light exposure due to the photo-cleavage of the chromophore (**Scheme 2.4**) [213, 214, 237].

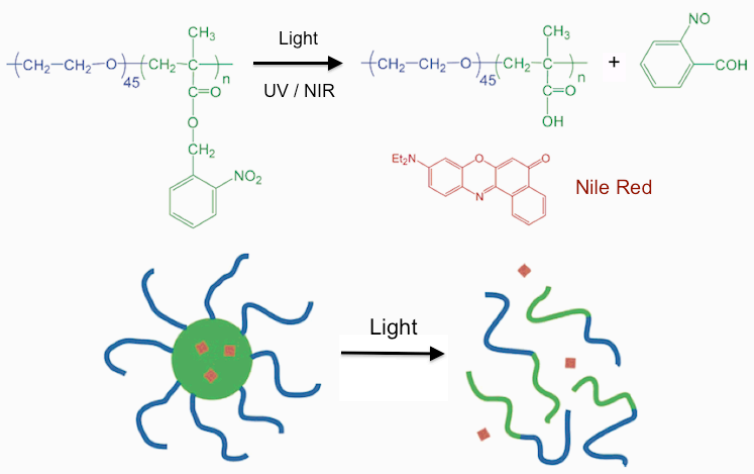

Scheme 2.4 – Photolysis of the 2-nitrobenzyl-containing amphiphilic block copolymer and chemical structure of Nile Red. Schematic illustration of the photocontrolled release of encapsulated Nile Red as a result of the photoinduced dissociation of the polymer micelle (adapted from [214]).

Other studies have explored the use of a photocleavable linker between the hydrophilic and hydrophobic blocks, rendering light-response to the formulation [238, 239].

After micelle formation, light can be applied to break BCP chains, but this strategy showed problems to successfully light-triggered release of drugs loaded in the micelle core, since the chain aggregation state of the micelle would not be loosened due to the removal of the hydrophilic corona. This problem was solved by positioning photocleavable moieties repeatedly along the hydrophobic main chain [240].

It is important to mention that the shift in hydrophilicity of the core-forming block is not always sufficient to induce a complete disruption of the initial micelles. Indeed, swelling or modifications in the characteristic size of micellar compartments as well as morphological transitions may result from the photocleavage process [186]. Finally, the magnitude of the photo-induced change may be affected by other parameters, such as the initial composition (block length ratio) and chain length of the starting photo-responsive block copolymer and kinetic of chain reorganization upon photocleavage, which is in some cases slow, especially in cases where the components of the micellar cores present a high glass transition.

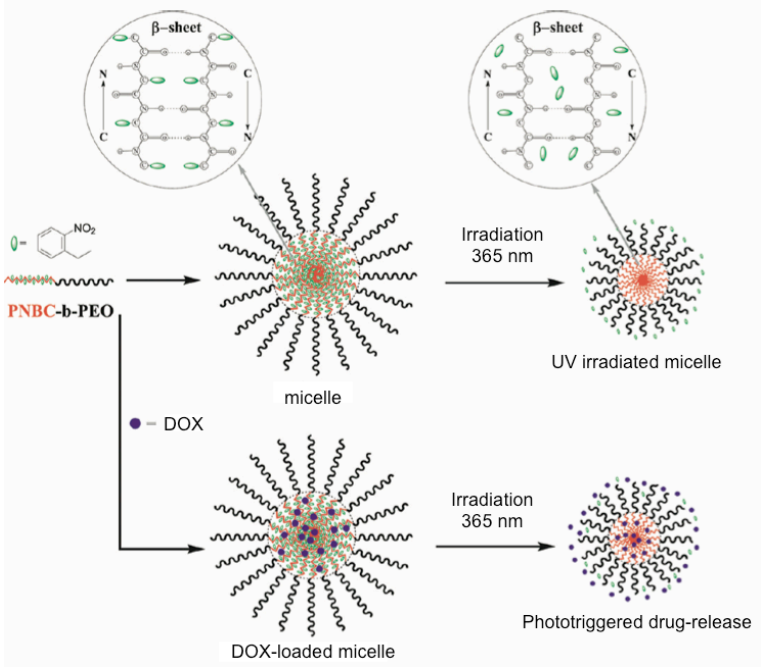

Scheme 2.5 – Schematic illustration of photoresponsive self-assembly and phototriggered drug-release of amphiphilic PNBC-*b*-PEO block copolymers in aqueous solution. The *o*-nitrobenzyl groups are gradually photocleaved from copolymers inducing the self-assemble NPs to become smaller, inducing drug release (adapted from [241]).

The photo-cleavage of moieties in NP formulations can induce drug delivery without disruption of the NP system. A typical example in which photocleavage does not lead to the disruption of micelles has been described for photo-responsive block copolymers containing

a poly(amino acid) block bearing photocleavable *o*-nitrobenzyl esters (**Scheme 2.5**). By synthesizing a poly(*S*-(-*o*-nitrobenzyl)-*L*-cysteine)-*block*-PEO diblock copolymer that forms micellar structures in water. After photo-cleavage of the *o*-nitrobenzyl moieties, shrinkage of the micellar core was monitored, with gradual release of doxorubicin (DOX) being monitored as a function of the irradiation time [241].

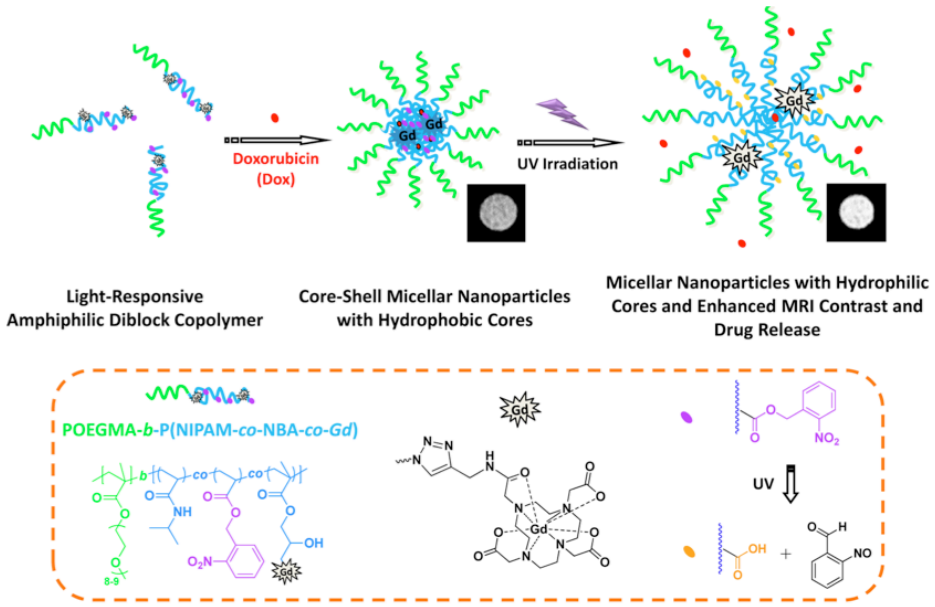

Scheme 2.6 – Schematic illustration for the preparation of light-responsive polymeric micelles of POEGMA-*b*-P(NIPAM-*co*-NBA-*co*-Gd) amphiphilic diblock copolymer showing light-triggered hydrophobicity to hydrophilicity transition within micellar cores and the concomitant enhancement of magnetic resonance imaging (MRI) contrast performance and release rate of physically encapsulated hydrophobic drug (DOX) (adapted from [221]). OEGMA, NIPAM, and NBA are oligo(ethylene glycol) monomethyl ether methacrylate, *N*-isopropylacrylamide, and *o*-nitrobenzyl acrylate, respectively.

A second example of a light-responsive that does not disrupt after light activation has been described for amphiphilic diblock copolymer micelles exhibiting light-triggered hydrophobicity/hydrophilicity transition within micellar cores (**Scheme 2.6**). POEGMA-*b*-P(NIPAM-*co*-NBA-*co*-*Gd*) diblock copolymer covalently labeled with Gd^{3+} complex (*Gd*) spontaneously self-assembles in aqueous solution into micellar NPs possessing hydrophobic P(NIPAM-*co*-NBA-*co*-*Gd*) cores and hydrophilic POEGMA coronas, which can physically encapsulate DOX as a model chemotherapeutic drug. Upon UV irradiation, hydrophobic NBA moieties within micellar cores are photo-cleaved, triggering micelle microstructural changes and core swelling. During this process, the microenvironment surrounding Gd^{3+} complexes changed from hydrophobic to hydrophilic, leading to the enhancement of MR imaging contrast performance and drug release [221]. Another example of a light-responsive

NP that does not disrupt after light activation has been described for amphiphilic gold NPs carrying hydrophilic poly(ethylene glycol) (PEG) and photo-responsive hydrophobic poly(2-nitrobenzyl acrylate) (PNBA) [222]. These NPs are optically traceable and form vesicles in aqueous solution, which can encapsulate drugs. Once the vesicles are irradiated by UV light, the PNAB is photo-cleaved, a change in the hydrophilicity/hydrophibicity balance occurs which favours the disassembly of the vesicles and the release of their payload.

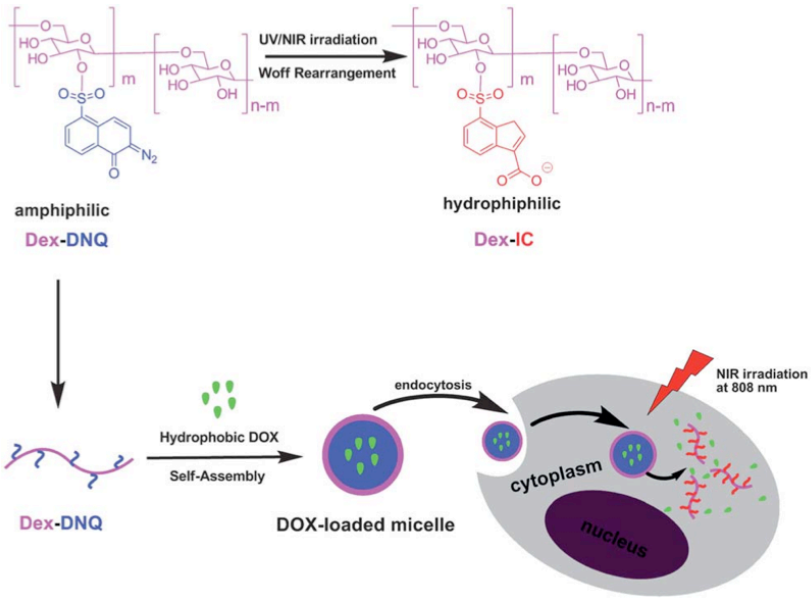

Scheme 2.7 – Schematic illustration of self-assembly and Wolff rearrangement of Dex-DNQ amphiphilic copolymer. The Wolff rearrangement of the DNQ molecules under NIR irradiation will dissociate the micelle structure and enhanced the intracellular release of DOX (adapted from [224]).

Systems that respond to near-infrared (NIR) wavelengths (750-1300 nm) are particularly attractive for biological applications due to the penetration and low attenuation of NIR radiation. The hydrophobic 2-diazo-1,2-naphthoquinone (DNQ) molecule is an attractive photo-trigger group because can undergo Wolff rearrangement via a two-photon process under NIR radiation yielding a hydrophilic 3-indenecarboxylic acid (3-IC) molecule with a pK_a of 4.5 (**Scheme 2.7**) [223, 224]. DOX-loaded dextran-graft-(2-diazo-1,2-naphthoquinone) (Dex-DNQ) amphiphilic copolymers have been synthesized. These amphiphiles can self-assemble into micelles on aqueous solution and dissociate after exposure to NIR radiation due to the Wolff rearrangement reaction of DNQ molecules. The dissociation of micelles leads to the release of DOX [224].

Specific inorganic NPs respond efficiently to NIR. For example, lanthanide-doped up-converting NPs (UCNPs) respond to NIR [242]. These NPs absorb NIR light (980 nm, 5 W) and emit photons in the UV and visible regions that, in turn, are absorbed by the

photoresponsive moieties of a micelle core-forming hydrophobic block. Photocleavage of the nitrobenzyl groups converts the polymethacrylate block into hydrophilic poly(methacrylic acid), which shifts the hydrophilic-hydrophobic balance toward the destabilization of micelles [243].

Mesoporous silica NPs (MSN) sensitive to NIR radiation have been also synthesized [227]. The pores of the NPs were filled with DOX and coated with a coumarin photo-responsive amphiphilic polymer. DOX was released after NP exposure at 800 nm via a two-photon absorption. Under these conditions, there was a shift in the hydrophilic–hydrophobic balance of the polymer filing the pores of the NPs, with the consequent release of the drug [227].

2.5.3.2 – Photo-disassembly of drug delivery systems by photo-degradation of NP components

Two main approaches have been followed in the photo-disassembly of drug delivery systems by the photo-degradation of NP components: (i) degradation of hydrophobic polymers containing photocleavable moieties forming the NP and (ii) degradation of hydrophobic polymers containing photocleavable moieties that fill the porous structure of inorganic NPs. In the first case, although similar to the hydrophobicity switch mechanism described in section **2.5.3.1**, the photoresponsive drug delivery systems offer the advantage of carrier disassembly into small pieces which might increase the kinetics of drug release and facilitate polymer biological elimination [174]. In the second case, porous inorganic micro/NPs are functionalized with polymers containing photolabile moieties that work as "gatekeepers" maintaining the encapsulated drug. The irradiation of these photoresponsive moieties induces their chemical degradation, the deprotection of the porous structure and drug release.

Rather than having photocleavable moieties as side-chain units of the hydrophobic core-forming blocks, they can be blocks in the main chain of the polymers. This strategy has been explored for systems in which the removal of the *o*-nitrobenzyl or coumarin protecting groups results in the degradation of polymeric particles and in the subsequent burst release of encapsulated molecules [176, 215]. A light-sensitive self-immolative polymer containing a quinone-methide backbone and photocleavable nitrobenzyl alcohol groups has been reported [176]. This polymer has the capacity to form NPs in aqueous solution which after UV light irradiation released their payload [176]. The same formulation design principle was

employed using 4-bromo-7-hydroxycoumarin protecting groups, with the objective of confer two-photon responsiveness to the formulation. Under UV and NIR irradiation of the photo-responsive protecting groups, a cascade of cyclization and rearrangement reactions is triggered, leading to backbone degradation [215]. Similar strategy has been also reported for the preparation of light-activatable NPs formed by 2-nitrophenylethylene glycol and diamines with different length and hydrophobicity. The photoactivation leads to a burst release of the encapsulated drugs [216].

Light-responsive particles have been also synthesized based on acetal-modified dextran (Ac-Dex) [244]. The high density of acetal groups makes Ac-Dex insoluble in water, while the unsubstituted biopolymer is readily soluble in water. Acid-catalyzed hydrolysis of Ac-Dex can be used to regenerate dextran, leading to dissolution of the particles in water. Therefore, polymer microparticles comprising blends of Ac-Dex and caged photoacids generator (PAG) have been prepared. The photolabile acids generated free acid upon illumination with UV light which induced the deprotection of the acetal groups of dextran and particle disassembly [228].

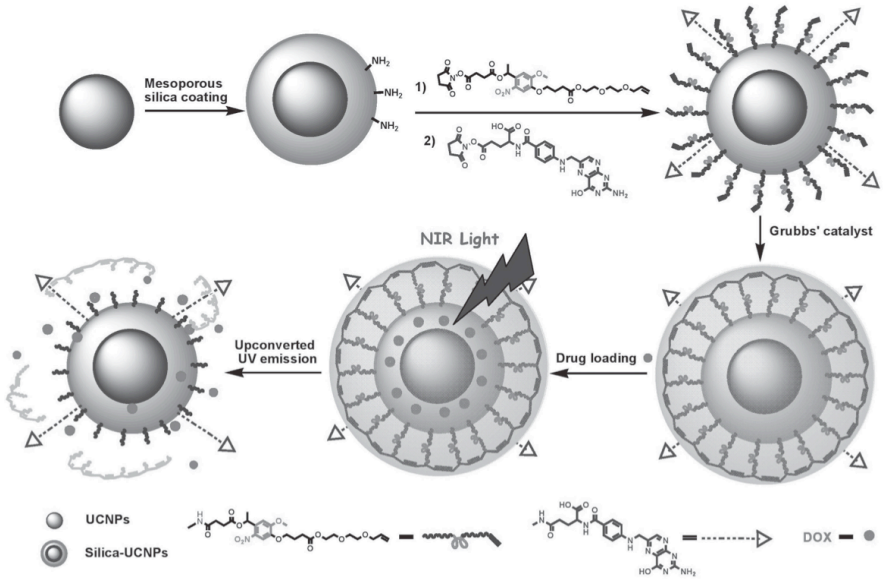

Scheme 2.8 – Schematic illustration of photo-controlled DOX delivery through photocaged mesoporous silica coated UCNPs (adapted from [229]).

MSNs have been also explored as light-activatable drug delivery systems using degradation of photocleavable moieties that fill the porous. In this case, the porous structure of the particles have been filed with polymeric "gatekeepers" containing nitrobenzyl [229] and coumarin derivatives [226, 227, 245]. For example, a light-responsive drug delivery nanocarrier for the on-demand delivery of antitumor drug DOX has been prepared (**Scheme**

2.8). Up-converting NPs (UCNPs) were first coated with a silica shell and then conjugated with a photo-activatable linker containing a terminal vinyl group. The linker was then crosslinked to form a polymeric shell in order to encapsulate antitumor drug molecules, DOX. NIR light irradiation of UCNPs triggered the cleavage of crosslinked photocaged linker and release of the drug [229]. A similar approach has been reported by others using an aminopropyl-functionalized MSN functionalized with a coumarin derivative for the delivery of the anticancer drug chlorambucil [226]. The exposure of the nanocarrier to a two-photon 800 nm NIR light and/or visible light (420 nm) promoted the photolysis of the coumarin derivative and the successful release of the drug, without detectable side products [226]. A similar strategy has been reported for MSNs [245]. In this case, photolabile coumarin-based molecules were attached to the surface of MSNs filled with a drug. These NPs were then coated with β-cyclodextrin molecules, blocking the pores and preventing the cargo from escaping. One-photon excitation at 376 nm or two-photon excitation at 800 nm cleaved the bond holding the coumarin to the nanopore, releasing both the bulky β-cyclodextrin cap and the cargo [245].

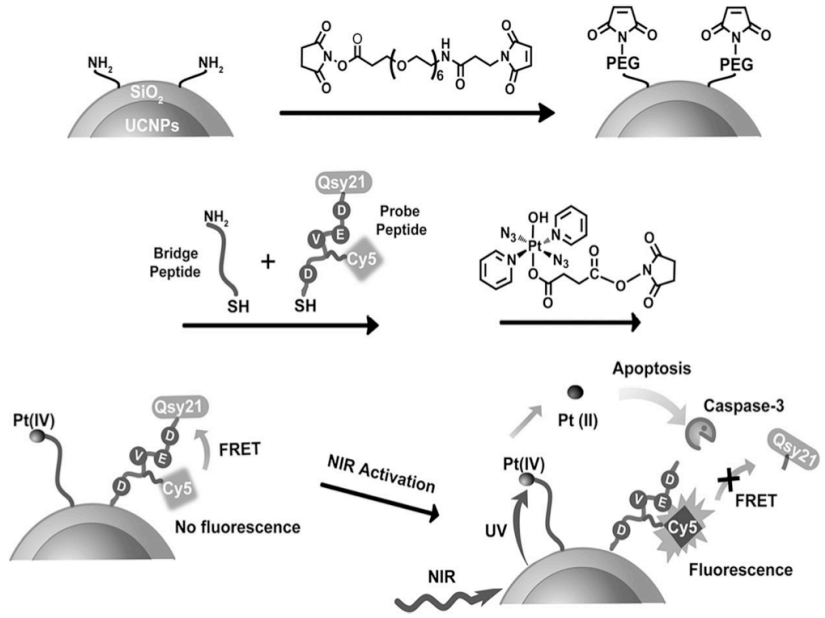

Scheme 2.9 – Schematic illustration of NIR light activation of platinum(IV) prodrug and intracellular apoptosis imaging through UCNPs (adapted from [230]).

Photo-degradation of NP components has been also used for biosensing (**Scheme 2.9**). In this case, the NPs absorbed NIR light (980 nm), converted the radiation in UV and visible light which was then absorbed by platinum present in the surface of the silica layer [230]. The platinum induced cell apoptosis mediated by caspase 3 which finally cleaved an

apoptosis sensing peptide on top of the NP. This formulation is an excellent example of a NP able to monitor in real time cell apoptosis [230].

2.5.3.3 – Light-activatable drug delivery systems based on photothermal effects

Very few organic chromophores absorb in the NIR, and even fewer are able to convert the absorbed energy into a chemical or thermal response that can be used to trigger drug release. For example, gold nanorods absorb light in the NIR region and convert it on heat for thermotherapy and/or to mediate drug release [218, 219]. This thermal effect can be used to induce changes in thermosensitive polymers coating gold carriers with the purpose of triggering drug release. Examples are poly(lactic-co-glycolic acid) (PLGA) NPs (glass transition temperature of 45 °C) entirely or half coated with a gold layer [246, 247], gold-shell-coated lipidic nanomicelles [248], polymer-coated gold nanocages [249] or gold nanorods combined with thermosensitive liposomes [250] have been designed, and some have shown significant anti-tumour activity in experimental models of breast cancer [247] and glioma [250].

The photothermal effect observed in inorganic NPs may be also used for the dehybrization of oligonucleotides and consequent release of drugs attached to the oligonucleotides. Au NPs functionalized with aptamer/hairpinDNA (apt/hp-Au NPs) have been used for the successful loading of the anticancer drug DOX. The release of the drug was induced by exposing the NPs to a continuous-wave (CW) laser [217]. Also a NIR light responsive drug delivery platform based on gold nanorods (AuNRs) was reported being incorporated within a mesoporous silica framework that was surface-functionalized with aptamer DNA [251]. Upon application to NIR light, the photothermal effect of the AuNRs led to a rapid rise in the local temperature, resulting in the dehybrization of the linkage DNA duplex that anchored the G-quadruplex DNA cap to the surface of the mesoporous silica-based materials, allowing the release of the entrapped guest. Importantly, the formulation employed DNA aptamer both as the capping and as targeting agent. With aptamer being in principle available for any kind of target, this proof of concept could open new research avenues for development of efficient drug delivery system [251].

The metal nanostructures are not ideal for regenerative medicine because the inorganic elements might affect cell viability [252]. However, recently, it was demonstrated that metal-free-non-light-sensitive polymeric NPs might be sensitive to NIR light [231]. In this case, the exposure of a suspension of PLGA NPs to a NIR laser at 980 nm induced the

release of the NP payload. This was due to the interaction of the NIR radiation with the water nanodomains within the polymeric NPs when they were suspended in an aqueous solution. Upon exposure to 980 nm NIR light, water molecules absorbed optical energy through vibrational transition and the excitation energy was converted into heat (**Scheme 2.10**) [231].

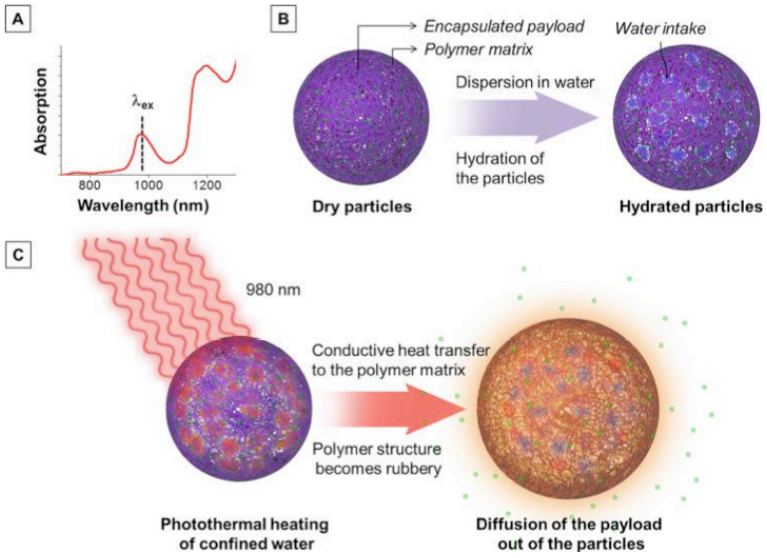

Scheme 2.10 – Schematic illustration of NIR-induced release mechanism: (A) absorption spectrum of water in the NIR region, (B) formation of isolated nanodomains of water in the polymeric structure, (C) release of encapsulated molecules following photothermal heating of water droplets inside the polymer particles (adapted from [231]).

2.5.3.4 – Photoisomerization

Photoisomerization is a process that involves a conformational change of a restrictive bond, usually a double bond. Two main molecules have been used on light-activatable NPs based on this process, specifically azobenzene [232, 253] and spiropyran [212, 225, 254]. These groups are characterized by a reversible photoisomerization reaction upon irradiation to UV or visible light. The first study reporting the use of azobenzene in nanocarriers was published in 1980 [255]. The study demonstrated the possibility of controlling the delivery properties of liposomes containing azobenzene mixed at various molar ratios with dipalmitoylphosphatidylcholine (DPPC) after UV irradiation [255]. Since this first study, the photoisomerization concept has been used very often in the preparation of photo-responsive micelles. These systems take advantage of the change in net dipole moment upon switching from the *trans* orientation (no net dipole moment) to the *cis* orientation. This leads to disruption in the hydrophobic–hydrophilic balance of the self-assembled micelles and causes

reorganization and subsequent release of encapsulated contents [256]. An example of such application was the preparation of giant asymmetric amphiphilic BCP vesicles in which the membrane is composed of two leaflets of polybutadiene (inner leaflet) and a side-on liquid crystalline polymer (LCP) with azobenzene mesogens (outer leaflet). Upon exposure to UV light, a LC-isotropic phase transition occurs in the outer leaflet resulting in a contraction of the outer monolayer along the membrane thickness direction, and the excess surface induces a curling instability that leads to the bursting of the vesicle membrane [257]. Other examples of photoisomerization have been reported for micelles formed by azobenzene-containing block copolymers [258], NPs containing azobenzene in the shell [253] and NPs containing azobenze in their backbone [259, 260].

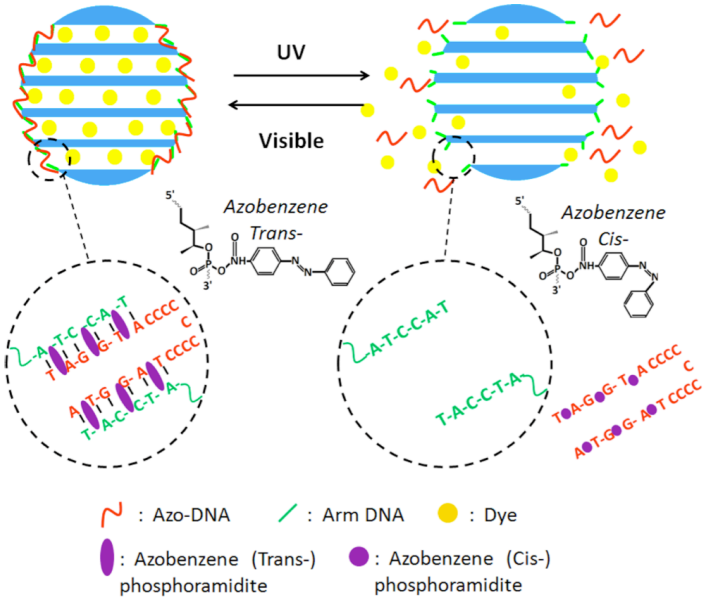

Scheme 2.11 – Schematic illustration of azobenzene-modified DNA-controlled reversible release system. Visible irradiation at 450 nm (azobenzene *trans*) leads to hybridization of the linker and the complementary DNA arm. Irradiation with UV (365 nm) converts azobenzene to the *cis* form, leading to dehybridization and pore opening (adapted from [232]).

Azobenzenes have been also used as nano-impellers and/or "gatekeepers" in MSNs for drug delivery applications [232, 261]. For example, azobenzene-modified nucleic acids have been immobilized in the pores of MSNs containing DOX (**Scheme 2.11**) [232]. The photoisomeration of azobenzene induced the dehybridization of DNA, causing uncapping of pore gates and the release of DOX. The same photoswitch principle was employed in up-converting NPs coated with DOX-loaded mesoporous silica. Upon absorption of NIR light (980 nm), the core-shell $NaYF_4$:TmYb upconverting NPs emitted photons in the UV and visible regions that, in turn, were absorbed by the azobenzene groups present in the pore

network of the mesoporous silica layer. The photoisomerization of azobenze resulted in the release of DOX [220]. A separate study has explored azobenzene-nanovalves in MSN by associating a two-photon paracyclophane-based fluorophore that activated azobenzene by a fluorescence resonance energy transfer (FRET) [262]. Also a nanoimpeller azobenzene approach in MSN was described where the activation of drug release activity occurred through the same two-photon excitation principle [233].

Spiropyrans (SP) are also promising photosensitive groups for the reversible modulation of nanocarriers. These molecules undergo photoisomerization into their hydrophilic zwitterionic merocyanine (MC) forms upon UV irradiation while the reverse process is triggered by visible light [208, 212]. Comparing with azobenzene moieties, the SP offer improved light responsiveness. This property has been explored for reversible light-induced disruption of micelles [225, 254]. Micelles containing SP have been tested in WI-38 and HeLa cells [225]. It is also possible to take advantage of a different feature conferred by SP, the reversible volume change upon phototriggering [212, 234]. By using a SP-based NP formulation, under UV irradiation is possible to verify that this nanocarrier shrinks from 103 to 49 nm, and this physical change in the NP structure could be explored to enhance the tissue penetration capabilities of the nanocarrier in HT-1080 tumors [234]. Through the encapsulation of docetaxel (Dtxl), the UV irradiated Dtxl-containing NPs were more effective in the treatment of HT-1080 tumors than free Dtxl or encapsulated Dtxl without irradiation. These results could be explained by the known contribution of Dtxl to relief the compression of tumor blood vessels [263], increasing tumor blood flow and improving the delivery of NPs. The conjugation of these factors induced tumor cell death, increased intratumoral vessel diameters and tumor perfusion enhancing the accumulation of Dtxl-containing NPs thought tumor tissue and inhibiting tumor growth [234]. Strategies like this may modified the tumor microenvironment to promote NPs tumor penetration and distribution. NPs containing SP that respond to NIR light have also been reported [235].

Although the reversible light-induced modulation of drug release seems to be a strategy more powerful than the irreversible disruption of nanocarriers, the enthusiasm has to be tempered by the fact that the nanocarrier response to light in reversible systems is usually much weaker than on irreversible systems. Moreover, the slow kinetics at which the photoactive moieties respond to light or relax to their initial state in the absence of light could be a severe limitation to their use in translational medicine. Finally, the complete reversibility is generally not achieved since the initial characteristic features of the system are usually not fully recovered during irradiation cycles [186].

2.6 – Opto-nanomedicine challenges

There are distinct strategies available for the light-regulation of drug release systems, each with their own specific advantages and disadvantages. Photolabile protective groups are conceptually easy to realize but inherently irreversible. However, if the functional groups of a molecule, which are responsible for its activity, are properly inserted and if the photoactivation process is clean, excellent results can be obtained. Photoswitching is reversible, but may be difficult to incorporate the photoswitch in such a way that photoisomerization dominates completely the drug delivery activity.

In the last five years, sophisticated stimuli-responsive drug delivery methodologies and light-responsive drug delivery systems have been reported; however, relatively few have been translated into clinical trials, and to the best of our knowledge no formulation is light-activatable [182, 264]. The translation of stimuli-responsive drug-delivery systems from the bench to the bedside is not straightforward. This can be explained by the complexity of their architectural design, which makes the potential pharmaceutical development more complex, specifically in terms of the manufacturing process, reproducibility and quality control [264]. Also, nontrivial optimizations and improvements are often required for the translation of each stimulus from preclinical experimental models to daily clinical practice. Although systems responsive to external stimuli are, from this point of view, more promising, major improvements would be needed to improve both tissue-penetration depth and focusing (to avoid damage to healthy tissues) [182, 265]. Moreover, the toxicity of these drug delivery systems is multifactorial, depending on composition, physicochemical properties, route of administration and dose. The benefit-to-risk ratio has therefore to be balanced according to the intended medical application [182]. To facilitate the translation of these technologies it is important to fully evaluate their biocompatibility *in vivo*. These studies should include not only an assessment of the biomaterial itself but also an assessment of local tissue reaction to the drug released [266]. The latter point is especially important in the case of sustained- or programmed-release systems, in which pharmacokinetics may differ substantially from those of injected doses. In particular, local drug levels may be much higher than the ones achieved by systemic delivery. Appropriate studies could range from local cytotoxicity studies to toxicogenomic analyses.

CHAPTER 3

HIGHLY EFFICIENT DRUG DELIVERY TO LEUKEMIC CELLS BY AN OPTO-NANOMEDICINE SYSTEM

3 – Highly efficient drug delivery to leukemic cells by an opto-nanomedicine system

3.1 – Abstract

The development of a nanoparticle system possessing a trigger to allow precise control of the timing, duration and magnitude of drug release is important for leukemia therapy. Here, we describe light-activatable polymeric nanoparticles (NPs) that rapidly release retinoic acid (RA) when exposed to a blue laser/UV light. These NPs reduce the clonogenicity of bone marrow tumor cells from patients with acute myeloid leukemia (AML) and induce the differentiation of RA-low sensitive leukemia cells expressing the chimeric promyelocytic leukemia zinc finger/RARα (PLZF/RARα) fusion protein. RA released from light-activated NPs was superior at inducing leukemia cell differentiation compared to RA released by passive diffusion. Further, we demonstrate the importance of temporal activation of the nanoformulation during the intracellular trafficking to maximize RA effect and show *in vivo* that leukemic cells loaded with NPs can be light-activated to release RA, thereby allowing greater spatio-temporal control of drug delivery.

Keywords: light, nanoparticles, retinoic acid, myeloid leukemia, cancer stem cells.

3.2 – Introduction

The differentiation of leukemic cells is a therapeutic platform very often used in the clinic to eradicate blood cancers, being the concentration of the inductive agent and the spatio-temporal control of its application very important variables for the success of the therapy [267]. Induction of leukemic cell differentiation by RA is a therapeutic strategy that has been used with great success in the treatment of acute promyelocytic leukemia (APL) [268, 269]. APL is a subtype of acute myeloid leukemia (AML) characterized by a unique translocation between chromosomes 15 and 17, which leads to the formation of the fusion oncogene PML-RARα involving the transcription factor RA receptor alpha (RARα). RA activates nuclear RA receptors (RARs) that forms heterodimers with retinoid X receptors (RXRs) which in turn binds to the RA response element (RARE) resulting in the activation

of target genes causing cell growth arrest, apoptosis and differentiation [270]. Despite its clear therapeutic efficacy, approximately 25% of patients receiving RA will develop serious complications including the "differentiation syndrome" [271]. Clinical trials of RA in other types of AML have been less successful, possibly because of the relatively higher concentrations of RA that are required to induce differentiation in non-APL AML. For both of these reasons, the design of a delivery system with precise temporal and dosage control will be important for cancer chemotherapy.

Micellar aggregates (core-shell micelles, vesicles, etc.) formed by amphiphilic block copolymers or small molecule surfactants have been reported as possible light-activatable drug delivery systems, with temporal and spatial control [213, 214]. Such polymer micelles could release the drugs at a required time and tumor location. In some cases the dissociation of the micelles occurs due to structural arrangements of the photo-sensitive molecule attached to the block copolymer or surfactant [178], the oxidation of the components of the micelles [272], or hydrophilic/hydrophobic balance due to the cleavage of the photo-sensitive molecule [237]. Recently, these studies have been extended to NPs that disassemble in response to light [176, 273]. To date however, it has yet to be shown that these systems can be used to deliver drugs intracellularly, either *in vitro* or *in vivo*, with precise temporal, spatial and dosage control. Here we show that light-activatable polymeric NPs can enhance the efficiency of RA delivery to leukemia cells either *in vitro* or *in vivo*. We further show that the timing of drug release following delivery by NPs can be tightly controlled, and that the efficiency of differentiation of leukemic cells induced by RA can be increased.

3.3 – Results

3.3.1 – Preparation and characterization of light-activatable polymeric nanoparticles

To prepare light-dissociable polymeric NPs, poly(ethyleneimine) (PEI, Mw of 25 kDa) was initially derivatized with 4,5-dimethoxy-2-nitrobenzyl chloroformate (DMNC) in DMSO, a light-sensitive photochrome (**Fig. 3.1A**). PEI was selected as initial NP block because it facilitates the cellular internalization of NPs and subsequent escape from endosomes [119, 133], while DMNC was selected because responds rapidly to light and the degradation products are relatively non-cytotoxic [236]. PEI-DMNC conjugates with different degree of substitution (PEI-$DMNC_{100}$; PEI-$DMNC_{50}$ and PEI-$DMNC_{25}$ with a

theoretical degree of substitution of 100%, 50% and 25% of the tertiary amines of PEI) have been synthesized and characterized by spectrophotometry and ^{1}H-NMR (**Figs. 3.2A to 3.2C**). Approximately 20% of the initial DMNC added to the reaction vial reacted with PEI. To prepare NPs, a solution of PEI-DMNC in DMSO was precipitated into an aqueous solution of dextran sulfate. NPs were formed because of the hydrophobicity of PEI-DMNC conjugate and the electrostatic interaction of PEI-DMNC (polycation) with dextran sulfate (DS, polyanion). To stabilize the NP formulation, zinc sulfate was added [133, 274]. NPs with a diameter between 150 (PEI-DMNC$_{100}$:DS NP) and 110 nm (PEI-DMNC$_{25}$:DS NP) (**Fig. 3.3A**) and a zeta potential between 20 (PEI-DMNC$_{100}$:DS NP) and 25 mV (PEI-DMNC$_{25}$:DS NP) were prepared.

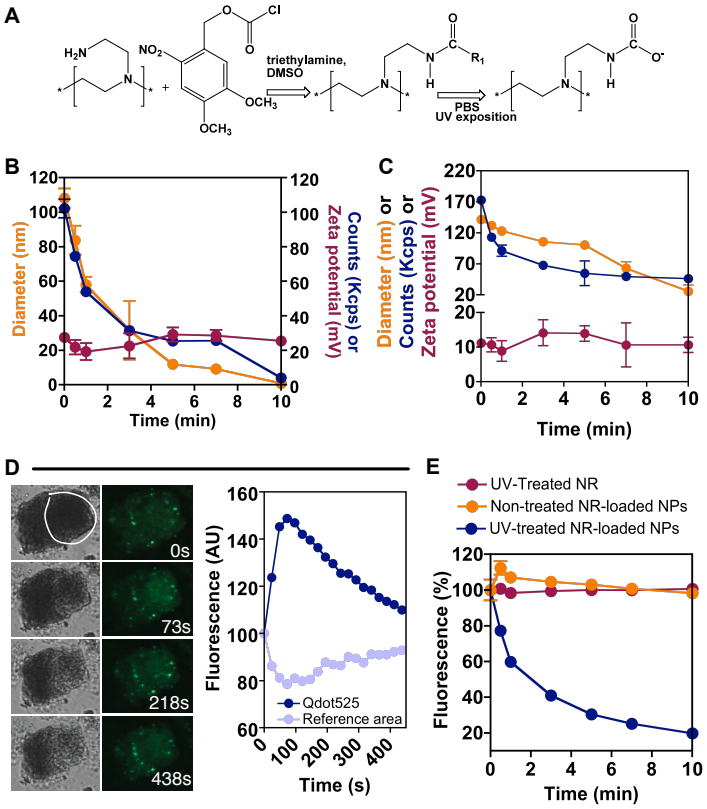

Figure 3.1 – Photo-disassembly of PEI-DMNC$_{25}$:DS NPs. (A) Schematic representation for the conjugation of PEI with DMNC and subsequent scission of the conjugate by UV light. (B) A suspension of NPs (n = 3) (2 mL, 50 μg/mL in water) was exposed to UV light (365 nm, 100 Watts) for up to 10 min. At each time, the size, zeta potential and number of NPs (kcps) in the suspension was evaluated by dynamic light scattering. (C) A suspension of NPs containing NR (n = 3) (2 mL, 50 μg/mL in water) was exposed to UV light (365 nm, 100 Watts) for up to 10 min. At each time, the size, zeta potential and number of NPs (kcps) in the suspension was evaluated by dynamic light scattering. (D) Confocal images showing light-disassembly of Qdot525-labeled NPs. A section of a NP aggregate (area delimited in the figure) was bleached continuously by a laser at 405 nm as confocal images were collected every 20 s. The images show the disassembly of the bleached area of the NP aggregate. Fluorescence intensity of the area bleached by the laser and reference area (i.e., not activated by the

laser) overtime. (E) Normalized fluorescence vs. time for the same NR-loaded NP formulation when exposed or not to UV light (365 nm, 100 Watts), showing the increase in the release rate with UV exposure. Nile Red in aqueous solution exposed to UV light is presented to demonstrate its photostability.

To demonstrate that PEI-DMNC:DS NP formulation could be photo-disassembled, a suspension of NPs (50 μg/mL) was exposed to UV light for up to 10 min and both the diameter, counts per second (i.e., number of NPs per volume unit) and zeta potential were assessed. The number of NPs decreased below half of the initial number after 1 min of UV exposure indicating NP disassembly (**Fig. 3.1B**). Under UV irradiation, the photolysis of DMNC disrupts the NPs because of the changing of hydrophilic/hydrophobic balance in the NP. In addition, the NPs that remained in suspension had a significant decrease in diameter from 110 to 5 nm after 10 min of UV exposure, while zeta potential was kept constant (25 mV). Importantly, UV light can be replaced by a blue laser (405 nm, 80 mW), which has minimal impact in cell biology, to induce the photo-disassembly of PEI-DMNC:DS NPs. As observed for UV-exposed NPs, blue light-exposed NPs have a decrease in number and in diameter overtime (**Fig. 3.3**).

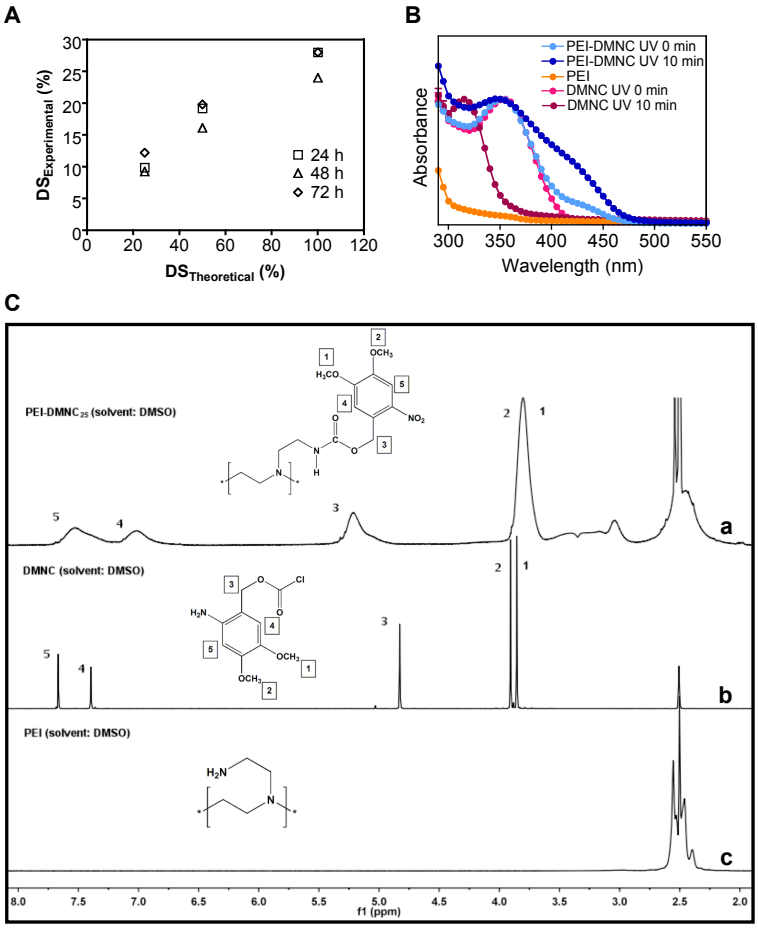

Figure 3.2 – Characterization of PEI derivatized with DMNC. (A) Degree of substitution (DS_n) of PEI with DMNC. The $DS_{theoretical}$ was calculated as molar ratio of DMNC to tertiary amines in PEI. The $DS_{experimental}$ was

determined by spectrophotometry. (B) Effect of 10 min-UV exposure (365 nm, 100 Watts) in the absorbance of DMNC (250 µg/mL, in DMSO), PEI (1 mg/mL, in DMSO), and PEI-$DMNC_{25}$ (1 mg/mL, in DMSO) conjugate. For DMNC, the absorption maximum at 355 nm reverted to baseline levels after 10 min of UV exposure, indicating the photo-cleavage of DMNC, and a new absorption peak was observed at 320 nm, due to the formation of 4,5-dimethoxy-2-nitrobenzyl alcohol (DMNA). For PEI-DMNC, there was a decrease in the intensity of the peak at 355 nm and a concomitant increase in the peak at 320 nm; however our results suggest that not all the attached DMNC molecules were photo-cleaved. (C) ^{1}H NMR spectra of PEI, DMNC and PEI-DMNC. ^{1}H NMR spectra of (a) PEI-DMNC conjugate in DMSO-d6, (b) DMNC in DMSO-d6 and (c) PEI in DMSO-d6, showing effective conjugation between PEI and DMNC.

The response of the NPs to UV light was mediated by DMNC coupled to one of the components of the NP, since NPs without DMNC did not respond to light (**Fig. 3.3**). In addition, the concentration of DMNC conjugated to PEI is important for the light-responsiveness of the NP. NPs formed by PEI with high degree of substitution with DMNC are less susceptible to photo-disassembly than NPs with PEI with low degree of substitution (**Fig. 3.3C**). Therefore, for subsequent studies the NP formulation having PEI with low degree of substitution was selected (PEI-$DMNC_{25}$:DS NP). To further confirm light-disassembly of the NPs, the NPs were conjugated with quantum dots (Qdots525) and their fluorescence monitored overtime after exposure of small regions of the NP to a blue confocal laser (405 nm). Our results show that fluorescence intensity increases after light exposure due to the disassembly of the NP and the decrease in the quenching of Qdot fluorescence after NP disassembly (**Fig. 3.1D**).

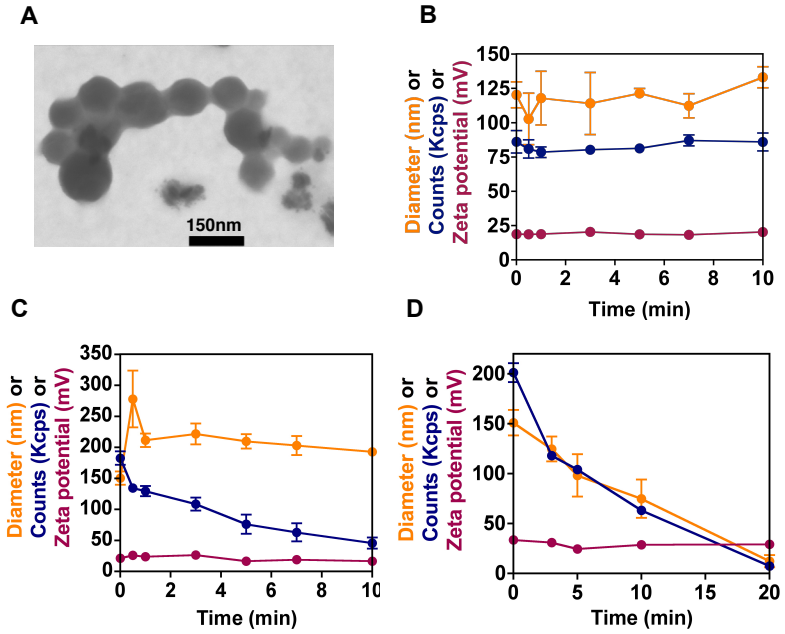

Figure 3.3 – Light-activation of NPs. (A) SEM of PEI-$DMNC_{25}$:DS NPs. (B,C,D) Blue laser (405 nm, 80 mW) activation of PEI:DS NPs (B), PEI-$DMNC_{100}$:DS (C) and PEI-$DMNC_{25}$:DS NPs (D). A suspension of

NPs (*n*=3) (100 μL, 100 μg, in water) was exposed to a blue laser up to 20 min. Then, the NP suspension was diluted up to 50 μg/mL in water and the size, zeta potential and number of NPs (Kcps) in the suspension was evaluated by dynamic light scattering.

To evaluate the characteristics of light-activatable polymeric NPs as a controlled release system, NPs were encapsulated with Niles Red (NR), a small hydrophobic dye with excellent photostability [176, 237]. NR fluorescence at about 530 nm shows good quantum yields in apolar solvents. When exposed to water its fluorescence emission shows a shift to approximately 640 nm and the quantum yield is significantly reduced [275]. The NP suspension was then exposed to UV light for up to 10 min and NP properties (diameter, counts, zeta potential) as well as release of NR were evaluated. As obtained for blank NPs, the number of NR containing NPs decreased overtime, indicating the encapsulated NR did not affect the photo-cleavage of the NPs (**Fig. 3.1C**). Then, the release of NR upon UV exposure was monitored by fluorescence spectroscopy (**Fig. 3.1E**). The fluorescence intensity (in percentage) of the NP suspension decreased to 20% of the initial value after 10 min of UV exposure, due to the controlled triggered burst release of NR in aqueous solution. In contrast, no significant release of NR was observed for NPs not exposed to UV light.

3.3.2 – Internalization and intracellular trafficking of light-activatable NPs

To evaluate NP internalization, chronic myelogenous leukemia (CML) K562 cells, human bone marrow acute promyelocytic leukemia (APL) NB4 cells and human myelomonoblastic U937 cells were exposed to variable concentrations of NPs and the concentration of NPs (containing Zn) internalized by each type of cell quantified by inductive coupled plasma mass spectrometry (ICP-MS) (**Fig. 3.4A**). NPs were highly stable in different cell culture media as evaluated by dynamic light scattering measurements (**Fig. 3.5**). Kinetic studies performed in NB4 and U937 cells (NP concentration of 10 μg/mL) show that NPs internalization peaked at 6 h (**Fig. 3.6A**). The three types of leukemic cells accumulated between 60 and 75 pg of NPs per cell following exposure for 4 h to cell culture medium containing 100 μg/mL of NPs (**Fig. 3.4A**). No significant differences were observed in the internalization profiles between cells. NP internalization by leukemia cell lines and primary AML cells was also characterized by flow cytometry (**Fig. 3.6B**). For this purpose, cells were exposed to light-sensitive NPs (with and without tetramethylrhodamine-5-(and-6)-isothiocyanate (TRITC) labeling) at concentrations of 10 μg/mL up to 24h, or just for 4 h (primary AML cells), washed to remove loosely bound NPs, resuspended in a Trypan Blue

solution to quench the extracellular fluorescence, and finally characterized by FACS. Over 95% of cell population was positive for the presence of NPs. Importantly, the NPs are retained in AML cells in culture for at least 5 days since no significant loss of fluorescence was observed by FACS (**Supplementary Fig. 3.6B.2**). All together, NPs were highly efficiently internalized by human leukemic cells and accumulate intracellularly for several days.

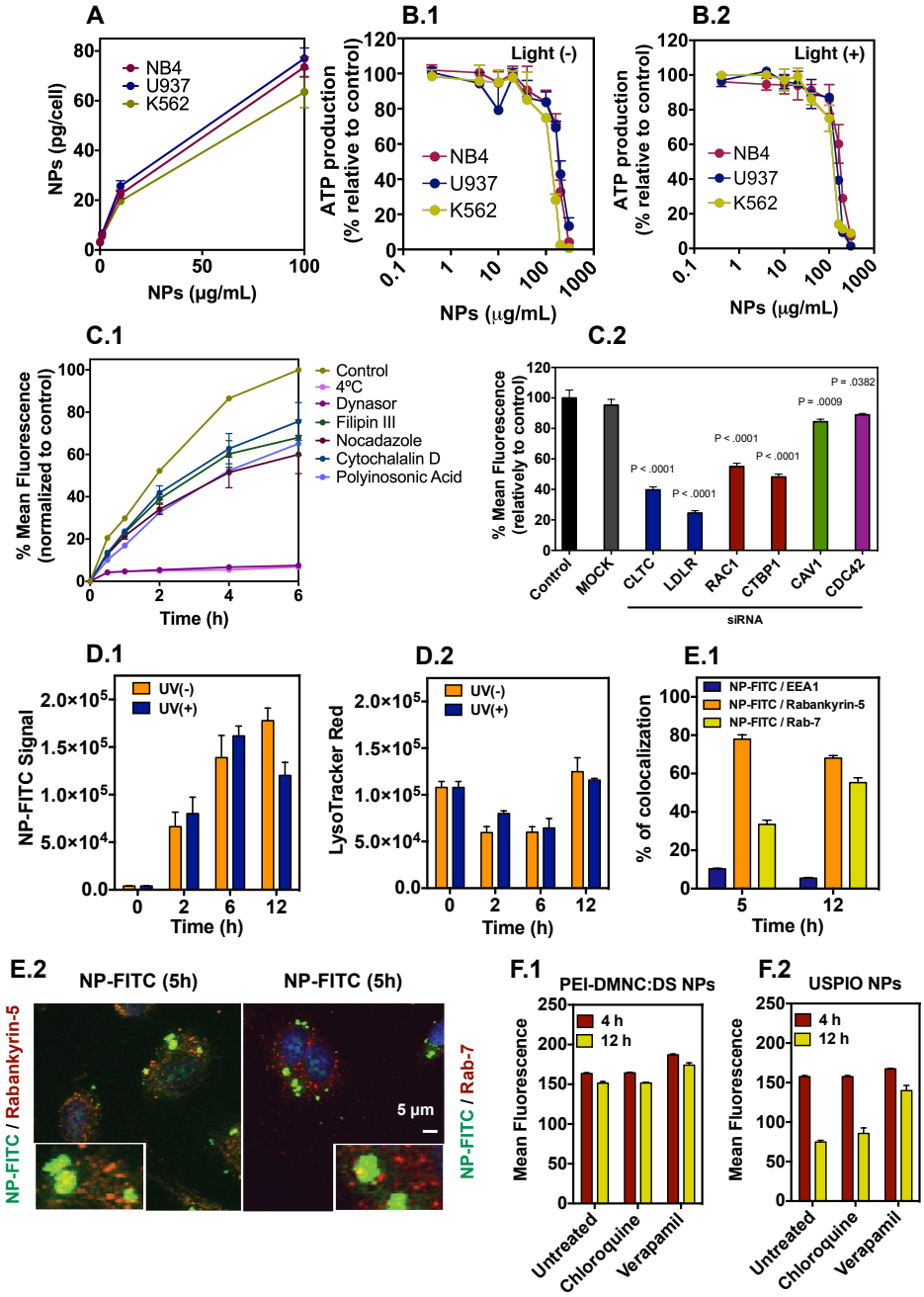

Figure 3.4 – Internalization, intracellular trafficking and cytoxicity of NPs. (A) Amount of NPs internalized by leukemia cell lines K562, NB4 and U937 as determined by ICP-MS (Zn quantification). Cells were incubated with NPs for 4 h, washed, lysed and Zn content of the NPs was quantified by ICP-MS. Results are expressed as Mean ± SEM (n = 3). (B) Cytotoxicity of NPs against K562, NB4 and U937 cells. Cells were

cultured in medium supplemented with light-sensitive RA^+ NPs for 4 h, washed, exposed or not to a UV light for 10 min, and then cultured for 20 h. Cell cytotoxicity was evaluated by an ATP kit. Results are expressed as Mean ± SEM (n = 3). (C) Internalization mechanisms of NPs. (C.1) Uptake of TRITC-NPs by U937 cells in the presence of several endocytosis inhibitors. Results are expressed as Mean ± SEM (n = 3). (C.2) Uptake of TRITC-NPs in U937 cells after silencing key regulators of CME (CLTC and LDLR), caveolin-mediated endocytosis (CAV1), GEEC-CCLIC pathways (CDC42) and macropinocytosis (RAC1 and CTBP1) with siRNAs. The results are expressed as Mean ± SEM (n = 3). P_{value} indicate significance relative to control. (D) Cellular trafficking of FITC-labeled NPs. HUVEC cells were incubated with FITC-labeled NPs (1 µg/mL) for 1 or 4 h, washed extensively, exposed or not to UV light (365 nm, 100 Watts), cultured in normal conditions for 1 or 2/8 additional hour/s, respectively, and stained with LysoTracker DND-99 before cell fixation. Results are expressed as Mean ± SEM (n = 3). (E) Intracellular trafficking of FITC-labelled NPs through endocytosis. Early endosome were stained with EEA1 antibody, early/late endosomes were stained with Rab-5 antibody and late endosome/lysosomes were stained with Rab7 antibody. Representative images of the intracellular distribution of FITC-labelled NPs in relation to early/late endosomes stained with Rab-5 antibodies (left image), and late endosome/lysosome stained with Rab7 antibody (right image). HUVEC cells were incubated with FITC-labelled NPs (1 µg/mL) for 4 h, washed extensively and cultured in normal conditions for 1 additional hour before cell fixation. Quantification of FITC-labelled NPs co-localized with EEA1, Rab-5 and Rab7 (right graph). HUVEC cells were incubated with 1 µg/mL for 4 hours, washed extensively and cultured in normal conditions for 1/8 additional hour/s before cell fixation. Results are expressed as Mean ± SEM (n = 3). (F) TRITC-labelled PEI-DMNC:DS NPs (10 µg/mL) or TRITC-labelled USPIO NPs (100 µg/mL) intracellular accumulation in Zn-induced U937 cells in the presence of the Pgp antagonist verapamil and of the endosome disruption agent chloroquine. Cells were exposed to culture medium with chemical agents, FITC-labelled NPs for 4 h, cultured for additional 8 h and finally characterized by FACS. Results are expressed as Mean ± SEM (n = 3).

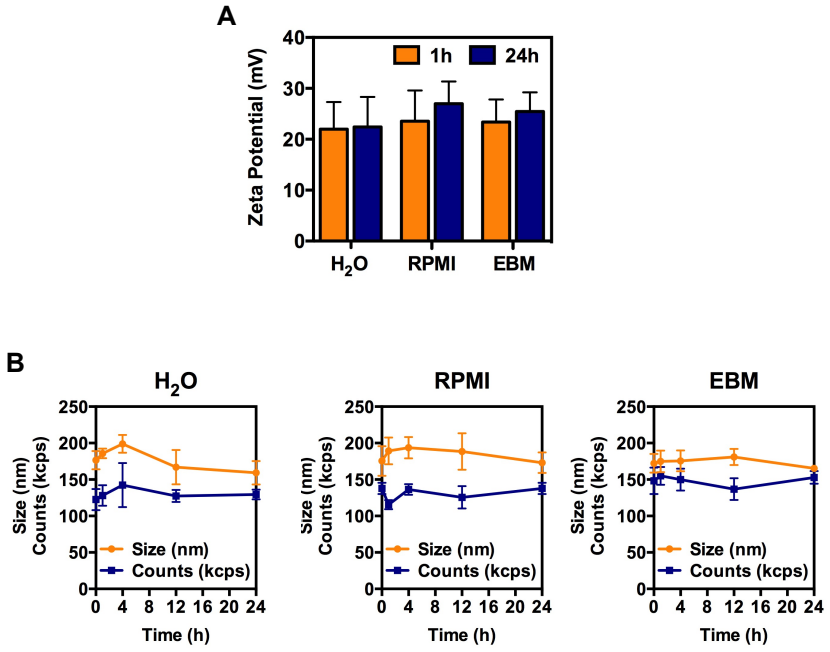

Figure 3.5 – Stability of NPs suspended in basal culture medium. (A) Zeta potential of NPs suspended in H_2O, basal RPMI medium or EBM medium. (B) Diameter (nm) and counts (Kcps) of NPs suspended in H_2O,

basal RPMI medium or EBM medium. A suspension of NPs (2 mL, 25 µg/mL) was prepared and diameter, counts and zeta potential determined by dynamic light scattering method (DLS) using a Zeta Plus Analyzer (Brookhaven). Results are expressed as Mean ± SEM (n = 3).

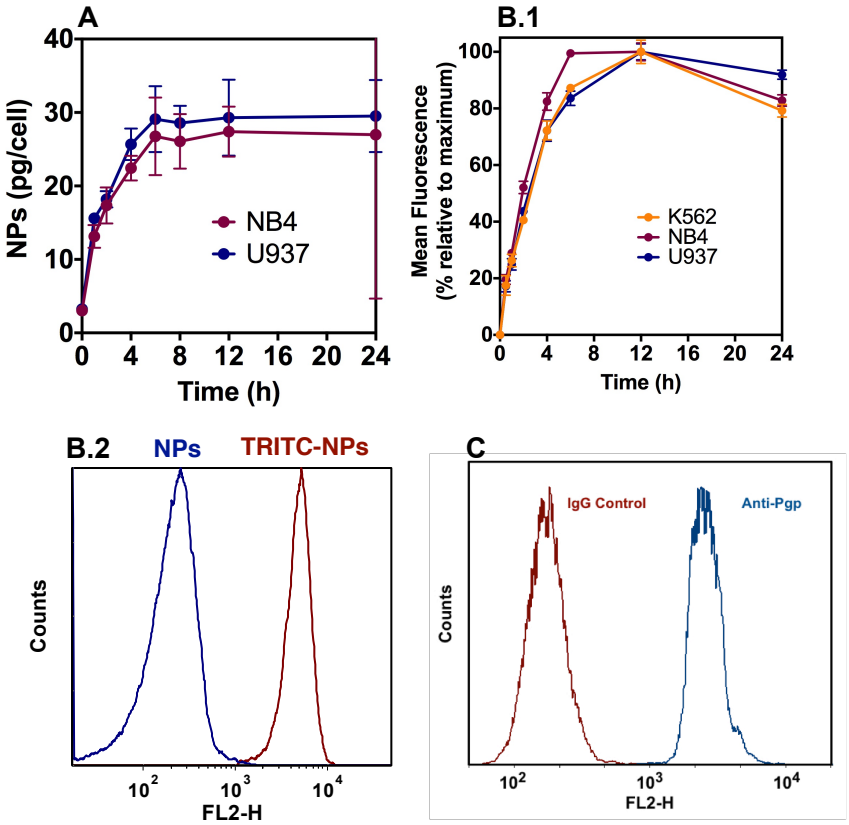

Figure 3.6 – Cellular uptake of NPs. (A) Quantification of NP internalization in leukemia cell lines NB4 and U937 as determined by ICP-MS analysis (Zn quantification). Cells were incubated with 10 µg/mL NPs up to 24 h. After each incubation period, the cells were extensively washed with PBS followed by the addition of an aqueous solution of nitric acid (1 mL, 69% (v/v)). The concentration of intracellular levels of Zn was quantified by ICP-MS. The concentration was normalised per cell. The estimation of NPs was done based on standard solutions. The results are expressed as Mean ± SEM (n = 3). (B.1) Uptake of TRITC-labeled NPs in leukemia cells as determined by FACS. Cells were cultured in medium supplemented with NPs for the time specified in the graph, washed and characterised by FACS. The results are expressed as Mean ± SEM (n = 3). (B.2) AML stem cells ($CD34^+CD38^-$) were labeled with TRITC-labeled NPs for 4 h and then cultured for 5 days. The histogram plot shows the percentage of cells labelled after 5 days. (C) Expression of Pgp in U937 cells as evaluated by FACS. A PE-conjugated mouse anti-human P-glycoprotein has been used (Abcam ab93590 – Clone UIC2).

NPs have no substantial effect in cell metabolism, as evaluated by an ATP assay, for concentrations up to 100 µg/mL. Cells were exposed to NPs for 4 h, washed to remove NPs not taken up by the cells, either exposed or not to UV light for 10 min, and finally cultured for additional 20 h (**Fig. 3.4B**). Because the activation of NPs by UV light or blue laser can induce double-stranded breaks into DNA we evaluated the effect of the radiation in the

phosphorylation of histone H2A (γH2AX) an early biomarker of DNA damage [276]. Our results indicate that neither UV nor blue light exposure for 10 min had significant impact in DNA damage (**Fig. 3.7**).

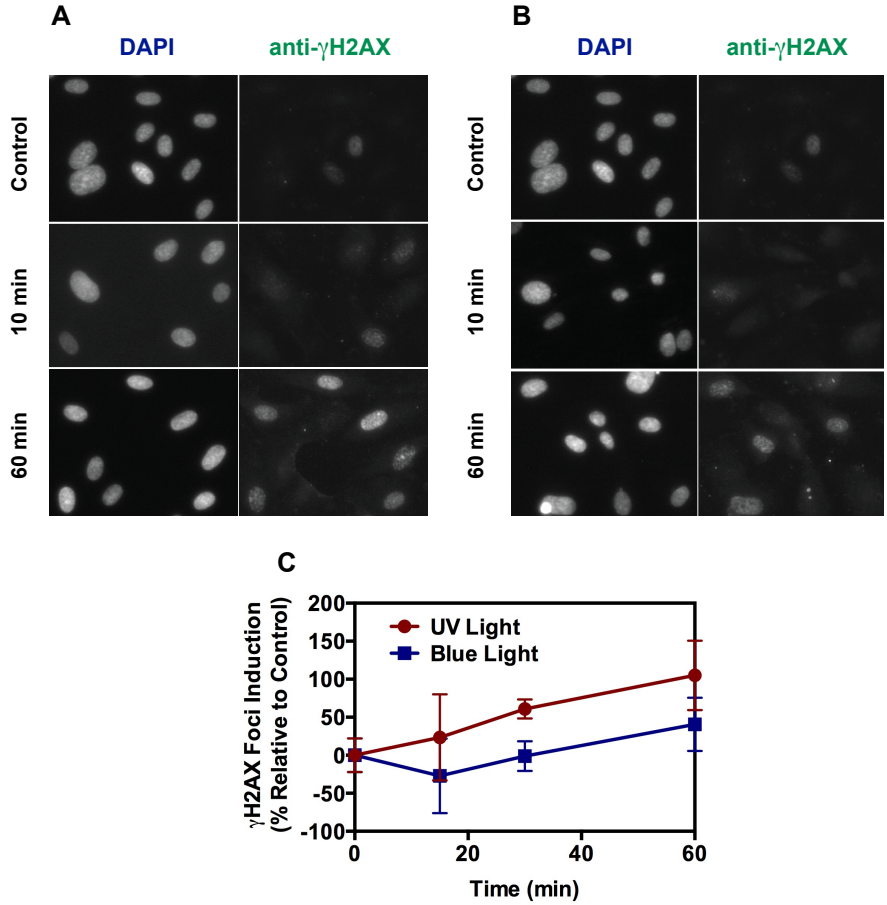

Figure 3.7 – Effect of UV light and Blue Light in DNA damage in HUVEC cells. Immunofluorescent staining of normal HUVEC cells mock treated or exposed to 10 min or 60 min of UV light (365 nm, 100 W) (A) or blue light (405 nm, 80 mW) (B) and allowed to recover for 6 h. Cells were then fixed and stained to readily identify γH2AX-containing foci, as biomarker for nuclear sites of DNA damage in affected cells. (C) Time-dependent increase of γH2AX after UV light (365 nm, 100 W) or blue light (405 nm, 80 mW) irradiation. Quantitative analysis of foci intensity were quantified using imageJ software and normalised to the control condition.

To identify the pathways of NP internalization, U937 cells were incubated in the presence of endocytosis chemical inhibitors at concentrations that were not cytotoxic for the cells (**Fig. 3.8A**), after which, fluorescently labelled NPs were added and the internalization monitored by flow cytometry. Filipin III inhibits cholesterol dependent internalization mechanisms, nocodazole inhibits microtubule dependent pathways, cytochalasin D inhibits all pathways dependent on actin (including macropinocytosis), dynasore inhibits clathrin-mediated endocytosis and polyinosinic acid inhibits scavenger receptors [277]. Whenever possible molecules that enter by a specific internalization pathway were used as positive

controls to show the efficacy of our inhibitors (**Fig. 3.8B**). Dynasore treatment (clathrin-mediated endocytosis (CME) inhibitor) reduced the uptake of NPs by 90%, compared to control cells (**Fig. 3.4C.1**). To confirm the endocytosis mechanisms involved in NP internalization, U937 cells were transfected with siRNAs to down-regulate key components of different endocytic mechanisms (**Fig. 3.4C.2**). We observed a ~60% and ~70% reduction on NPs uptake upon downregulation of clathrin heavy chain (CLTC), and low-density lipoprotein receptor (LDLR), respectively, confirming a role for CME. The knockdown of macropinocytosis regulators (Rac1 and CTBP1), led to a ~40% and ~50% decrease in NPs uptake, suggesting that macropinocytosis was also involved in NPs internalization. Downregulation of Caveolin 1 (CAV1), involved in caveolin-mediated endocytosis, and GPI-anchored protein-enriched early endocytic compartment/clathrin-independent carriers (GEEC-CLIC) pathways (CDC42) had no significant impact in NPs uptake. To further elucidate the intracellular trafficking of the NPs, we used adherent cells (HUVECs) to facilitate the characterization by confocal microscopy. The intracellular trafficking of the NPs was assessed first by performing a LysoTracker staining to see the general distribution of the FITC-labeled NPs in the endolysosomal system (**Fig. 3.4D**). During the first few hours of incubation with FITC-labeled NPs there was a clear drop in the intensity of LysoTracker in the cell suggesting a decrease in the pH of the endosomal vesicles by the presence of PEI (a strong base) in the cell and also possible vesicle disruption as the FITC-labeled NPs signal was increased in the cytoplasm. At later time points (12 hours) of incubation with FITC-labeled NPs the intensity of LysoTracker reached control levels suggesting that the endolysosomal system regained its normal characteristics **(Fig. 3.4D)**. To fully characterize the route of FITC-labeled NPs inside the endolysosomal system a time-dependent colocalization study of FITC-labeled NPs with the specific markers: EEA1 for early endosomes, Rab-5 for early/late endosomes and Rab-7 for late endosome/lysosomes was done. For short incubation times (1-2 h) not many vesicles are seen with FITC-labeled NPs; instead there is a diffuse distribution of green allover the cytoplasm (ca. 80-90% of the fluorescence). This is consistent with a rapid escape of the NPs from endosomes after entering the cell likely due to their buffering capacity, leading to osmotic swelling and rupture of endosomes[133]. For later time points (over 5 hours) of incubation with FITC-labeled NPs there is a clear accumulation of FITC-labeled NPs inside vesicles that are mostly Rab-5 and/or Rab-7 positive with very low EEA-1 colocalization. The high colocalization with Rab-5 and the size of the vesicles containing NPs suggests that macropinocytosis is also an entrance route for these NPs **(Fig. 3.4E)**. Taken together, our results indicate that the

major endocytic mechanism for the internalization of the NPs is clathrin-mediated endocytosis. Our siRNA results indicate that macropinocytosis might be also involved but at minor extent. It is likely that both endocytic pathways are interconnected as demonstrated recently for lipid NPs [278]. Our results further show that the internalization of the NPs is rapid and in the first 2 h a significant percentage of NPs tend to escape the endolysomal compartment, while the ones that did not escape accumulate in early/late endosomes.

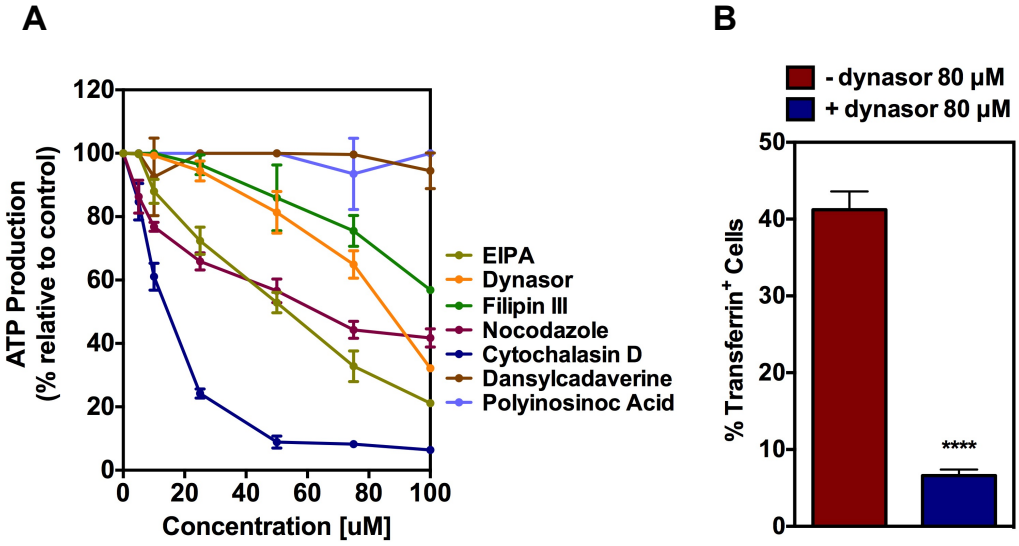

Figure 3.8 – (A) Cytotoxicity of chemical inhibitors against U937 cells. Cells were cultures in medium supplemented with growing concentrations of chemical inhibitors for 24h. Cell cytotoxicity was evaluated by an ATP kit. Results are expressed as Mean ± SEM (n = 3). (B) Transport of FITC-labeled transferrin (1 µg/mL) known to selectively enter cells via clathrin-mediated endocytosis. Dynasor at concentration of 80 µM inhibits the internalisation of transferrin in U937 cells. Cells were exposed to culture medium with and without dynasor for 30 min, exposed to FITC-labeled transferrin for 3 min, at 4 ºC, and finally characterized by FACS. Results are expressed as Mean ± SEM (n = 3). **** Denotes statistical significance (P<0.0001).

Next, we asked whether NPs would be effluxed by leukemic cells overtime. It is known that tumor cells high express P-glycoprotein (Pgp), a membrane transporter that is responsible for the efflux of drugs [279] and NPs [280]. Therefore, we studied by flow cytometry the effects of the Pgp antagonist verapamil [280] and the endosome disruption agent chloroquine [281] in the intracellular accumulation of NPs on RA-resistant Zn-induced U937-B412 cells. Our results showed that the intracellular accumulation of the NPs in U937 was similar with or without inhibition of Pgp or promoting endosomal escape by chloroquine (**Fig. 3.4F.1**). In contrast, the intracellular accumulation of control ultra small paramagnetic iron NPs (USPIO) required the inhibition of Pgp (**Fig. 3.4F.1**). Overall, our results show the unique properties of our NP formulation to accumulate in leukemic cells.

3.3.3 – Remotely activation of the NP formulation and leukemia cell differentiation

To evaluate the feasibility of remotely trigger the disassembly of a specific population of NPs during their intracellular trafficking, we transfected HUVECs with Qdot525-labelled NPs (10 μg/mL) for 4 h. When a small region of the cell having NPs is excited by blue light laser (405 nm) under a confocal microscope, NP fluorescence increases as compared to a reference region not excited with UV light (**Fig. 3.9A**). This increase is due to the disassembly of the NPs and a decrease in the quenching of the quantum dots immobilized in the NPs. The efficacy of our light-activatable NPs for delivering RA was further assessed in leukemic cell lines and primary AML cells. All the leukemic cell lines express all three RA receptors, although RARα is higher expressed than RARβ and RARγ (**Fig. 3.10**). Complexes of RA with PEI were formed by the electrostatic interactions of the carboxyl groups of RA with the amine groups of PEI. The NP formulation contained approximately 120 μg of RA per mg of NP, had an average diameter of 160 nm and a zeta potential of 22 mV. In order to assess the efficiency of the RA^+ NPs in delivering RA inside leukemic cells and induce an RA-dependent signaling pathway a RARE reporter cell line was generated using NB4 cells. The RA-dependent induction of a RARE element driving the transcription of the firefly luciferase gene was used to evaluate the kinetics of RA-induction using RA^+ NPs or RA in solution. These luciferase assays showed that RA^+ NPs are able to induce high levels of luciferase activity shortly after light activation (**Fig. 3.9B**). RA^+ NPs were more efficient and quicker at inducing transcription from the RARE-luciferase locus than RA in solution. To assess if this high efficiency is related with a higher amount of RA being delivered inside the cells using the NPs, radioactive RA was used. Cells were incubated in the presence of [^{3}H]RA (1 μM and 10 μM) and [^{3}H]RA-NPs (1 μg/mL and 10 μg/mL) at 37 ºC for 4 h. After 24 and 72 h, cells were washed and the amounts of [^{3}H]RA internalized were measured. Comparable results were obtained for NB4 (**Fig. 3.9C**), K562 and U937 cell lines (**Fig. 3.11**). The uptake of [^{3}H]RA was higher using the NPs when comparing with [^{3}H]RA available in solution reaching its peak at 24 h. Considering that there was a smaller amount of RA in the NP formulation than the one available when cells were incubated with RA in solution the rational for NP utilization as a carrier for RA is well justified both from an efficiency point of view as from an uptake yield perspective (values below 2% were obtained for [^{3}H]RA in solution comparing with values above 20% obtained when NPs are employed).

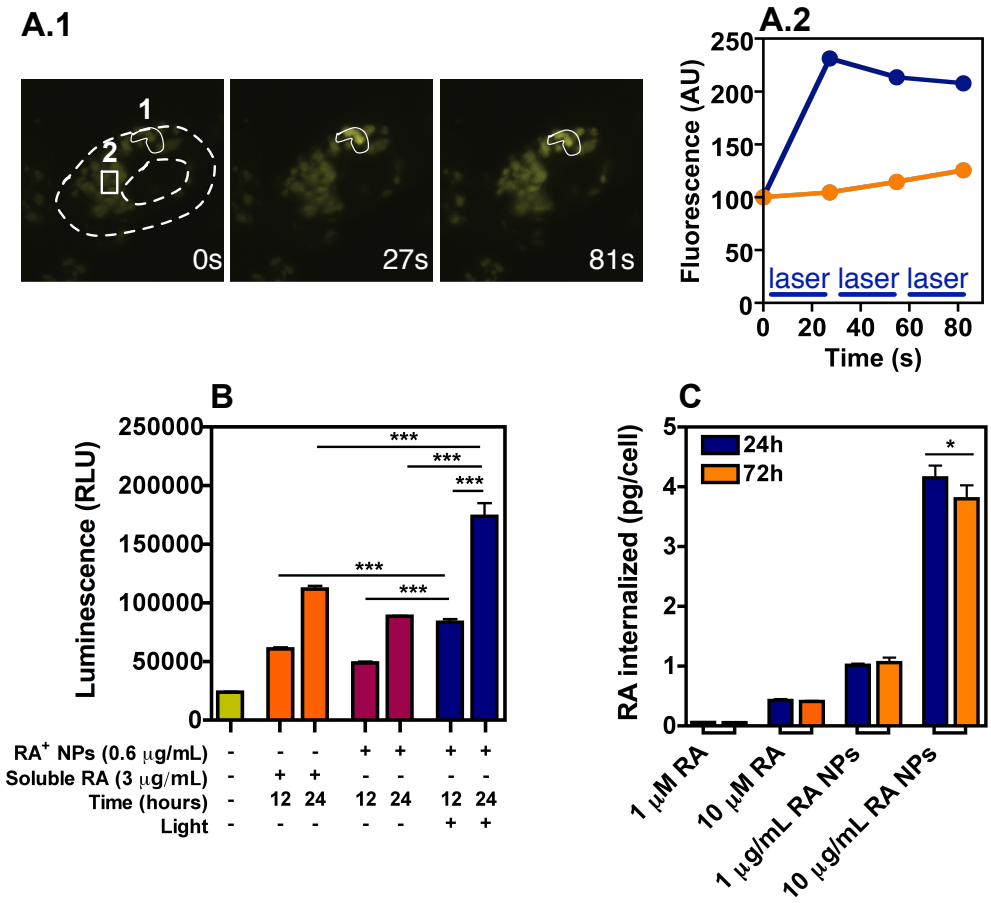

Figure 3.9 – Intracellular photo-disassembly of NPs and release of RA. (A) Confocal imaging of HUVEC cells after exposure for 4 h to QDot525-labelled NPs. A small section of the cell (region 1, created by a mask) was then exposed to blue light laser cycles (405 nm) in a Zeiss confocal microscope and the intensity of fluorescence at 525 nm monitored. In parallel, the fluorescence of another section of the cell (region 2) not excited with the laser was monitored as a control. Our results show that the fluorescence intensity in region 2 maintains overtime while in region 1 the intensity increases. Blue dots and line presents the blue light laser-exposed area of Qdot525-labelled NPs; orange dots and line presents the control unexposed area of Qdot525-labelled NPs. Dashed areas show cell membrane and nucleus. (B) Intracellular release of RA as evaluated by a RARE luciferase assay. NB4-RARE cells were cultured with soluble RA (10 μM; 3 μg of RA per mL) in culture medium for the entire duration of the experiment, or light-activatable RA^+ NPs (5 μg/mL; 0.6 μg of RA per mL). Cells were exposed to NPs for 1 h, washed with PBS, and resuspended in cell medium. Some samples were exposed to UV light (365 nm, 100 Watts) for 5 min. The cells were then cultured for 12/24 h before luciferase luminescence reading. Results are expressed as Mean ± SEM (n = 3). (C) [^{3}H]-RA uptake by NB4 cells. NB4 cells were cultured with soluble ^{3}H-RA (1 and 10 μM) in culture medium for the entire duration of the experiment, or light-activatable ^{3}H-RA^+ NPs (1 and 10 μg/mL). Cells were exposed to NPs for 4 h, cells washed with PBS and then resuspended in cell medium for additional 20/68 h before scintillation counting. Results are expressed as Mean ± SEM (n = 3). *P<0.05, **P<0.01, ***P<0.001.

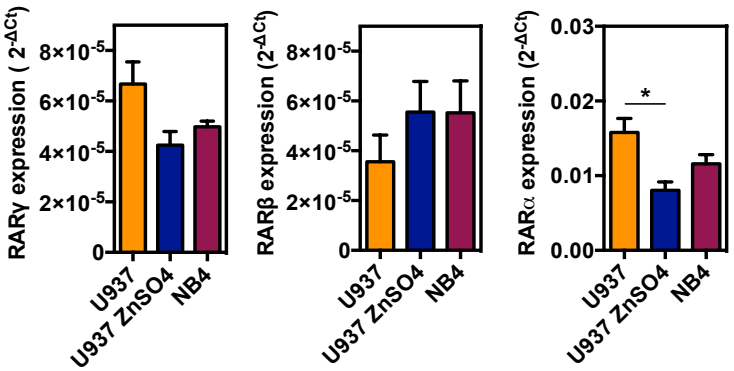

Figure 3.10 – Expression of RAR-α, RAR-β and RAR-γ genes (normalized to GAPDH) in human leukemia cell lines as assessed by qRT-PCR analysis. Results are expressed as Mean ± SEM (n = 3).

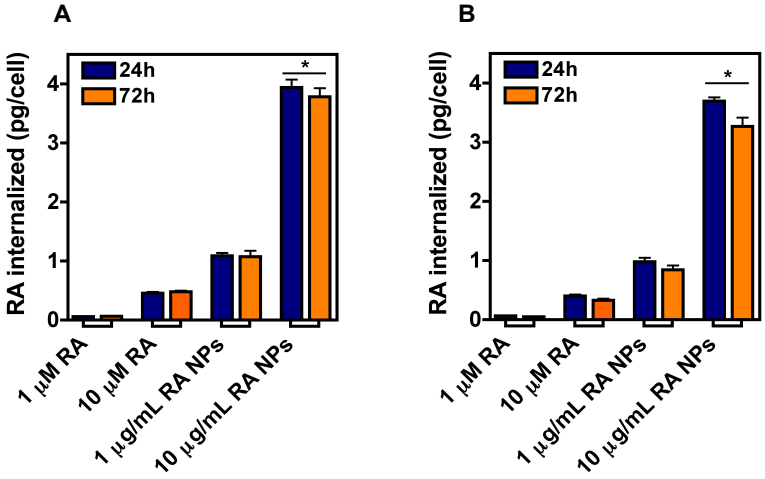

Figure 3.11 – Tritium-labeled RA uptake assay in K562 (A) and U937 (B) cells. K562 and U937 cells were cultured with soluble ^{3}H-RA (1 and 10 μM) in culture medium for the entire duration of the experiment, or light-activatable ^{3}H-RA^{+} NPs (1 and 10 μg/mL). NPs were added to cell culture for 4 hours. Then, the cells were washed with PBS, and fresh cell medium added and the cells remained in culture for 24/72 hours before scintillation counting.

Recent studies reported that lipid-based NPs are able to release siRNA cargo in the cytosol only during a limited window of time when the NPs reside in a specific compartment sharing early and late endosomal characteristics [278, 282]. To demonstrate the temporal control afforded by RA^{+} NP formulation, we have transfected NB4 and Zn-induced U937-B412 cells with RA^{+} NPs and light-activated the formulation at different time points. The effect of the intracellular release of RA was evaluated in terms of differentiation of the cells into the myeloid lineage (expression of CD11b marker at day 3) (**Fig. 3.12A**). Cells that were incubated with NPs for 4 to 8 h and subsequently activated by light showed the highest differentiation into the myeloid lineage. Interestingly, cells exposed to NPs above 8 h showed lower capacity to differentiate, which might indicate less efficiency of RA to escape

from the endolysomal compartment. Importantly, cells incubated with NPs for 1 h showed high level of differentiation, which indicates that the uptake of the NPs is rapid and the endosomal escape efficient. Then, we asked whether cells exposed for the same time (4 h) to NPs (therefore having the same internalization levels of NPs) but activated at different times (up to 44 h) during the intracellular transport of the NPs would have differences in their differentiation pattern (**Fig. 3.12B**). Our results show that even after 44 h following NP internalization, the NPs can be activated and the delivery of RA in the cytosol can be relatively efficient. Similar results were obtained when the effect of the temporal intracellular release of RA was evaluated by the induction of the RA-dependent signaling pathway of the RARE reporter cell line generated using NB4 cells. (**Fig. 3.12A.3 and 3.12B.3**). Overall, these results show that the NPs can be accumulated in the intracellular environment and activated in a time window of almost 2 days without loosing their capacity to differentiate the cells. Importantly, a single activation procedure seems to be sufficient to activate RA release from the NPs, since no significant increase in efficiency was observed when multiple rounds of light activation was performed **(Fig. 3.12C)**.

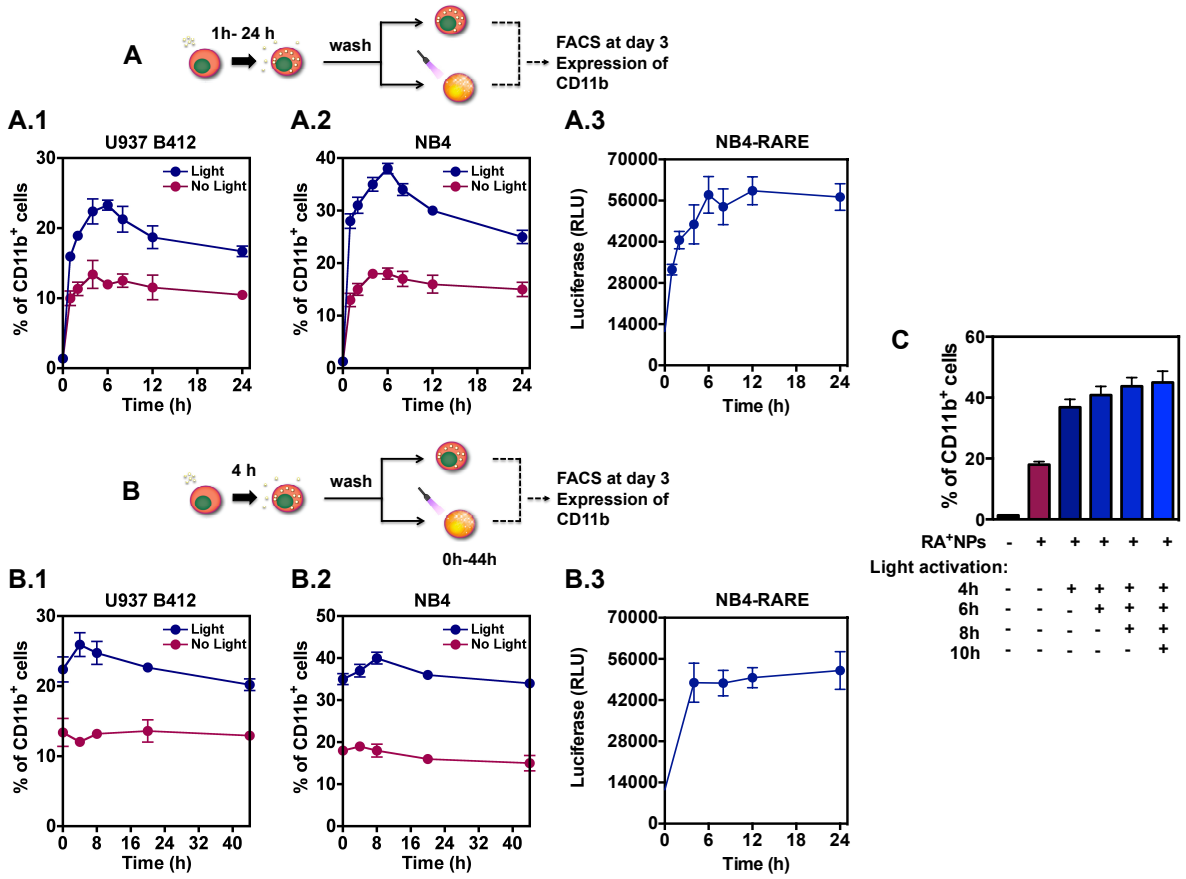

Figure 3.12 – Effect of time in the activation of RA$^+$ NPs within the cells. (A) Schematic representation of the methodology. Zn-induced U937-B412 (A.1), NB4 (A.2) or NB4-RARE-luciferase reporter (A.3) cells were

cultured with RA^+ NPs (1 μg/mL) for variable period of times (1 up to 24 h), washed with PBS, resuspended in cell culture media, exposed to UV light (365 nm, 100 Watts) for 5 min, and cultured for 12 h (luciferase measurements) or 72 h (flow cytometry analyses). Results are expressed as Mean ± SEM (n = 3). (B) Schematic representation of the methodology. Zn-induced U937-B412 (B.1), NB4 (B.2) or NB4-RARE-luciferase reporter (B.3) cells were cultured with RA^+ NPs (1 μg/mL) for 4 h, washed with PBS, resuspended in cell culture media, exposed to UV light (365 nm, 100 Watts) for 5 min at variable periods of time (0 up to 44 h), and cultured for 12 h (luciferase measurements) or 72 h (flow cytometry analyses). Results are expressed as Mean ± SEM (n = 3). In A.3 and B.3, the activation of RA-dependent signaling pathway was measured by luminescence while cell differentiation was evaluated by the expression of CD11b. (C) Effect of multiple light activation in CD11b expression in Zn-induced U937-B412 cells. Cells were cultured with RA^+ NPs (10 μg/mL) for 4 h, washed with PBS, resuspended in cell culture media, exposed to multiple 5 min-cycles of UV light (365 nm, 100 Watts) during the 72 h of culture. Myelocytic differentiation ($CD11b^+$ cells) of human leukemia Zn-induced U923-B412 cells was determined by FACS. Results are expressed as Mean ± SEM (n = 3).

Next, we evaluated the capacity of RA^+ NPs to induce the differentiation of different leukemic cells lines. We studied RA^+ NPs effects in the K562 CML cell line, which undergoes limited erythroid differentiation in the presence of RA [283]. K562 cells were incubated for 4 h with NPs, washed, and further cultured for 1 to 6 days. The frequency of erythroid differentiation, as assessed by benzidine staining was 100-1000 fold higher in cells treated with RA^+ NPs than in cells continuously exposed to RA in the culture medium (**Fig. 3.13A.1**). Importantly, light-activation of RA^+ NPs further increased the numbers of $benzidine^+$ cells (**Fig. 3.13A.2**). We complemented these results by examining the effect of soluble RA and light-sensitive RA^+ NPs in the induction of human acute promyelocytic leukemia (APL)-derived NB4 cells differentiation. This process was monitored the expression of CD11b, a marker of myeloid maturation. RA^+ NPs were much more effective (from 100 up to 1000 fold) than soluble RA in inducing CD11b expression (**Fig. 3.13B.1**). Furthermore, cells treated with RA^+ NPs activated by light showed higher (from 1.5 to 2 fold) differentiation into the myeloid lineage than cells treated with non-activated RA^+ NPs (**Fig. 3.13B.2**). Importantly, the differentiation effect exerted by the NPs is mediated by the intracellular delivery of RA since the supernatant of NPs suspended in media for 6 days at 37 °C had no significant effect in the differentiation of NB4 cells (data not shown). We also evaluated the differentiation capacity of light-activatable RA^+ NPs in APL cells having chimeric PLZF/RARα fusion protein resulting from a translocation between chromosomes 11 and 17 [284, 285]. APL caused by PLZF/RARα is morphologically indistinguishable from APL caused by PML/RARα and exhibits impaired sensitivity to RA [286, 287]. We have analyzed the differentiation of a U937 promonocytic leukemia clone transduced with a

zinc-inducible U937 cell system expressing the PLZF/RARA fusion protein (U937-B412). Our results show that the induction of PLZF/RARα expression by zinc in U937-B412 cells decreases their ability to differentiate into myeloid cells ($CD11b^+$ cells) as compared to cells without PLZF/RARα expression (**Fig. 3.13C and Fig. 3.14**). However, U937-B412 cells treated with RA^+ NPs were more prone to differentiate into myeloid cells (approximately 1000 fold) than cells treated with soluble RA (**Fig. 3.13C.1**). Moreover, cells treated with light-activated RA^+ NPs show higher (from 2 to 4 fold depending on the differentiation time and NP concentration) capacity for myelocytic differentiation than cells treated with non-activated RA^+ NPs (**Figs. 3.13C.2 and 3.13C.3**).

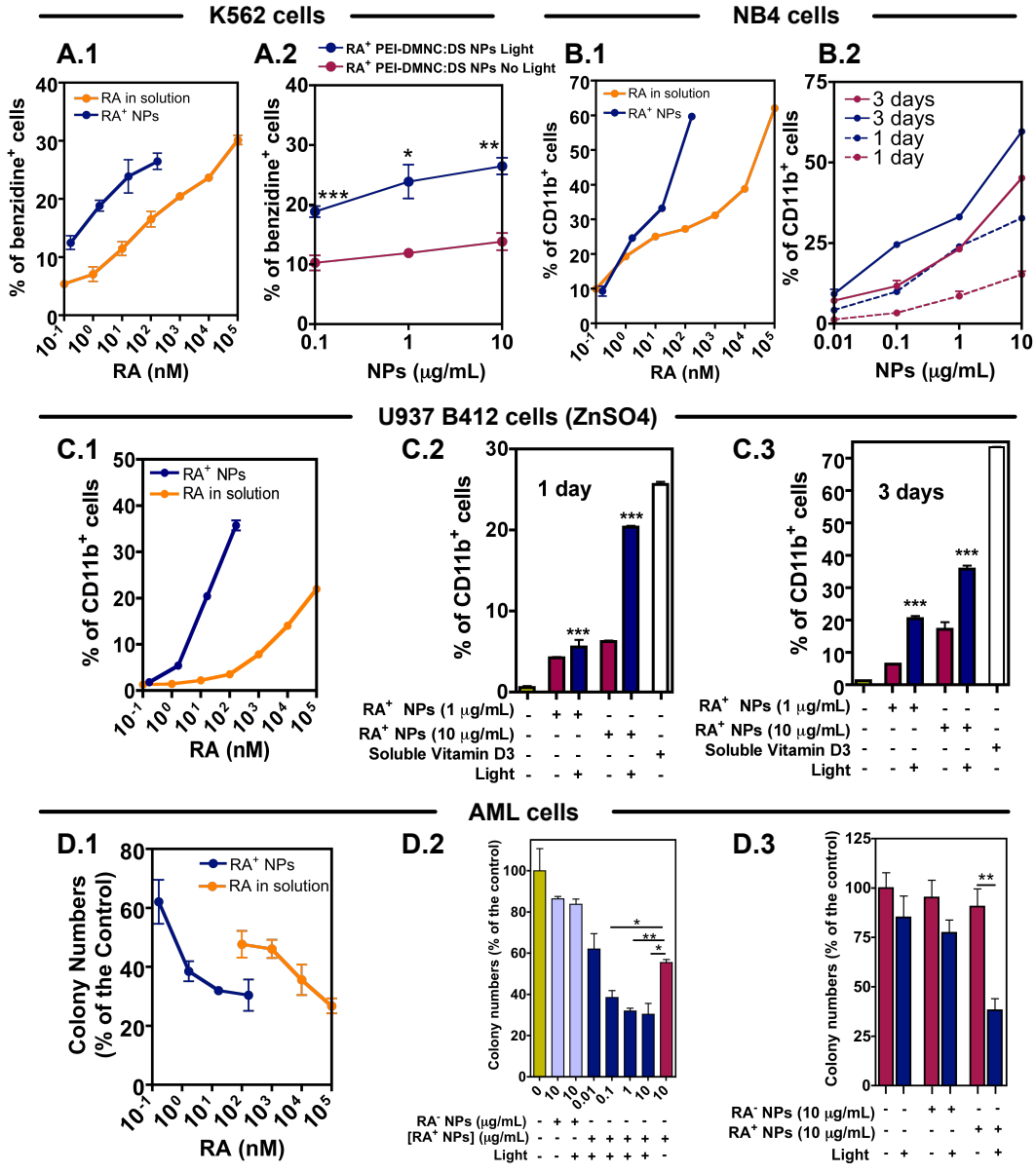

Figure 3.13 – Effect of RA^+ NPs on human leukemia cells. In the case of cells treated with NPs, cells were treated with RA^+ NPs for 4 h, washed, activated or not with UV light (365 nm, 100 Watts) for 5 min, and then

cultured for a certain period of time. In case of cells treated with soluble RA, cells were cultured in media containing soluble RA for the entire period of culture. (A.1) Erythroid differentiation of human leukemia K562 cells cultured with light-activated NPs or soluble RA. K562 cells were cultured for 6 days. (A.2) Percentage of benzidine$^+$ cells in K562 cells after 6 days of culture. (B.1) Myelocytic differentiation (CD11b$^+$ cells) of human leukemia NB4 cells cultured with light-activated NPs or soluble RA. NB4 cells were cultured for 3 days. (B.2) Percentage of CD11b$^+$ cells in NB4 cell cultures after 1 and 3 days of culture. (C.1) Myelocytic differentiation (CD11b$^+$ cells) of human Zn-induced U937-B412 cells cultured with light-activated NPs or soluble RA. Zn-induced U937-B412 cells were cultured for 3 days. (C.2 and C.3) Percentage of CD11b$^+$ cells in Zn-induced U937-B412 cell cultures after 1 day (C.2) or 3 days (C.3) of culture. Cells cultured with 10^{-7} M of vitamin D3 for 1 or 3 days were used as positive controls. (D.1 and D.2) Differentiation of AML stem cells cultured with light-activated NPs or soluble RA. Cell differentiation was evaluated by a colony forming unit assay at day 14. (D.2) AML stem cells were cultured for 14 days with RA in medium (10^2 – 10^5 nM) or RA$^+$ NPs (0.01 – 10 μg/mL) or blank NPs (10 μg/mL), exposed or not to UV light. Cell differentiation was evaluated by a colony forming unit assay at day 14. (D.3) Long-term culture-initiating cell assay results. AML stem cells were cultured on feeder layers for 5 weeks and then on methylcellulose medium for 14 days with blank NPs (10 μg/mL) or RA$^+$ NPs (10 μg/mL) exposed or not to UV light. Results are expressed as a mean percentage of control plates containing only AML cells. Results are expressed as Mean ± SEM (n = 3). *P<0.05, **P<0.01, ***P<0.001.

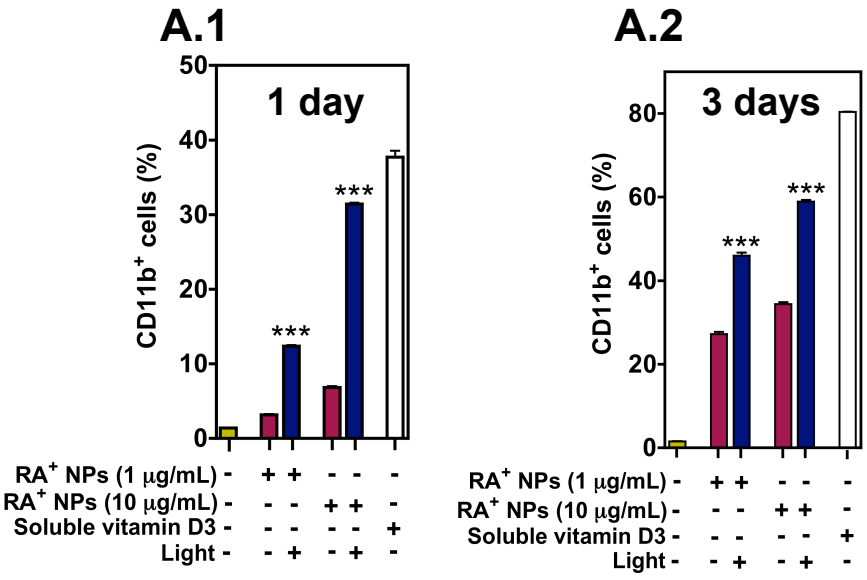

Figure 3.14 – Myelocytic differentiation of human leukemia U937-B412 cells without zinc-induction. (A.1) Percentage of CD11b$^+$ cells in U937-B412 cells cultures without zinc-induction after being exposed for 1 day to various concentrations of light-sensitive RA$^+$ NPs, exposed or not to UV light (365 nm, 100 Watts, 5 min) after a 4h-period of internalization and 1300 rpm centrifugation washing step, or cultured with 10^{-7} M of vitamin D3 (Sigma) in culture medium during 1 day. (A.2) Percentage of CD11b$^+$ cells in U937-B412 cells cultures without zinc-induction after being exposed for 3 day to various concentrations of light-sensitive RA$^+$

NPs, exposed or not to UV light (365 nm, 100 Watts, 10 min) after a 4h-period of internalization and 1300 rpm centrifugation washing step, or cultured with 10^{-7} M of vitamin D3 (Sigma) in culture medium during 3 day.

The potential of our optonanomedicine system was further assessed against $CD34^+$ primary leukemic cells isolated from the bone marrow aspirates of patients with AML taken at diagnosis. We evaluated their clonogenic potentials in short term (blast colony-forming cells, CFC) and long term (long-term culture-initiating cell, LTC-IC) assays following treatment with RA or RA^+ NPs. Our results indicate that light-activatable RA^+ NPs were more effective than soluble RA at decreasing the number of CFCs (from 100 to 1000 fold) (**Fig. 3.13D.1**). Cell treatment with blank NPs (RA^- NPs) activated or not with light had no significant effect in the CFC number relative to control (**Fig. 3.13D.2**). Our results further indicate that RA^+ NPs activated by light are more effective in decreasing the number of CFCs as well as LTC-ICs (**Fig. 3.13D.3**) than non-activated RA^+ NPs.

3.3.4 – Remotely activation of the NP formulation *in vivo*

Next, we evaluated if RA^+ NPs can function *in vivo*. NB4 cells were cultured with RA^+ NPs for 4 h, washed and activated *ex-vivo* by exposure to a 405 nm blue laser (80 mW) for 5 min, embedded in Matrigel and then injected into a cylindrical poly(dimethylsiloxane) (PDMS) construct that has been previously implanted subcutaneously in NOD/SCID recipients (**Fig. 3.15A**). The PDMS cylinder was used to restrict cell position inside the animal. After 5 days, human cells were isolated from the implants and CD11b expression measured by flow cytometry (**Figs. 3.15B.1–3.15B.3**). Consistent with the *in vitro* data, CD11b expression was statistical higher in NB4 cells treated with *ex vivo* light-activated RA^+ NPs than in cells treated with RA^+ NPs without light activation (**Fig. 3.15C**). The experiment was then repeated but this time with *in vivo* activation. One day after implantation the recipients were exposed to a 405 nm blue optical fibre for 5 min at the sites of the implants that contained the cells (**Fig. 3.15D**). After 3 days the recipients were sacrificed, human cells isolated and CD11b expression was assessed. CD11b expression was higher in NB4 cells from mice that had been exposed to the blue laser demonstrating that internalised RA^+ NPs can be activated to release RA *in vivo* in a highly controlled manner (**Fig. 3.15E**).

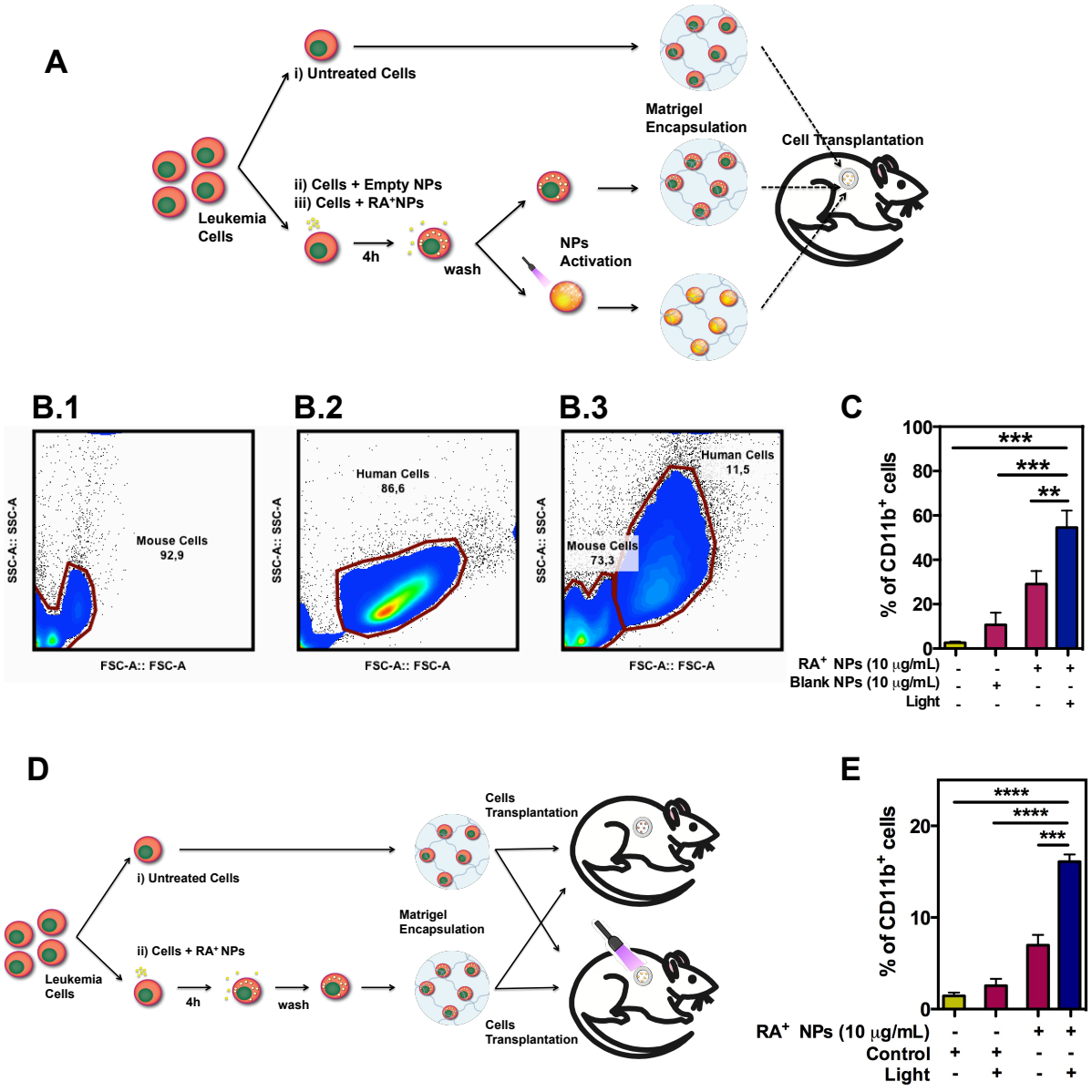

Figure 3.15 – *In vivo* differentiation of NB4 cells exposed to light-activatable RA$^+$ NPs. (A) Schematic representation of the *in vivo* experimental set up. Cells were treated with blank or RA$^+$ NPs (10 μg/mL) for 4 h, washed, and then activated or not with a blue optical fiber (405 nm, 80 mW) for 5 min. Cells were then resuspended in a 1:1 (v/v) Matrigel solution and subcutaneously injected in a PDMS cylinder construct implanted in the dorsal region of mice. After 5 days, cells were removed from the construct and characterized by FACS, for CD11b expression. (B) Representative flow cytometry plots. Representative flow cytometry plots showing mice recipient cells (B.1), human leukemia NB4 cells (B.2) and a mixture of mice recipient cells with human leukemia NB4 cells (B.3). (C) Percentage of CD11b$^+$ cells in human leukemia NB4 cells collected 5 days after subcutaneously injection. Results are expressed as Mean ± SEM (n = 4). *P<0.05, **P<0.01, ***P<0.001. (D) Schematic representation of the *in vivo* set up. Cells were treated with RA$^+$ NPs (10 μg/mL) for 4 h, washed and then encapsulated in a 1:1 (v/v) Matrigel solution and subcutaneously injected in a PDMS cylinder construct implanted in the dorsal region of mice. After 24 h, some experimental groups were activated *in vivo* with a blue optical fiber for 5 min. (E) Percentage of CD11b$^+$ cells in human leukemia NB4 cells

collected 3 days after the *in vivo* activation. Results are expressed as Mean ± SEM (n = 3). ***P<0.001, ****P<0.0001.

3.4 – Discussion

In this study, we developed an efficient light-activatable polymeric NP for the spatio-temporal release of RA in leukemic cells. We showed the efficiency of the release both *in vitro* and *in vivo*. The efficiency is due to a combination of several factors including (i) high internalization in terms of kinetics (in the first 4-6 h) and in magnitude (60 and 75 pg of NPs per cell following exposure for 4 h to cell culture medium containing 100 μg/mL of NPs), (ii) high endolysomal escape (80% of the NPs escape the endolysomal compartment in the first 2 h; this is approximately 18 pg of NPs per cell), (iii) durable intracellular accumulation of the NPs (no exocytosis mediated by Pgp; accumulation for more than 5 days in $CD34^+$ cells) and (iv) fast disassembly of the NPs once activated by UV or blue light (minutes range).

The NP formulation described here is irreversible disassembled by a photochemical process (UV or blue laser). Several light-activatable polymeric NPs have been reported[273], however the internalization and intracellular trafficking of these NPs containing bioactive agents and their effect in the modulation/differentiation of cells both *in vitro* and *in vivo* has not been studied. Here, we demonstrate the precise spatial and temporal control in the release of RA. We show for the first time that cells transfected with light-activatable NPs can be activated after 2 days while maintaining the same inductive properties. This gives an opportunity to use cells as "Trojan horses" for activation at specific sites of human body.

Although several NP formulations have been reported for the release of RA, including from our group [133, 136], no formulation can release high doses of RA (120 μg of RA per mg of NP) in minutes-range. This is very important to enhance the differentiation of leukemic cells, in particular in APL caused by PLZF/RARα, which exhibits impaired sensitivity to RA [286, 287]. In this case, the light-activated RA^+ NPs enhanced 2-4 fold the differentiation of the leukemic cells as compared to cells treated with non-activated RA^+ NPs.

Our results show that the release of RA induces efficiently the terminal differentiation of leukemic cell lines (NB4, K562 and U937) and $CD34^+$ cells isolated from the bone marrow of AML patients, at levels that were not possible with soluble RA.

Previously, liposomes [140] and block copolymer NPs [146] have been used for the release of RA in myeloid leukemia cell lines. However, no significant differences were observed between liposome/NP formulations and soluble RA in their capacity to induce leukemia cell differentiation into myeloid cells. It is possible that the enhanced differentiation observed with our formulation is due to a combined effect of high concentration of RA with zinc release from the NP formulation, which is important for the activity of zinc-finger proteins. Because the therapeutic efficiency of liposome RA formulations have been demonstrated in clinical trials (the formulation had a better pharmacokinetic profile than oral RA (non-liposome), maintained higher and sustained plasma drug concentrations, and induced less molecular remissions in APL patients [141, 288]), the formulation described in this work might add therapeutic value.

Light-activatable NPs are mainly internalized by clathrin-mediated endocytosis (dynasore inhibits 90% of NP uptake) and they rapidly (first 2 h) escape the endosomal compartment. Clathrin-mediated endocytosis has been reported for lipid NPs [278]; however, macropinocytosis has also been identified as a major entry pathway of NPs [278, 282]. Our siRNA data indicates that macropinocytosis is also involved in the internalization of the NPs but at minor extent than clathrin-mediated endocytosis. The mechanism of escape of the NPs from the endosomal compartment (13 pg of NPs per cell, i.e. 40% of the internalized NPs, in the first 2 h) is unclear. We could not detect endosomes bursting during NP trafficking by live cell imaging. It is possible that the positive NPs interact with the ionic lipids of endosomes creating small holes and facilitating their escape as previously reported for lipid NPs[278]. The high escape of the NPs from the endosomal compartment likely decreased their exocytosis, which is very beneficial for the therapeutic effect of our formulation. Exocytosis is a very often process in NPs taken up by normal [289] and leukemic cells. Exocytosis might occur by the induction in the expression of Pgp that is an energy-dependent drug efflux pump. Indeed, previous studies have highlighted the role of p-glycoprotein-associated multi-drug resistance (MDR) in retinoid-resistant disease [290].

In summary, we have established an opto-nanomedicine approach for the treatment and study of leukemic (stem) cells either *in vitro* or *in vivo*. This approach allows remote control in the release of biomolecules with spatio-temporal resolution. These light-activatable NPs might be suitable for general therapeutic and regenerative medicine applications.

3.5 – Methods

3.5.1 – Preparation and characterization of poly(ethyleneimine) (PEI) conjugated with 4,5-dimethoxy-2-nitrobenzyl chloroformate (DMNC)

DMNC (DS100: 194.1 mg; DS25: 48.5 mg, Sigma) was slowly added to a solution of PEI in DMSO (2 mL containing 50 mg/mL PEI, Sigma) containing triethylamine (DS_{100}: 98.2 μL; D_{25}: 24.5 μL, Sigma), and the reaction flask cooled to 0 ºC by immersion on ice. Then, the reaction was allowed to proceed for 24 h at 25 ºC with stirring. At the end, the PEI-DMNC conjugate was purified by dialysis (Spectra/Por® 1 Regenerated Cellulose dialysis membrane, MWCO 6000-8000 Da, Spectrum) against DMSO overnight at room temperature. Reaction yields above 54% were obtained using a dialysis purification methodology. For NMR characterization, PEI-DMNC (in DMSO) was precipitated in water, washed, freeze-dried, and then dissolved (10 mg/mL) in DMSO-d6 and ^{1}H NMR spectra were acquired using a Bruker Avance III 400 MHz spectrometer.

3.5.2 – Preparation of NPs

Non-activatable NPs were prepared by the electrostatic interaction of PEI (polycation) with dextran sulfate (DS, polyanion) in water, at room temperature, as previously described by us [133]. Briefly, an aqueous DS solution (1 mL, 10 mg/mL) was added drop-by-drop to an aqueous solution of PEI (5 mL, 10 mg/mL) and stirred for 5 min. Then, an aqueous solution of $ZnSO_4$ (0.6 mL; 1 M) was added and stirred for 30 min. The NP suspension was then dialyzed (Spectra/Por® 1 regenerated cellulose dialysis membrane, MWCO 6000-8000 Da, Spectrum) for 24 h, in the dark, against an aqueous solution of mannitol (5 %, w/v), lyophilized for 1 day and stored at 4 ºC before use.

Light-activatable NPs were prepared by adding a PEI-DMNC solution (66.7 μL, 150 mg/mL, in DMSO) to an aqueous solution of DS (5 mL, 0.4 mg/mL) and stirred for 5 min. Then, an aqueous solution of $ZnSO_4$ (120 μL, 1 M) was added and stirred for 30 min. The NP suspension was then dialyzed (Spectra/Por® 1 Regenerated Cellulose dialysis membrane, MWCO 6000-8000 Da, Spectrum) for 24 h, in the dark, against an aqueous solution of mannitol (5 %, w/v), lyophilized for 1 day and stored at 4 ºC before use. In some cases, PEI-

DMNC was labeled with Qdot525. For that purpose, an aqueous solution of 1-ethyl-3-(3-dimethyllaminopropyl)carbodiimide hydrochloride (EDC); 500 μL of EDC (10 mg/mL, aqueous solution at pH 6.0)) was added to a suspension of Qdots525 (0.16 mmoles, in 310 μL of PBS). After 5 min, PEI-DMNC solution (200 μL, 25 mg/mL in DMSO) was added to the previous solution and allowed to react for 1 h, in the absence of light, at room temperature.

For the preparation of NR-containing NPs, initially a NR solution (60 μL, 2% w/v, in DMSO) was added to a solution of PEI–DMNC (66.7 μL, 150 mg/mL in DMSO) and maintained at room temperature for 30 min, under stirring. The solution was then carefully added to an aqueous solution of DS (5 mL, 0.4 mg/mL) and stirred for 5 min. The NPs in suspension were treated with an aqueous solution of $ZnSO_4$ (120 μL; 1 M) for 30 min. NR that was not encapsulated in the NPs was removed by centrifugation (2,000 g for 3 min). The NP suspension was then dialyzed (Spectra/Por® 1 Regenerated Cellulose dialysis membrane, MWCO 6000-8000 Da, Spectrum) for 24 h, in the dark, against an aqueous solution of mannitol (5 %, w/v), lyophilized for 1 day and stored at 4 ºC before use. For the preparation of RA-containing NPs, a RA solution (24 μL, 50 mg/mL, in DMSO) was added to a solution of PEI-DMNC (66.7 μL, 150 mg/mL in DMSO). The subsequent steps were similar to the ones described above for NR-containing NPs.

For the preparation of fluorescently labeled NPs, NPs (2 mg) were resuspended in 0.1 M carbonate/bicarbonate buffer (1 mL, pH 8.3) followed by the addition of FITC or TRITC (5 mL in DMSO, 3-fold molar excess). The NP suspension was stirred for 1 h in the absence of light and then dialyzed (Spectra/Por® 1 regenerated cellulose dialysis membrane, MWCO 6000-8000 Da, Spectrum) for 24 h against an aqueous solution of mannitol (5 %, w/v), lyophilized, and stored at 4 ºC before use.

3.5.3 – Characterization of the NPs

The diameter of the NPs was measured by photon correlation spectroscopy (PCS) using quasi-elastic light scattering equipment (Zeta-Pals™ Zeta Potential Analyzer, Brookhaven Instruments Corp., Holtsville, NY) and ZetaPlus™ Particle Sizing Software (version 4.03). To measure NP diameter, the NP suspension (2 mL, 50 μg/mL in water for molecular biology) was added to a cuvette and allowed to stabilize for 10 min. The sample was then vortexed for 5 s and subjected to NP size analysis in the ZetaPlus™ for 3 min (3

times; all data were recorded at 90º). After each reading the cuvette was again vortexed for 5 s and exposed to UV light (365 nm) or blue light (405 nm) for a certain period of time (see below). The values of NP diameter and NP counts were recorded. The average diameters described in this work are number-weighted average diameters. The zeta potential of NPs was determined in a 1 mM KCl pH 6 solution, at 25 °C (2 mL, 50 μg/mL). All data were recorded with at least 5 runs (in triplicate) with a relative residual value (measure of data fit quality) of 0.03. The diameter of NPs was also confirmed by ultra-high-resolution analytical FE-SEM SU-70 with a dedicated detector of STEM. Diluted NP suspensions (in H_2O) were placed on a 400-mesh 3 mm copper grid coated with a carbon support film (Taab Labs Ltd.) and dried overnight.

3.5.4 – Cell Culture

Human umbilical vascular endothelial cells (HUVECs) were obtained from Lonza and cultured in EGM-2 medium (Lonza) in a CO_2 incubator at 37 ºC, 5 % CO_2 in a humidified atmosphere, with media changes performed every other day. Cells were passaged every 2-5 days and used for experiments between passage 4 and 6. Human chronic myelogenous leukemia K562 cells, kindly provided by Dr. Veronica Buckle (Weatherall Institute of Molecular Medicine) were cultured in RPMI-1640 (Gibco) in a CO_2 incubator at 37 ºC, 5 % CO_2 in a humidified atmosphere, supplemented with 10 % fetal bovine serum (FBS) (Gibco) and 100 U/mL PenStrep (Lonza). Human bone marrow acute promyelocytic leukemia NB4 cells, kindly provided by Dr. Arthur Zelent (Institute of Cancer Research, Royal Cancer Hospital) were cultured in RPMI-1640 (Gibco) in a CO_2 incubator at 37 ºC, 5 % CO_2 in a humidified atmosphere, supplemented with 10 % FBS (Gibco) and 100 U/mL PenStrep (Lonza). Human myelomonoblastic cell lines U937-MT and U937-B412 [291], kindly provided by Dr. Estelle Duprez (Centre de Recherche en Cancérologie de Marseille, France), were maintained at exponential growth in RPMI-1640 medium suplemented with 10% FBS (Gibco) and 100 U/mL of PenStrep. U937-MT is the empty vector control and U937-B412 contains PLZF/RARα cDNA under the control of the zinc inducible human-metallothionein promoter [291]. For PLZF/RARα induction cells were stimulated with 0.1 mM $ZnSO_4$ for at least 24 h.

3.5.5 – NP cytotoxicity studies

NPs were suspended in a solution of milli-Q water with PenStrep (5 μL/mL of 10000 U/mL stock solution, Lonza) and Fungizone (2.5 μg/mL, Sigma-Aldrich) for 30 min, centrifuged (14,000 g for 10 min), and finally resuspended in serum free cell culture medium. K562, NB4 and U937 cells (0.1×10^6 cells/condition) were incubated in serum free RPMI-1640 for 4 h in a 96-well plate containing variable amounts of PEI-DMNC:DS NPs. Once the incubations were terminated the cells were washed gently with medium to remove NP excess, and half of the samples were exposed to UV light (365 nm, 100 W) for 10 min. The cells were then cultured for 20 h in 100 μL of complete medium (RPMI-1640 medium supplemented with 10 % FBS (Gibco) and 100 U/mL PenStrep). A CellTiter-Glo® luminescent cell viability assay (ATP, Promega, USA) was performed according to the recommendations of the vendor.

3.5.6 – Assessment of histone γH2AX phosporylation (DNA damage) induced by UV light or blue light irradiation

HUVEC cells (passage 4) were cultured on 1 % gelatin-coated slides until subconfluency in EGM-2, followed by exposure to UV light (365 nm, 100 W) or blue light (405 nm, 80 mW) for 1, 3, 5, 10, 15, 30 or 60 min, in triplicates. Control conditions did not receive any light radiation. Following treatment, the medium was replaced by fresh medium and the cells were incubated for additional 6 h on normal culture conditions. The cells were then fixed with 4 % paraformaldehyde (Electron Microscopy Sciences) for 10 min at room temperature and then washed with PBS. The cells were then permeabilized with 1 % (v/v) Triton-X, blocked with PBS + 2 % BSA and stained for 1 h with anti-human primary γH2AX antibody (clone: N1-431, BD Biosciences). Detection was done with secondary antibody anti-mouse Cy3 conjugate (Jackson ImmunoResearch). Cell nuclei were stained with 4',6-diamidino-2-phenylindole (DAPI) (Sigma), and the slides were mounted with mounting medium (Dako) and examined with a Zeiss inverted fluorescence microscope.

3.5.7 – NP internalization studies

NP internalization studies were performed initially by flow cytometry in K562 and AML cells derived from human bone marrow aspirates of AML patients. K562 or AML cells (0.1×10^6 cells/condition) were incubated for 4 h in serum free RPMI-1640 or serum free Ex-Vivo medium (Lonza) containing TRITC-labeled NPs (10 μg/mL), respectively, in a 6 well plate. Once the incubations were terminated, the cells were centrifuged at 1300 rpm, 20 ºC for 5 min, washed one time with cold trypan blue solution (200 μL; 600 μg/mL), re-washed 3 times with cold PBS and then resuspended in PBS containing 2.5 % FBS (500 μL), ready for FACS analysis. A total of 10,000 events were recorded per measurement. In some conditions, AML cells were cultured in StemSpan SFEM (Stemcell Technologies) supplemented with a human cytokine cocktail containing SCF (50 ng/mL, Stemcell Technologies), TPO (15 ng/mL) and Flt-3L (50 ng/mL, PeproTech) plus PenStrep (10,000 U/mL, Lonza) and Fungizone (25 μg/mL, Sigma) for 5 days after NPs internalization for 4 h.

NP internalization was also monitored by inductive coupled plasma mass spectrometry (ICP-MS). In this case, the intracellular levels of Zn were measured before and after cell exposure to NPs. K562, NB4 and U937 cells (0.1×10^6 cells/well) were plated in 24 well plates and incubated in serum free RPMI-1640 from 1 to 24 h with variable amounts of PEI-DMNC:DS NPs. After incubations, NPs that have were not internalized by the cells were washed three times with PBS an the cells centrifuged followed by the addition of an aqueous solution of nitric acid (1 mL, 69 % (v/v)). The samples (n = 3) were analyzed by ICP-MS for the concentration of intracellular levels of Zn. The concentration of Zn was normalized per cell. The estimation of NPs was done based on controlled standard solutions.

3.5.8 – NP uptake studies

U937 cells were cultured on 24 well plates (1×10^5 cells/well) and inhibited by one of the following chemicals during 30 min before adding a suspension of TRITC-labelled NPs (5 μg/mL): dynasor (80 μM), cytochalasin D (10 μM), nocodazole (50 uM), filipin III (100 μM) and polyinosinic acid (100 μg/mL). The inhibitor concentrations were based in values reported in literature and further validated by us to have no cytotoxic effect over the period of the assay (6 h), as confirmed by ATP assay. The incubation of the cells with NPs for different times was performed in the presence of the inhibitor. As controls, we used cells

without NPs and cells incubated with NPs without inhibitor. At the end of each time point, cells were centrifuged at 1300 rpm, 20 ºC for 5 min with PBS, washed one time with cold trypan blue solution (200 μL; 600 μg/mL), re-washed 3 times with cold PBS and then resuspended in PBS containing 2.5 % FBS (500 μL) for FACS analysis. A total of 10,000 events were obtained per measurement. To validate the inhibitory activity of dynasor we performed uptake studies of FITC-labeled transferrin, known to selectively enter cells via clatherin-mediated endocytosis. Briefly, U937 cells were cultured on 24 well plates (1×10^5 cells/well) and treated or not with dynasor (80 μM, 30 min pre-incubation), followed by addition of 1 μg/mL FITC-labeled transferrin (Life Technologies). The transferrin was allowed to bind for 3 min at 4 ºC. Cells were then evaluated as before.

The NP uptake mechanism was also studied on U937 cells by silencing specific proteins of clathrin-mediated endocytosis (CLTC and LDLR), caveolin-mediated endocytosis (CAV1), GEEC-CCLIC pathways (CDC42) and macropinocytosis (RAC1 and CTBP1) by siRNA (Thermo Fisher). Transfection was performed in a 24 well plate with 0.5×10^5 cells in antibiotic-free complete medium with 100 nM siRNA and 1.5 μL of Lipofectamine RNAiMAX (Life Technologies) transfection reagent for 24 h. After this initial period, the transfection medium was replaced by complete medium and the cells incubated for another 48 h. Then, cells were cultured with TRITC-labelled NPs (5 μg/mL) for 6 h. Once the incubations were terminated, the cells were centrifuged at 1300 rpm, 20 ºC for 5 min, with PBS, washed one time with cold trypan blue solution (200 μL; 600 μg/mL), re-washed 3 times with cold PBS and then resuspended in PBS containing 2.5 % FBS (500 μL) for FACS analysis. Non-transfected cells or cells transfected with lipofectamine but without siRNAs (MOCK) were used as controls. In all FACS analysis, a total of 10,000 events were recorded per run. All conditions were performed in triplicate.

3.5.9 – Intracellular trafficking analysis

HUVEC cells (passage 4) were cultured on 1% gelatin-coated slides until subconfluency in EGM-2. The cells were then incubated with 1 μg/mL FITC-labeled NPs for 1 or 4 hours, washed extensively, exposed or not to UV light (365 nm, 100 W), cultured in normal conditions for 1 or 2/8 additional hour/s, respectively. For LysoTracker staining, at time points 2, 6 and 12 hours, the cells were incubated with 50 nM LysoTracker Red DND-99 (Invitrogen). After 30 min of incubation, the coverslips were washed extensively with

PBS, followed by cell fixation with 4 % paraformaldehyde (Electron Microscopy Sciences) for 10 min at room temperature and then washed with PBS. Cell nuclei were stained with DAPI (Sigma), and the slides were mounted with mounting medium (Dako) and examined with a Zeiss LSM 50 confocal microscope.

Co-localization analysis was performed by culturing HUVEC cells (passage 4) on 1 % gelatin-coated slides until subconfluency in EGM-2. Cells were treated with 1 μg/mL FITC-labeled NPs for 1 or 4 hours, washed extensively and cultured in normal conditions for 1 or 1/8 additional hour/s, respectively. Then the cells were fixed with 4 % paraformaldehyde (Electron Microscopy Sciences) for 10 min at room temperature, blocked with 2 % (w/v) BSA, and when necessary, permeabilized with 0.5 % (v/v) Triton-X. Cells were then stained for 1 h with anti-human primary antibodies (EEA1, clone: C45B10, Cell Signaling), Rabankyrin-5 (ANKFY1 (D-15), Santa Cruz Biotechnology), or Rab 7 (clone: D95F2, Cell Signaling). In each immunofluorescence experiment, an isotype-matched IgG control was used. Binding of primary antibodies to specific cells was detected with anti-rabbit or anti-goat IgG Cy3 conjugate (Jackson ImmunoResearch). Cell nuclei were stained with DAPI (Sigma), and the slides were mounted with mounting medium (Dako) and examined with a Zeiss LSM 50 confocal microscope. Co-localization analysis was done in ImageJ through assessment of the percentage of overlapping objects. Two objects are considered to be co-localizing when their intensity profile is overlaping more than 40 %. For this analysis the number (percentage of FITC-labeled NPs foci that are positive for EEA-1/Rab-5/Rab-7) and the intensity volume (percentage of FITC-labeled NPs in the EEA-1/Rab-5/Rab-7-positive compartments) were used. This approach was found to be more adequate than classical co-localization tools in ImajeJ or other softwares that measure pixel co-occurrence and correlation analyses, because it allowed us to (i) discriminate between background and vesicle/ NP-foci fluorescence and (ii) interpret the results in terms of percentage of NP-foci that are localized to vesicles in another channel of interest.

3.5.10 – Intracellular accumulation of NPs

To determine exocytose of NPs, NP uptake assays were performed in the presence of Pgp antagonist verapamil or the endosome disruption agent chloroquine. U937 cells were cultured on 24 well plates (1×10^5 cells/well) and chloroquine (100 μM, no pre-incubation) and verapamil (100 μM, 60 min pre-incubation) conditions were tested. The chemical agents

concentrations were based on values reported in the literature and further validated by us to have no cytotoxic effect over the period of the assay (12 h). After the pre-incubation with the chemical agents, TRITC-labelled PEI-DMNC:DS NPs (10 μg/mL) or TRITC-labelled poly-L-lysine USPIO NPs (100 μg/mL) were added to the cells, maintaining the chemical agents concentration. As controls we used cells incubated without NPs and cells incubated with NPs without chemical agents. At the end of each experiment, the cells were centrifuged at 1300 rpm, 20 ºC for 5 min with PBS, washed one time with cold trypan blue solution (200 μL; 600 μg/mL), re-washed 3 times with cold PBS and then resuspended in PBS containing 2.5 % FBS (500 μL) for FACS analysis. A total of 10,000 events were recorded per measurement, and all conditions were performed in triplicate.

3.5.11 – RARE cell line generation

The cignal lenti RARE reporter kit (CLS-016L SABiosciences) was used for the establishment of a RA reporter NB4 cell line. For that purpose, rectronectin solution (15 μg/cm^2, 30 μg, 500 μL on PBS, Takara) was plated in a 24-well plate 2 hours prior to cell seeding. The plate was kept at room temperature and was washed one time, immediately before seeding, with PBS. NB4 cells (1×10^5) were plated in 175 μL of RPMI-1640 medium (Gibco) supplemented with 0.5 % FBS and 100 U/mL PenStrep and to this condition 125 μL of cignal lentiviral particles were added to a total experimental volume of 300 μL. After a gentle swirl of the plate the cells were incubated 20 hours at 37 ºC in a humidified incubator with 5 % CO_2 atmosphere. In the following day, cells were washed and allowed to recover in the incubator for 24 hours cultured in 500 μL of fresh RPMI-1640 medium supplemented with 10 % FBS and 100 U/mL PenStrep. After that, 2 μg/mL of puromycin (Invitrogen) was added to the culture medium for selection of transduced cells. Evaluation of selection efficiency in puromycin-containing medium was performed every 3 days for a period of 5 weeks.

3.5.12 – Luciferase assay

To assess the biological effect of RA in RAR-regulated signalling pathway activity, luciferase reporter assay was performed. NB4-RARE cells (2.5×10^4 cells/condition) were plated in v-shaped 96-well plates and cultured with soluble RA (10 μM) or light-activatable

RA^+ NPs (5 μg/mL). The NPs were suspended in serum free medium and added to cells for 1 h. The cells were then washed by centrifugation (1300 rpm, 5 min) to remove non-internalized NPs, and half of the samples were exposed to blue light (405 nm, 80 mW, 5 min). The cells were then cultured for 12/24 hours in RPMI-1640 medium supplemented with 10 % FBS and 100 U/mL PenStrep. After these incubation times, the conditions were centrifuged (1500 rpm, 3 min), excess medium carefully aspirated and the cells washed with 100 μL of PBS. After a new centrifugation and removal of PBS, 60 μL of cell lysis buffer (8 mM of magnesium chloride; 1 mM DL-Dithiothreitol; 1 mM Ethylenediaminetetraacetic acid; 25 mM of 1 M Trizma Base with 1 M Sodium phosphate monobasic; 15 % Glycerol; and 1 % Triton X-100), was added to each condition. The plate was kept on ice, under agitation for 15 min to allow complete lysis and then the plate was placed on -80 ºC for the amount of time necessary for the samples to freeze. After these steps, the plate was removed from the -80 ºC, put on ice and allowed to defrost at slow rate.

For the preparation of the luminescence reading, 40 μL of ATP (100 μM, Sigma) was added to 1960 μL of reading buffer solution (8 mM of magnesium chloride; 1 mM DL-Dithiothreitol; 1 mM Ethylenediaminetetraacetic acid; 25 mM of 1 M Trizma Base with 1 M Sodium phosphate monobasic; and 15 % Glycerol) to a final concentration of 2 μM ATP. On a second tube, 2 mL of D-Luciferin working solution (167 μM, Sigma) was prepared protected from light. The injection system of the luminometer was primed until ready. Following that step, the luminometer software was programmed to set the temperature to 37 ºC, and under stirring for the duration of the experiment accept 50 μL of sample per condition in a 96-white plate, inject 100 μL of ATP working solution 3 seconds after reading cycle begins; inject 100 μL of D-Luciferin working solution 4 seconds after reading cycle begins and read the luminescence 5 seconds after reading cycle begins. The luciferase luminescence was quantified in a microplate luminometer reader LumiStar Galaxy (BMG Labtech). All conditions were performed in triplicate.

3.5.13 – [^{3}H]RA internalization studies

[11, 12-^{3}H(N)]-Retinoic acid, 50.4 Ci/mmol, was purchased from Perkin Elmer. [^{3}H]RA solution for cell culture assays was prepared on the day of experiments by dissolving [^{3}H]RA in DMSO with unlabelled RA in a 1:1000 ratio to a final concentration of 10 μM of RA. [^{3}H]RA solution in DMSO for the preparation of NPs was prepared on the day of

experiments using a 1:4000 ratio of labelled to unlabelled RA. Experiments were initiated by the adding the [^{3}H]RA solution (1 μM and 10 μM; representing less than 1% in volume of the total cell culture medium) or [^{3}H]RA-NP suspension (1 μg/mL and 10 μg/mL) to cultures (60,000 cells/condition, 24-well plate, 1 mL) of K562, NB4 and U937 cells. In case of soluble RA, cells (K562, NB4 or U937; 60,000 cells/condition, 24-well plate) were cultured with medium containing [^{3}H]RA (1 μM and 10 μM; 1 mL of medium) for 24 or 72 h, washed with PBS (2 times), harvested, lysed with lysis buffer (100 μL) and kept on ice until scintillation counting procedure. In case of RA-containing NPs, cells (same conditions as for soluble RA) were cultured with [^{3}H]RA-NPs (1 μg/mL and 10 μg/mL) for 4 h, washed with PBS and cultured for additional 20 or 68 h in the respective culture medium. Cells were then collected to eppendorfs, washed with PBS, centrifuged (1500 rpm, 5 min), lysed with lysis buffer (see above) and kept on ice until scintillation counting procedure. The lysed samples (100 μL) were mixed with liquid scintillation fluid (1 mL; Packard Ultima Gold) and the scintillations counted in a TriCarb 2900 TR Scintillation analyser (Perkin Elmer).

3.5.14 – Time-activation of NPs within cells

NB4 and Zn-induced U937-B412 cells (6.0×10^4 cells/condition) were plated in 24-well plates and transfected with RA^+ NPs (1 μg/mL) for different time periods (1, 2, 4, 6, 8, 12 and 24 h). The cells were then washed by centrifugation (1300 rpm, 5 min) to remove non-internalized NPs, and immediately exposed to UV light (365 nm, 100 W, 5 min). In a second experimental setup, NB4 and Zn-induced U937-B412 cells (6.0×10^4 cells/condition) were plated in 24-well plates and transfected with RA^+ NPs (1 μg/mL) for 4 h. The cells were then washed by centrifugation (1300 rpm, 5 min) to remove non-internalized NPs, cultured in normal conditions and exposed to UV light (365 nm, 100 W, 5 min) at different time points (0, 4, 8, 20 and 44 h). The effect of the intracellular release of RA was evaluated in terms of differentiation of the cells into the myeloid lineage (as assessed by the expression of CD11b) at day 3, as assessed by flow cytometry. All conditions were performed in triplicate.

NB4-RARE cells (2.5×10^4 cells/condition) were plated in v-shaped 96-well plates and transfected with RA^+ NPs (1 μg/mL) for different time points (1, 2, 4, 6, 8, 12 and 24 h). The cells were then washed by centrifugation (1300 rpm, 5 min) to remove non-internalized NPs, and immediately exposed to UV light (365 nm, 100 W, 5 min). For the second

experimental setup, NB4-RARE cells (2.5×10^4 cells/condition) were plated in v-shaped 96-well plates and transfected with RA^+ NPs (1 μg/mL) for 4 h. The cells were then washed by centrifugation (1300 rpm, 5 min) to remove non-internalized NPs, cultured in normal conditions and exposed to UV light (365 nm, 100 W, 5 min) at different time points (0, 4, 8, 20 and 44 h). The cells were then cultured for 12 hours after each condition light activation in RPMI-1640 medium supplemented with 10 % FBS and 100 U/mL PenStrep. After these procedures luciferase luminescence was quantified as described above for the luciferase assays. All conditions were performed in triplicate.

3.5.15 – Multiple activation of NPs within cells

Myelocytic differentiation of Zn-induced U937 cells was assessed by the quantification of CD11b expression by flow cytometry. U937-B412 cells (6.0×10^4 cells/condition) were cultured with $ZnSO_4$ (0.1 mM) in culture medium up to 24 h prior to experiment to induce the expression of PLZF/RARα. Then cells were transfected with RA^+ NPs (1 μg/mL) for 4 h, washed, placed in normal culture medium and then different activated by UV light (365 nm, 100 W, 5 min). Cells without light activation were used as control. The following conditions were tested: i) single light activation at 4 h; ii) light activations at 4 h and 6 h; iii) light activations at 4 h, 6 h and 8 h and iv) light activations at 4 h, 6 h, 8 h and 10 h. After 3 days, expression of CD11b on U937 cell surface was measured by staining with a fluorescent (PE)-conjugated anti-CD11b mAb (BD Biosciences) using FACS. All conditions were performed in triplicate.

3.5.16 – K562 differentiation assay

Erythroid differentiation of K562 cells was assessed by cytochemical staining with benzidine solution. K562 cells (6.0×10^4 cells/condition) were exposed to a wide range of free-RA concentrations for 6 days. Since RA display a very low solubility, DMSO was used to dissolve RA to the culture medium before cell culture experiments (final concentration of DMSO was below 0.01 % in culture medium). To investigate the effect of RA^+ NPs on K562 differentiation, K562 cells (6.0×10^4 cells/condition) were transfected with RA^+ NPs (from 0.01 up to 10 μg/mL; in serum-free medium) for 4 h, washed by centrifugation (1300 rpm, 5 min) to remove NP excess, and part of the samples exposed to UV light (365 nm, 100 W, 5

min). The cells were then cultured for 6 days in complete medium (RPMI-1640 medium supplemented with 10 % FBS (Gibco) and 100 U/mL PenStrep), after which they were stained by a benzidine solution (to stain the heme groups of erythrocytes).

The benzidine stock solution was prepared by dissolving benzidine dihydrochloride (20 mg, Sigma) in glacial acetic acid (292 μL) and water (9.7 mL) solution. The working solution was prepared by mixing part of the benzidine stock solution (1 mL) with 30 % H_2O_2 (20 μL, Panreac). The staining was performed by mixing 50 μL of K562 cells (in the evaluated condition medium) with benzidine working solution at a 1:1 (v/v) ratio, at room temperature for 3 minutes. Following the staining the number of positive cells was determined using a hemocytometer. The staining was performed in three individual experiences for all conditions.

3.5.17 – NB4 differentiation assay

Myelocytic differentiation of NB4 cells was assessed by quantifying the CD11b expressing population, using flow cytometry. NB4 cells (6.0×10^4 cells/condition) were plated in 24-well plates and cultured with soluble RA or light-activatable RA^+ NPs. The NPs were suspended in serum free medium and added to cells for 4 h. The cells were then washed by centrifugation (1300 rpm, 5 min) to remove non-internalized NPs, and half of the samples were exposed to UV light (365 nm, 100 W, 5 min). The cells were then cultured for 6 days in RPMI-1640 medium supplemented with 10 % FBS (Gibco) and 100 U/mL PenStrep with half medium changes every 3 days. Conditioned medium (CM) was obtained from the centrifugation of RA^+ NPs (10 μg/mL) in culture medium for 6 days. After 1, 3 and 6 days, expression of CD11b on NB4 cell surface was measured by FACS using a fluorescent (PE)-conjugated anti-CD11b antibody (BD Biosciences, ICRF44 clone). All conditions were performed in triplicate.

3.5.18 – U937 differentiation assay

Myelocytic differentiation of U937 cells was assessed by the quantification of CD11b expression by flow cytometry. U937-B412 cells (6.0×10^4 cells/condition) were cultured either with or without $ZnSO_4$ (0.1 mM). To induce the expression of PLZF/RARα in U937-B412 cells they were treated for 24 h with $ZnSO_4$ (0.1 mM). Then cells were treated with

soluble RA or light-activatable RA^+ NPs (transfection for 4 h followed by light activation for 5 min) for 3 days. After 1 and 3 days, expression of CD11b on U937 cell surface was measured by staining with a fluorescent (PE)-conjugated anti-CD11b mAb (BD Biosciences) using FACS. All conditions were performed in triplicate.

3.5.19 – Relative gene expression of RAR-α, RAR-β and RAR-γ (normalized to GAPDH) in leukemia cell lines

RNA was extracted using TRIzol® (Ambion) and RNAeasy mini kit (Qiagen) and cDNA was obtained from 1 μg RNA using TaqMan® Reverse Transcription Reagents (Invitrogen), according to supplier's instructions. Gene expression levels of RAR-α, RAR-β and RAR-γ (normalized to GAPDH) in NB4 and U937-B412 Zn-induced or not were quantified with Power SYBR® Green PCR Master Mix using a 7500 Fast Real-Time PCR System (Applied Biosystems, Foster City, USA). Specific primer pairs were CCATCCTCAGAACTCACAA and ACCAGCGAGAATTAATACCT for RAR-α, CACCTAGAGGATAAGCACTT and GGACTCACTGACAGAACA for RAR-β, CCACCTTCTTGCTCCTAC and CTTTCACCCTCTGTTCCT for RAR-γ, AGCCACATCGCTCAGACACC and GTACTCAGCGCCAGCATCG for GAPDH, forward and reverse, respectively. Thermal cycling conditions were 30 s at 94 °C, 30 s at 60 °C and 33 s at 72 °C, for 40 cycles, followed by a melting curve.

3.5.20 – AML differentiation assay

AML bone marrow mononuclear cells isolated by Ficoll-Histopaque (GE Healthcare) gradient centrifugation, enriched using the MACS CD34 isolation kit (Miltenyi Biotec) and cryopreserved were kindly provided by Dr. Rajeev Gupta (Department of Haematology, UCL Cancer Institute). The isolated $CD34^+$ AML cells were maintained in StemSpan SFEM (Stemcell Technologies) supplemented with a human cytokine cocktail containing SCF (50 ng/mL, Stemcell Technologies), TPO (15 ng/mL) and Flt-3L (50 ng/mL, PeproTech) plus PenStrep (10,000 U/mL, Lonza) and Fungizone (25 μg/mL, Sigma) up to 3 days. Prior to the colony-forming cell (CFC) and long-term culture-initiating cell (LTC-IC) assays, AML cells were incubated for 4 h in Ex-Vivo (Lonza) serum free medium, with and without blank NPs or RA^+ NPs in a 24 well plate. After that time, the cells were washed to remove loosely

bound NPs. For the CFC assays (2.0 x 10^5 cells/condition) AML cells were plated in triplicate in MethoCult H4230 (3 mL, StemCell Technologies) supplemented with SCF [50 ng/mL], IL-3 [10 ng/mL], and Flt-3L [50 ng/mL], all human, plus PenStrep (10,000 U/mL, Lonza) and Fungizone (25 μg/mL, Sigma) in 6-well plate. For some conditions UV light (365 nm, 100 W, 5 min) was used to activate RA^+ NPs. Cultures were scored after 14 days for the presence of clusters and colonies containing >20 cells using an inverted microscope. LTC-IC assays were performed in triplicate in a 6-well plate gelatinized for 2 hours prior to adding the feeders. The feeder layer was composed of a 1:1 mixture of irradiated (80 Gy) SL/SL (1.5×10^4 cells/condition) and M210B4 mouse fibroblasts (1.5×10^4 cells/condition), kindly provided by Dr. Rajeev Gupta (Department of Haematology, UCL Cancer Institute). AML cells (1×10^6 cells/condition) were plated in Myelocult H5100 medium (StemCell Technologies), supplemented with Flt-3L [50 ng/mL], hydrocortisone [10^{-6} M] (StemCell Technologies) and PenStrep (10,000 U/mL, Lonza) and fungizone (25 μg/mL, Sigma). For some conditions UV light (365 nm, 100 Watts, 5 min) was used to trigger RA release. After the cells were inoculated, weekly half medium changes were performed (with Flt-3L [100 ng/mL]) for the duration of the culture. After 5 weeks, all cells were harvested and placed into methylcellulose based assay for the detection of AML-CFC as described above.

3.5.21 – *In vivo* study

All animal work has been conducted according to relevant national and international guidelines and approved by the Bioethics Committee of University of Salamanca. On the day before injecting the cells, PDMS cylindrical constructs (∅internal = 1.0 cm; ∅external = 1.5 cm) were implanted subcutaneously on NOD/SCID mice (Jackson Laboratory) maintained in pathogen-free conditions with irradiated chow. For the *ex-vivo* activation studies in the day of the experiment, NB4 cells were suspended in serum free medium with (i) no NPs, (ii) with empty NPs (10 μg/mL) or RA^+ NPs (10 μg/mL) for 4 h. At the end, cells were washed by centrifugation (1300 rpm, 5 min), and the ones treated with RA^+ NPs were either activated or not with a blue laser (405 nm, 80 mW) for 5 min. NB4 cells (5×10^6 cells per PDMS construct) were injected subcutaneously in the center of the PDMS construct embedded in Matrigel (200 μL, BD Biosciences). Five days after injection of the cells, animals were sacrificed by cervical dislocation and cells within the cylindrical construct were collected and characterized by flow cytometry. For the *in vivo* activation studies in the day of the

experiment, NB4 cells were suspended in serum free medium with (i) no NPs, (ii) with RA^+ NPs (10 μg/mL) for 4 h. At the end, cells were washed by centrifugation (1300 rpm, 5 min), and 5×10^6 NB4 cells per PDMS construct were injected subcutaneously in the center of the PDMS construct embedded in Matrigel (200 μL, BD Biosciences). One day after injection, some of both conditions under study were either activated or not with a blue optical fiber (405 nm, 80 mW) for 5 min. Three days after injection of the cells, animals were sacrificed by cervical dislocation and cells within the cylindrical construct were collected and characterized by flow cytometry.

CHAPTER 4
CONCLUSIONS AND FUTURE WORK

4.1 – General conclusions

An estimated 200 000 cases of leukemia occur annually which result in 145 000 deaths [2]. The work carried out in this thesis focused in the development of a new therapeutic approach to treat acute myelocytic leukemia (AML) that represents 37% of the cases. Current therapies include chemotherapy followed or not by stem cell transplantation. The combination of RA and anthracyclin-based chemotherapy is currently the standard therapy for myelocytic leukemia (AML), specifically APL [141]. Unfortunately, ca. 25% of the patients die in a 5-years period of time. In addition, when the treatment is successful side effects are typically observed. The hypothesis of this thesis is that controlled drug delivery systems able to increase the intracellular concentration of RA and the time of its presentation will increase its therapeutic efficacy in leukemia cells (**Fig. 4.1**). Regarding the time of RA presentation, the hypothesis in this thesis is that leukemic cells might act as carriers to transport NPs to the bone marrow. Once the cells are at the bone marrow, NPs inside the cells can be activated and release RA to induce the differentiation of the transporting cells. This differentiation process will impact the homeostasis of the niche and might block the resistance observed after conventional therapy.

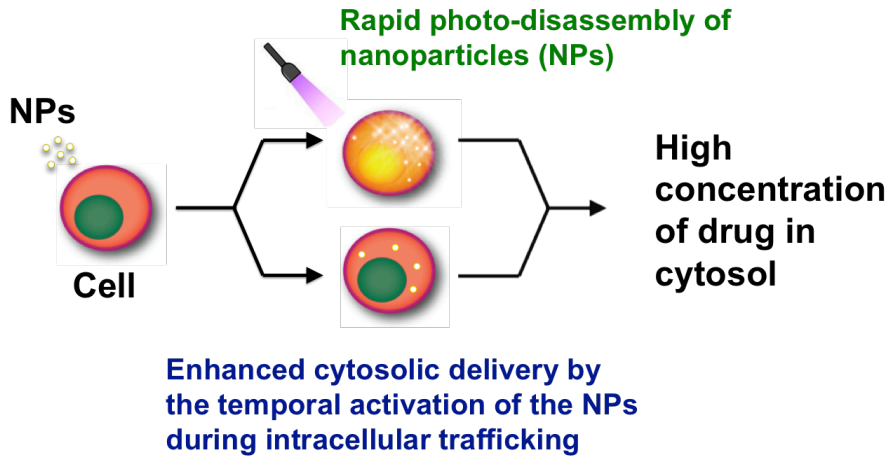

Figure 4.1 – Schematic illustration of therapeutic hypothesis. Drug delivery systems that enhance the intracellular concentration of the differentiating agent and the time of its presentation will increase therapeutic efficacy.

In this thesis we show for the first time the preparation of light-activatable polymeric NPs that are able to encapsulate and release rapidly (minutes range) RA when exposed to light. NPs were prepared by first modifying chemically a polycationic polymer (polyethyleneimine) with a light-sensitive compound, which promoted light-responsiveness to the conjugate, and then complexing it with dextran sulphate and RA. These NPs had an effective diameter ranging from 140-170 nm and a positive zeta potential of (+ 22 mV), being stable in cell culture medium. Our results show that PEI-DMNC:DS NPs are good carriers of RA with the capacity to encapsulate 120 μg of RA per mg of NP. We further show the light-sensitive properties of RA^+ PEI-DMNC:DS NPs after UV light (365 nm) or blue laser (405 nm, 80 mW) exposure, in conditions that do not damage cell DNA. In addition, we show that RA^+ PEI-DMNC:DS NPs are rapidly internalize by HUVECs, leukemia cell lines and $CD34^+$ primary leukemic cells isolated from the bone marrow aspirates of patients with AML. Leukemia cells internalize RA^+ PEI-DMNC:DS NPs mainly by clathrin-mediated endocytosis and at minor extent by macropinocytosis. Importantly, NPs escape rapidly endosomal compartment and accumulate in the overall cell cytoplasm, without inducing cytotoxicity for concentrations below 100 μg/mL. Our results further show that RA^+ PEI-DMNC:DS NPs can remain inside cells for very long periods of time (at least 48 h), while keeping their light-sensitive properties. This is a unique property that opens the possibility to activate the cells when they reach the bone marrow and interfere directly with the stem cell niche (work being carried out).

Light-activatable NPs are very effective to deliver RA within leukemic cells. Our results show that RA^+ NPs induce higher activation of RA receptors as soluble RA and this is because light-activatable NPs can release up to 4 pg of RA per cell, while cells treated with soluble RA had 0.05 pg per cell. It should be noted that the release of RA in current polymeric nanoparticles [146] or liposomes [140, 141] is by passive diffusion or mediated by the degradation of the NP matrix. This is a slow process without any possibility of control [146]. Therefore, our light-activatable NP formulation can release higher doses of RA than conventional formulations at the desired time.

Light activated RA^+ NPs successfully induced the differentiation of both RA-responsive and RA-resistant leukemia cell lines. Light activated RA^+ NPs induce 1.92 (± 0.17) times higher levels of erythroid differentiation in K562, 1.19 (± 0.01) times of granulocytic differentiation in NB4 and 1.45 (± 0.03) times of granulocytic differentiation in U937 cells as compared to non-activated NPs. In addition, light-activated RA^+ NPs induce 1.83 (± 0.17) times higher levels of erythroid differentiation in K562, 1.12 (± 0.01) times of

granulocytic differentiation in NB4 and 1.44 (± 0.04) times of granulocytic differentiation in U937 cells as compared to 1 μM RA in solution. It should be noted that RA^+ NPs contain 10 times less RA than the one used in solution. This experimental result is particularly important in the RA-resistant cell line U937-PLZF/RARA where the high RA intracellular release is able to overcome the low sensitivity of the cell. Cells treated with light activated RA^+ NPs show a 4-fold higher differentiation profile after 24 h than cells treated with non-activated NPs.

Our results also show that light activated RA^+ NPs decrease the clonogenic potential of $CD34^+$ leukemia cells from bone marrow aspirates of human AML patients. When AML stem cells were treated with light-activated RA^+ NPs we are able to observe 69.6 ± 9.2 % and 61.8 ± 10.1 % less colonies of undifferentiated stem cells, in CFC and LTC-IC colony assays, respectively. The results also demonstrate that cells treated with blank NPs (RA^- NPs) activated or not with light had no significant effect in the CFC number relatively to control, and reinforce the notion that triggered burst release of RA is more effective in decreasing the number of CFCs as well as LTC-ICs as non-activated conditions.

Human leukemia cells loaded with RA^+ NPs can be activated *in vivo* by a blue laser and differentiate successfully into the myelocytic lineage. Our results show that cells cultured with RA^+ NPs for 4 hours, washed, activated with a blue laser for 5 min, embedded in matrigel and injected subcutaneously in a cylindrical construct implanted in the animal the day before to restrict cell positioning *in vivo*, successfully differentiate into the myelocytic lineage, something that wasn't observed for the conditions treated with blank NPs or non-activated RA^+ NPs. Importantly, the same observation was monitored when instead of performing the activation of RA^+ NPs *ex vivo*, the light activation procedure took place *in vivo*. To the best of our knowledge, the results described in this thesis are the first demonstration of the *in vivo* activation of light-activatable NP formulations to modulate cell activity/differentiation.

The light-activatable NP formulation described in this thesis compares favourably to other formulations to treat leukemia. Nanoformulations that are under evaluation in clinical trials (**Chapter 2**, **Section 2.4**, **Table 5**) or are clinically approved for leukemia therapy [104, 106], still fail to deliver efficiently the therapies, even presenting superior pharmacokinetics comparing to conventional therapies [91, 182]. Until now, available therapies and formulations fail to achieve high transfection efficiency, accumulation in the cytoplasm and release the drug in a tuneable and precise fashion with therapeutic relevance. In fact, the release over a long period of time of low concentrations of drug could lead to the

development of MDR [292], compromising the therapeutic outcome. The formulation presented in this thesis might overcome this issue since a high concentration of RA is released in the cell cytoplasm inducing a rapid cell differentiation process. Importantly, this effect is mediated by the light-activation of the formulation, since the magnitude of this effect was not observed with the non-activated NP formulation. Overall, the combination of high RA encapsulation capacity, high internalization efficiency and intracellular stability, the rapid degradation and RA release when exposed to light create a unique therapeutic value proposition to reach new levels of control over cellular processes. The capacity that the formulation presents to remain intracellularly without loosing RA and light responsiveness capability over a long period of time provides a new opportunity for therapeutic intervention, allowing physicians to tailor the therapeutic process in a controlled fashion. Among the most interesting opportunities of intervention is the HSC niche, that due to their characteristics promotes chemoresistance and maintenance of a poll of leukemic cells that are responsible for future relapses. The direct intervention in the bone marrow could open new therapeutic avenues for blood-related cancers.

Importantly, the presented light-activatable NP formulation might also offer opportunities in other therapeutic fields or regenerative medicine applications. For example, our formulation could be employed to increase the efficiency of intracellular siRNA delivery, since current approaches lack full success [278, 282].

4.2 – Future work

The present dissertation illustrates the potential application of light-activatable polymeric NPs in the intracellular release of bioactive agents in cells. Micro- and nanoscale science and technology has captured the public and scientific imagination like few techno-scientific projects before. From its speculative beginnings as an envisioned “science of the very small”, it quickly developed into a multi-billion dollar enterprise, reshaping science policy and traditional scientific disciplines [293]. Researchers that wish to value their findings and take their research to the next level should learn how to do it. The number of startup companies involved in the interface of nanotechnology and biotechnology is increasing at a surprising rate and governments, corporations and venture capitalist invested $17.8 billion in nanoscale products and nanotechnology systems in 2010 [294]. For some entrepreneurs, nanotechnology will be their business, but for a wider pool of companies will

use nanotechnology to improve their existing products. The true challenge for researchers that what to become entrepreneurs with their existing technologies is asking: how does my technology apply to existing products, and does it create a tangible increase in its value proposition?

Future work should address the potential clinical translation opportunities of light-activatable polymeric NPs, based on the results presented on this dissertation. Two possible areas that could particularly benefit from the work developed are: (i) ocular drug delivery [295]; and (ii) topical drug delivery [296]. Ocular drug transport barriers pose a challenge for drug delivery comprising the ocular surface epithelium, the tear film and internal barriers of the blood-aqueous and blood-retina barriers. Ocular drug delivery efficiency depends on the barriers and the clearance from the choroidal, conjunctival vessels and lymphatic. Traditional drug administration reduces the clinical efficacy especially for poor water soluble molecules and for the posterior segment of the eye. Light-activatable polymeric NPs could overcome these barriers, increase the drug penetration at the target site and importantly, control drug delivery levels by the use of laser sources commonly used in ocular treatments, with lower doses and without any toxicity compared to the conventional eye drops. Also the treatment of the human skin opens opportunities for clinical translation of light-activatable polymeric NPs presented in this dissertation. Human skin not only functions as a permeation barrier (mainly because of the stratum corneum layer) but also provides a unique delivery pathway for therapeutic and other active agents. These compounds penetrate via intercellular, intracellular, and transappendageal routes, resulting in topical delivery (into skin strata) and transdermal delivery (to subcutaneous tissues and into the systemic circulation). Light-activatable polymeric NPs would be especially suitable in the approach of the pathology, pathogenesis, and topical treatment approaches of dermatological diseases, such as psoriasis, contact dermatitis, and skin cancer. By combining the advantages of nanosized drug carrier, high drug-loading capacity and controlled triggered burst release using methodologies already employed in the clinic, light-activatable polymeric NPs open new research and clinical opportunities that should be addressed in future work.

Based on the constraints regarding the wavelength sensitivity of the studied light-activatable polymeric NPs, and the restrictions regarding deep tissue nanoformulation activation, further work is required to evaluate the feasibility of the use of fibre-optics *in vivo*, to modulate nanoformulation triggered burst release, and measure the effects of these manipulations in real-time. However, these tools rely on fibre-optic probes, attached to a power source and surgically inserted into the tissue, to transmit light and stimulate photo-

activation *in vivo*, representing important constrains that should be taken into account. With this in mind, an alternative is the development of near infrared light-sensitive NPs. Some of this work has been already started in our lab. Our preliminary data show that is possible to activate NPs located centimetres far from the skin.

In leukemia, cancer-propagating cells (CPCs) are able to rebuild the niche to evade chemotherapy. A great challenge in leukemia is to target CPCs inside the niche. Our technology is currently being tested to target the stem cell niche. Cells will act as "Trojan Horses", transporting the NPs until the bone marrow. The differentiation of the cells will be then induced by light. Finally the differentiation of the cells will modulate the homeostasis of the niche (**Fig. 4.2**) (work being carried out).

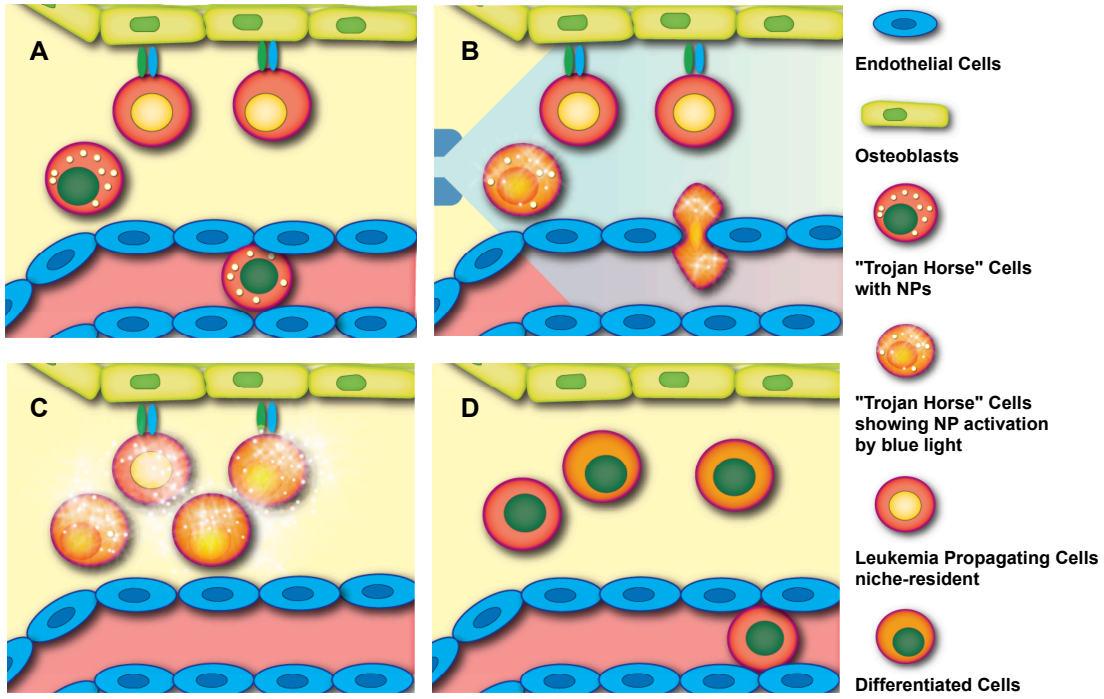

Figure 4.2 – Schematic representation of the trojan horse strategy for induction of differentiation and exhaustion of the leukemia cancer niche. (A) Syngeneic "Trojan horse" leukemia cells are employed to transport RA^+ NPs to the bone marrow niche. (B) Remote blue light activation induces controlled intracellular release of RA in the "Trojan horse" cells. (C) Niche-resident leukemia propagating cells receive paracrine signalling from the "Trojan horse" cells. (D) The paracrine effect successfully induces differentiation of the niche-resident leukemia propagating cells.

The light-activatable NPs developed in the present thesis might have potential for different regenerative medicine applications. For example, the light-activatable NPs might be useful to modulate stem cell niche in order to enhance HSC engraftment after transplantation. RA has been described as a key regulator of HSC development [297] and the

release of this molecule at the bone marrow niche is still unclear. However, many other molecules could be employed through the developed nanocarrier to facilitate HSC expansion and engraftment.

Additional studies are needed to further confirm the mechanisms and *in vivo* behaviour of light-activatable polymeric NPs. In Chapter 3, the use of these NPs to study *in vivo* light-activation raised several intriguing questions concerning their biological activity. Future work should focus in addressing the effective delivery of light-activatable polymeric NPs to the niche, addressing all concerns regarding the safety of the procedure, the successful induction of cell differentiation only after homing in the diseased niche and through the assessment of the impact that light-activation alone could have in such delicate microenvironment. These answers will open clear possibilities to take the formulation further into clinical trials for the treatment of leukemia stem cells.

The translation of scientific knowledge to the clinic is an essential step towards the creation of a strong economic base capable of leveraging new scientific discoveries. The need to invest in research on bioengineering, especially on bionanomedicine, is heightened by the current healthcare crisis and the coming demographic challenges that are increasing healthcare costs to a critical level. Only through innovation and convergent technologies it would be possible to push medicine towards a more personalized, accessible and affordable level with more effective prevention and treatment, which no longer accepts harmful side effects as a trade-off for effective cure [298]. Although engineering approaches to scientific studies are guiding nanotechnology towards success, future breakthrough materials and enabling tools will still face significant hurdles to their implementation. Considerable economic obstacles must be overcome to achieve the successful commercialization of nanomedicine-based products, since securing the substantial financial funds is daunting. Furthermore, large pharmaceutical companies have been slow to embrace nanotechnology-based products and have left many of the initial studies and most of development and investment risk to start-up companies. Another, very different obstacle, involves the general public's perception of nanotechnology. In general, scientists and engineers, including those working in nanomedicine, have failed to accurately and successfully communicate results to a lay audience and follow though on promised potential technological outcome. These obstacles should be taken into consideration as future efforts converge on solid scientific, technical and clinical goals, accelerating nanomedicine´s progress in conjugation with improved public communication and awareness by making better use of abundant media resources.

References

1. Degos, L. and Z.Y. Wang, *All trans retinoic acid in acute promyelocytic leukemia.* Oncogene, 2001. **20**(49): p. 7140-7145.

2. Jemal, A., et al., *Global cancer statistics.* CA Cancer J Clin, 2011. **61**(2): p. 69-90.

3. Robak, T. and A. Wierzbowska, *Current and emerging therapies for acute myeloid leukemia.* Clin Ther, 2009. **31 Pt 2**: p. 2349-70.

4. Norsworthy, K., L. Luznik, and I. Gojo, *New treatment approaches in acute myeloid leukemia: review of recent clinical studies.* Rev Recent Clin Trials, 2012. **7**(3): p. 224-37.

5. Roboz, G.J., *Current treatment of acute myeloid leukemia.* Curr Opin Oncol, 2012. **24**(6): p. 711-9.

6. Leung, W., et al., *Late effects of treatment in survivors of childhood acute myeloid leukemia.* J Clin Oncol, 2000. **18**(18): p. 3273-9.

7. Berman, E., *Long-Term and Late Effects of Treatment in Adults Facts*. 2012, Leukemia & Lymphoma Society.

8. Hanahan, D. and R.A. Weinberg, *The hallmarks of cancer.* Cell, 2000. **100**(1): p. 57-70.

9. Hanahan, D. and R.A. Weinberg, *Hallmarks of cancer: the next generation.* Cell, 2011. **144**(5): p. 646-74.

10. Society, A.C., *Cancer Facts & Figures 2014*. 2014, American Cancer Society: Atalanta.

11. O'Brien, C.A., A. Kreso, and J.E. Dick, *Cancer stem cells in solid tumors: an overview.* Semin Radiat Oncol, 2009. **19**(2): p. 71-7.

12. Esteller, M., *Epigenetics in cancer.* N Engl J Med, 2008. **358**(11): p. 1148-59.

13. Schwartz, G.K. and M.A. Shah, *Targeting the cell cycle: a new approach to cancer therapy.* J Clin Oncol, 2005. **23**(36): p. 9408-21.

14. Malumbres, M. and M. Barbacid, *Cell cycle, CDKs and cancer: a changing paradigm.* Nat Rev Cancer, 2009. **9**(3): p. 153-66.

15. Collins, K., T. Jacks, and N.P. Pavletich, *The cell cycle and cancer.* Proc Natl Acad Sci U S A, 1997. **94**(7): p. 2776-8.

16. Wang, J.C. and J.E. Dick, *Cancer stem cells: lessons from leukemia.* Trends Cell Biol, 2005. **15**(9): p. 494-501.

17. Reya, T., et al., *Stem cells, cancer, and cancer stem cells.* Nature, 2001. **414**(6859): p. 105-11.

18. Jordan, C.T., M.L. Guzman, and M. Noble, *Cancer stem cells.* N Engl J Med, 2006. **355**(12): p. 1253-61.

19. Lapidot, T., et al., *A cell initiating human acute myeloid leukaemia after transplantation into SCID mice.* Nature, 1994. **367**(6464): p. 645-8.

20. Bonnet, D. and J.E. Dick, *Human acute myeloid leukemia is organized as a hierarchy that originates from a primitive hematopoietic cell.* Nat Med, 1997. **3**(7): p. 730-7.

21. Eppert, K., et al., *Stem cell gene expression programs influence clinical outcome in human leukemia.* Nat Med, 2011. **17**(9): p. 1086-93.

22. Konopleva, M.Y. and C.T. Jordan, *Leukemia stem cells and microenvironment: biology and therapeutic targeting.* J Clin Oncol, 2011. **29**(5): p. 591-9.

23. Lutz, C., et al., *Identifying leukemia stem cells--is it feasible and does it matter?* Cancer Lett, 2013. **338**(1): p. 10-4.

24. Jordan, C.T., *The leukemic stem cell.* Best Pract Res Clin Haematol, 2007. **20**(1): p. 13-8.

25. Becker, M.W. and C.T. Jordan, *Leukemia stem cells in 2010: current understanding and future directions.* Blood Rev, 2011. **25**(2): p. 75-81.

26. Hogan, C.J., E.J. Shpall, and G. Keller, *Differential long-term and multilineage engraftment potential from subfractions of human CD34+ cord blood cells transplanted into NOD/SCID mice.* Proc Natl Acad Sci U S A, 2002. **99**(1): p. 413-8.

27. le Viseur, C., et al., *In childhood acute lymphoblastic leukemia, blasts at different stages of immunophenotypic maturation have stem cell properties.* Cancer Cell, 2008. **14**(1): p. 47-58.

28. Gibbs, K.D., Jr., et al., *Decoupling of tumor-initiating activity from stable immunophenotype in HoxA9-Meis1-driven AML.* Cell Stem Cell, 2012. **10**(2): p. 210-7.

29. Goardon, N., et al., *Coexistence of LMPP-like and GMP-like leukemia stem cells in acute myeloid leukemia.* Cancer Cell, 2011. **19**(1): p. 138-52.

30. Taussig, D.C., et al., *Leukemia-initiating cells from some acute myeloid leukemia patients with mutated nucleophosmin reside in the CD34(-) fraction.* Blood, 2010. **115**(10): p. 1976-84.

31. Taussig, D.C., et al., *Hematopoietic stem cells express multiple myeloid markers: implications for the origin and targeted therapy of acute myeloid leukemia.* Blood, 2005. **106**(13): p. 4086-92.

32. Bakker, A.B., et al., *C-type lectin-like molecule-1: a novel myeloid cell surface marker associated with acute myeloid leukemia.* Cancer Res, 2004. **64**(22): p. 8443-50.

33. van Rhenen, A., et al., *The novel AML stem cell associated antigen CLL-1 aids in discrimination between normal and leukemic stem cells.* Blood, 2007. **110**(7): p. 2659-66.

34. Hosen, N., et al., *CD96 is a leukemic stem cell-specific marker in human acute myeloid leukemia.* Proc Natl Acad Sci U S A, 2007. **104**(26): p. 11008-13.

35. Jan, M., et al., *Prospective separation of normal and leukemic stem cells based on differential expression of TIM3, a human acute myeloid leukemia stem cell marker.* Proc Natl Acad Sci U S A, 2011. **108**(12): p. 5009-14.

36. Majeti, R., et al., *CD47 is an adverse prognostic factor and therapeutic antibody target on human acute myeloid leukemia stem cells.* Cell, 2009. **138**(2): p. 286-99.

37. Saito, Y., et al., *Identification of therapeutic targets for quiescent, chemotherapy-resistant human leukemia stem cells.* Sci Transl Med, 2010. **2**(17): p. 17ra9.

38. Hoang, V.T., A. Zepeda-Moreno, and A.D. Ho, *Identification of leukemia stem cells in acute myeloid leukemia and their clinical relevance.* Biotechnol J, 2012. **7**(6): p. 779-88.

39. Essers, M.A. and A. Trumpp, *Targeting leukemic stem cells by breaking their dormancy.* Mol Oncol, 2010. **4**(5): p. 443-50.

40. Lane, S.W., D.T. Scadden, and D.G. Gilliland, *The leukemic stem cell niche: current concepts and therapeutic opportunities.* Blood, 2009. **114**(6): p. 1150-7.

41. Schofield, R., *The relationship between the spleen colony-forming cell and the haemopoietic stem cell.* Blood Cells, 1978. **4**(1-2): p. 7-25.

42. Scadden, D.T., *The stem cell niche in health and leukemic disease.* Best Pract Res Clin Haematol, 2007. **20**(1): p. 19-27.

43. Scadden, D.T., *The stem-cell niche as an entity of action.* Nature, 2006. **441**(7097): p. 1075-9.

44. Morrison, S.J. and D.T. Scadden, *The bone marrow niche for haematopoietic stem cells.* Nature, 2014. **505**(7483): p. 327-34.

45. Calvi, L.M., et al., *Osteoblastic cells regulate the haematopoietic stem cell niche.* Nature, 2003. **425**(6960): p. 841-6.

46. Stier, S., et al., *Osteopontin is a hematopoietic stem cell niche component that negatively regulates stem cell pool size.* J Exp Med, 2005. **201**(11): p. 1781-91.

47. Fleming, H.E., et al., *Wnt signaling in the niche enforces hematopoietic stem cell quiescence and is necessary to preserve self-renewal in vivo.* Cell Stem Cell, 2008. **2**(3): p. 274-83.

48. Nilsson, S.K., et al., *Osteopontin, a key component of the hematopoietic stem cell niche and regulator of primitive hematopoietic progenitor cells.* Blood, 2005. **106**(4): p. 1232-9.

49. Adams, G.B., et al., *Stem cell engraftment at the endosteal niche is specified by the calcium-sensing receptor.* Nature, 2006. **439**(7076): p. 599-603.

50. Katayama, Y., et al., *Signals from the sympathetic nervous system regulate hematopoietic stem cell egress from bone marrow.* Cell, 2006. **124**(2): p. 407-21.

51. Kollet, O., et al., *Osteoclasts degrade endosteal components and promote mobilization of hematopoietic progenitor cells.* Nat Med, 2006. **12**(6): p. 657-64.

52. Avecilla, S.T., et al., *Chemokine-mediated interaction of hematopoietic progenitors with the bone marrow vascular niche is required for thrombopoiesis.* Nat Med, 2004. **10**(1): p. 64-71.

53. Ara, T., et al., *Long-term hematopoietic stem cells require stromal cell-derived factor-1 for colonizing bone marrow during ontogeny.* Immunity, 2003. **19**(2): p. 257-67.

54. Sacchetti, B., et al., *Self-renewing osteoprogenitors in bone marrow sinusoids can organize a hematopoietic microenvironment.* Cell, 2007. **131**(2): p. 324-36.

55. Zhang, J., et al., *Identification of the haematopoietic stem cell niche and control of the niche size.* Nature, 2003. **425**(6960): p. 836-41.

56. Sugiyama, T., et al., *Maintenance of the hematopoietic stem cell pool by CXCL12-CXCR4 chemokine signaling in bone marrow stromal cell niches.* Immunity, 2006. **25**(6): p. 977-88.

57. Arai, F. and T. Suda, *Regulation of hematopoietic stem cells in the osteoblastic niche.* Adv Exp Med Biol, 2007. **602**: p. 61-7.

58. Yoshihara, H., et al., *Thrombopoietin/MPL signaling regulates hematopoietic stem cell quiescence and interaction with the osteoblastic niche.* Cell Stem Cell, 2007. **1**(6): p. 685-97.

59. Cancelas, J.A., et al., *Rac GTPases differentially integrate signals regulating hematopoietic stem cell localization.* Nat Med, 2005. **11**(8): p. 886-91.

60. Yang, L. and Y. Zheng, *Cdc42: a signal coordinator in hematopoietic stem cell maintenance.* Cell Cycle, 2007. **6**(12): p. 1445-50.

61. Zhang, C.C. and H.F. Lodish, *Insulin-like growth factor 2 expressed in a novel fetal liver cell population is a growth factor for hematopoietic stem cells.* Blood, 2004. **103**(7): p. 2513-21.

62. Kiel, M.J., G.L. Radice, and S.J. Morrison, *Lack of evidence that hematopoietic stem cells depend on N-cadherin-mediated adhesion to osteoblasts for their maintenance.* Cell Stem Cell, 2007. **1**(2): p. 204-17.

63. Kiel, M.J., et al., *Hematopoietic stem cells do not depend on N-cadherin to regulate their maintenance.* Cell Stem Cell, 2009. **4**(2): p. 170-9.

64. Williams, D.A., et al., *Fibronectin and VLA-4 in haematopoietic stem cell-microenvironment interactions.* Nature, 1991. **352**(6334): p. 438-41.

65. Ishikawa, F., et al., *Chemotherapy-resistant human AML stem cells home to and engraft within the bone-marrow endosteal region.* Nat Biotechnol, 2007. **25**(11): p. 1315-21.

66. Colmone, A., et al., *Leukemic cells create bone marrow niches that disrupt the behavior of normal hematopoietic progenitor cells.* Science, 2008. **322**(5909): p. 1861-5.

67. Zhang, B., et al., *Altered microenvironmental regulation of leukemic and normal stem cells in chronic myelogenous leukemia.* Cancer Cell, 2012. **21**(4): p. 577-92.

68. Schepers, K., et al., *Myeloproliferative neoplasia remodels the endosteal bone marrow niche into a self-reinforcing leukemic niche.* Cell Stem Cell, 2013. **13**(3): p. 285-99.

69. Trumpp, A., M. Essers, and A. Wilson, *Awakening dormant haematopoietic stem cells.* Nat Rev Immunol, 2010. **10**(3): p. 201-9.

70. Adams, G.B., et al., *Therapeutic targeting of a stem cell niche.* Nat Biotechnol, 2007. **25**(2): p. 238-43.

71. Doan, P.L. and J.P. Chute, *The vascular niche: home for normal and malignant hematopoietic stem cells.* Leukemia, 2012. **26**(1): p. 54-62.

72. Liang, G.W., et al., *Enhanced therapeutic effects on the multi-drug resistant human leukemia cells in vitro and xenograft in mice using the stealthy liposomal vincristine plus quinacrine.* Fundam Clin Pharmacol, 2008. **22**(4): p. 429-37.

73. Murati, A., et al., *Myeloid malignancies: mutations, models and management.* BMC Cancer, 2012. **12**: p. 304.

74. Rocquain, J., et al., *Combined mutations of ASXL1, CBL, FLT3, IDH1, IDH2, JAK2, KRAS, NPM1, NRAS, RUNX1, TET2 and WT1 genes in myelodysplastic syndromes and acute myeloid leukemias.* BMC Cancer, 2010. **10**: p. 401.

75. Appelbaum, F.R., et al., *Acute myeloid leukemia.* Hematology Am Soc Hematol Educ Program, 2001: p. 62-86.

76. Pollyea, D.A., H.E. Kohrt, and B.C. Medeiros, *Acute myeloid leukaemia in the elderly: a review.* Br J Haematol, 2011. **152**(5): p. 524-42.

77. Bennett, J.M., et al., *Proposals for the classification of the acute leukaemias. French-American-British (FAB) co-operative group.* Br J Haematol, 1976. **33**(4): p. 451-8.

78. Abdul-Hamid, G., *Classification of Acute Leukemia*, in *Acute Leukemia - The Scientist's Perspective and Challenge*, M. Antica, Editor. 2011, InTech.

79. Vardiman, J.W., et al., *The 2008 revision of the World Health Organization (WHO) classification of myeloid neoplasms and acute leukemia: rationale and important changes.* Blood, 2009. **114**(5): p. 937-51.

80. Henderson, E.S.S., R.J., *Evidence That Drugs in Multiple Combinations Have Materially Advanced the Treatment of Human Malignancies.* Cancer Res., 1969. **29**: p. 2272-2280.

81. Warrell, R.P., Jr., et al., *Acute promyelocytic leukemia.* N Engl J Med, 1993. **329**(3): p. 177-89.

82. Wang, Z.Y. and Z. Chen, *Acute promyelocytic leukemia: from highly fatal to highly curable.* Blood, 2008. **111**(5): p. 2505-15.

83. Tallman, M.S., D.G. Gilliland, and J.M. Rowe, *Drug therapy for acute myeloid leukemia.* Blood, 2005. **106**(4): p. 1154-63.

84. Ashley, N. and J. Poulton, *Mitochondrial DNA is a direct target of anti-cancer anthracycline drugs.* Biochem Biophys Res Commun, 2009. **378**(3): p. 450-5.

85. Miller, A.A., *Body surface area in dosing anticancer agents: scratch the surface!* J Natl Cancer Inst, 2002. **94**(24): p. 1822-3.

86. Rowe, J.M., *Is there a role for intensifying induction therapy in acute myeloid leukaemia (AML)?* Best Pract Res Clin Haematol, 2009. **22**(4): p. 509-15.

87. Gupta, V., M.S. Tallman, and D.J. Weisdorf, *Allogeneic hematopoietic cell transplantation for adults with acute myeloid leukemia: myths, controversies, and unknowns.* Blood, 2011. **117**(8): p. 2307-18.

88. Cornelissen, J.J. and B. Lowenberg, *Role of allogeneic stem cell transplantation in current treatment of acute myeloid leukemia.* Hematology Am Soc Hematol Educ Program, 2005: p. 151-5.

89. Fernandez, H.F., *New trends in the standard of care for initial therapy of acute myeloid leukemia.* Hematology Am Soc Hematol Educ Program, 2010. **2010**: p. 56-61.

90. Skrtic, M., et al., *Inhibition of mitochondrial translation as a therapeutic strategy for human acute myeloid leukemia.* Cancer Cell, 2011. **20**(5): p. 674-88.

91. Krishnan, V. and A.K. Rajasekaran, *Clinical nanomedicine: a solution to the chemotherapy conundrum in pediatric leukemia therapy.* Clin Pharmacol Ther, 2014. **95**(2): p. 168-78.

92. Brown, G. and P. Hughes, *Retinoid differentiation therapy for common types of acute myeloid leukemia.* Leuk Res Treatment, 2012. **2012**: p. 939021.

93. Gudas, L.J. and J.A. Wagner, *Retinoids regulate stem cell differentiation.* J Cell Physiol, 2011. **226**(2): p. 322-30.

94. Congleton, J., R. MacDonald, and A. Yen, *Src inhibitors, PP2 and dasatinib, increase retinoic acid-induced association of Lyn and c-Raf (S259) and enhance MAPK-dependent differentiation of myeloid leukemia cells.* Leukemia, 2012. **26**(6): p. 1180-8.

95. Patatanian, E. and D.F. Thompson, *Retinoic acid syndrome: a review.* J Clin Pharm Ther, 2008. **33**(4): p. 331-8.

96. Altucci, L. and H. Gronemeyer, *The promise of retinoids to fight against cancer.* Nat Rev Cancer, 2001. **1**(3): p. 181-93.

97. Feynman, R., *There's Plenty of Room at the Bottom.* Engineering and Science, 1960. **23**(5): p. 22-36.

98. Drexler, E., *Engines of Creation: The Coming Era of Nanotechnology*. 1986, New York: Anchor Books.

99. Ferreira, L., et al., *New opportunities: the use of nanotechnologies to manipulate and track stem cells.* Cell Stem Cell, 2008. **3**(2): p. 136-46.

100. Zhang, L., et al., *Nanoparticles in medicine: therapeutic applications and developments.* Clin Pharmacol Ther, 2008. **83**(5): p. 761-9.

101. Ferrari, M., *Frontiers in cancer nanomedicine: directing mass transport through biological barriers.* Trends Biotechnol, 2010. **28**(4): p. 181-8.

102. Chou, L.Y., K. Ming, and W.C. Chan, *Strategies for the intracellular delivery of nanoparticles.* Chem Soc Rev, 2011. **40**(1): p. 233-45.

103. Svenson, S., *What nanomedicine in the clinic right now really forms nanoparticles?* Wiley Interdiscip Rev Nanomed Nanobiotechnol, 2014. **6**(2): p. 125-35.

104. Kaspers, G.J., et al., *Improved outcome in pediatric relapsed acute myeloid leukemia: results of a randomized trial on liposomal daunorubicin by the International BFM Study Group.* J Clin Oncol, 2013. **31**(5): p. 599-607.

105. Raj, T.A., A.M. Smith, and A.S. Moore, *Vincristine sulfate liposomal injection for acute lymphoblastic leukemia.* Int J Nanomedicine, 2013. **8**: p. 4361-9.

106. Feldman, E.J., et al., *Pharmacokinetics of CPX-351; a nano-scale liposomal fixed molar ratio formulation of cytarabine:daunorubicin, in patients with advanced leukemia.* Leuk Res, 2012. **36**(10): p. 1283-9.

107. Richly, H., et al., *Plasma and cellular pharmacokinetics of doxorubicin after intravenous infusion of Caelyx/Doxil in patients with hematological tumors.* Int J Clin Pharmacol Ther, 2009. **47**(1): p. 55-7.

108. Suzuki, R., et al., *Effective anti-tumor activity of oxaliplatin encapsulated in transferrin-PEG-liposome.* Int J Pharm, 2008. **346**(1-2): p. 143-50.

109. Kato, K., et al., *Phase II study of NK105, a paclitaxel-incorporating micellar nanoparticle, for previously treated advanced or recurrent gastric cancer.* Invest New Drugs, 2012. **30**(4): p. 1621-7.

110. Langer, C.J., et al., *Phase III trial comparing paclitaxel poliglumex (CT-2103, PPX) in combination with carboplatin versus standard paclitaxel and carboplatin in the treatment of PS 2 patients with chemotherapy-naive advanced non-small cell lung cancer.* J Thorac Oncol, 2008. **3**(6): p. 623-30.

111. Hrkach, J., et al., *Preclinical development and clinical translation of a PSMA-targeted docetaxel nanoparticle with a differentiated pharmacological profile.* Sci Transl Med, 2012. **4**(128): p. 128ra39.

112. Cucinotto, I., et al., *Nanoparticle albumin bound Paclitaxel in the treatment of human cancer: nanodelivery reaches prime-time?* J Drug Deliv, 2013. **2013**: p. 905091.

113. Ferreira, L., *Nanoparticles as tools to study and control stem cells.* J Cell Biochem, 2009. **108**(4): p. 746-52.

114. Sahay, G., D.Y. Alakhova, and A.V. Kabanov, *Endocytosis of nanomedicines.* J Control Release, 2010. **145**(3): p. 182-95.

115. Nel, A.E., et al., *Understanding biophysicochemical interactions at the nano-bio interface.* Nat Mater, 2009. **8**(7): p. 543-57.

116. Paulo, C.S., R. Pires das Neves, and L.S. Ferreira, *Nanoparticles for intracellular-targeted drug delivery.* Nanotechnology, 2011. **22**(49): p. 494002.

117. Liang W., L.J.K.W., *Endosomal Escape Pathways for Non-Viral Nucleic Acid Delivery Systems*, in *Molecular Regulation of Endocytosis*, B. Ceresa, Editor. 2012, Intech.

118. Lin, Q., et al., *Lipid-based nanoparticles in the systemic delivery of siRNA.* Nanomedicine (Lond), 2014. **9**(1): p. 105-20.

119. Boussif, O., et al., *A versatile vector for gene and oligonucleotide transfer into cells in culture and in vivo: polyethylenimine.* Proc Natl Acad Sci U S A, 1995. **92**(16): p. 7297-301.

120. D. S. Zhuk, P.A.G., V. A. Kargin, *Advances in the chemistry of polyethyleneimine.* Russ. Chem. Rev., 1965. **34**(7): p. 515-527.

121. C. R. Dick, G.E.H., *Characterization of Polyethylenimine.* Journal of Macromolecular Science: Part A - Chemistry: Pure and Applied Chemistry, 1970. **4**(6): p. 1301-1314.

122. Hobel, S. and A. Aigner, *Polyethylenimines for siRNA and miRNA delivery in vivo.* Wiley Interdiscip Rev Nanomed Nanobiotechnol, 2013.

123. Behr, J.-P., *The Proton Sponge: a Trick to Enter Cells the Viruses Did Not Exploit* CHIMIA International Journal for Chemistry, 1997. **51**(1-2): p. 34-36.

124. Godbey, W.T., K.K. Wu, and A.G. Mikos, *Size matters: molecular weight affects the efficiency of poly(ethylenimine) as a gene delivery vehicle.* J Biomed Mater Res, 1999. **45**(3): p. 268-75.

125. Abdallah, B., et al., *A powerful nonviral vector for in vivo gene transfer into the adult mammalian brain: polyethylenimine.* Hum Gene Ther, 1996. **7**(16): p. 1947-54.

126. Kunath, K., et al., *Low-molecular-weight polyethylenimine as a non-viral vector for DNA delivery: comparison of physicochemical properties, transfection efficiency and in vivo distribution with high-molecular-weight polyethylenimine.* J Control Release, 2003. **89**(1): p. 113-25.

127. Thomas, M. and A.M. Klibanov, *Enhancing polyethylenimine's delivery of plasmid DNA into mammalian cells.* Proc Natl Acad Sci U S A, 2002. **99**(23): p. 14640-5.

128. Breunig, M., et al., *Breaking up the correlation between efficacy and toxicity for nonviral gene delivery.* Proc Natl Acad Sci U S A, 2007. **104**(36): p. 14454-9.

129. Jager, M., et al., *Branched and linear poly(ethylene imine)-based conjugates: synthetic modification, characterization, and application.* Chem Soc Rev, 2012. **41**(13): p. 4755-67.

130. Peng, M., et al., *Investigation of the degradation mechanism of cross-linked polyethyleneimine by NMR spectroscopy.* Polymer Degradation and Stability, 2007. **93**(2): p. 476-482.

131. Chollet, P., et al., *Side-effects of a systemic injection of linear polyethylenimine-DNA complexes.* J Gene Med, 2002. **4**(1): p. 84-91.

132. Tiyaboonchai, W., J. Woiszwillo, and C.R. Middaugh, *Formulation and characterization of DNA-polyethylenimine-dextran sulfate nanoparticles.* Eur J Pharm Sci, 2003. **19**(4): p. 191-202.

133. Maia, J., et al., *Controlling the neuronal differentiation of stem cells by the intracellular delivery of retinoic acid-loaded nanoparticles.* ACS Nano, 2011. **5**(1): p. 97-106.

134. Guasch, A., W.M. Deen, and B.D. Myers, *Charge selectivity of the glomerular filtration barrier in healthy and nephrotic humans.* J Clin Invest, 1993. **92**(5): p. 2274-82.

135. Carmen Moga, C.H., *Low Density Lipoprotein Apheresis for the Treatment of Familial Hypercholesterolemia*, in *IP-18 Information Paper*. 2004, Alberta Heritage Foundation for Medical Research: Alberta. p. 55.

136. Santos, T., et al., *Polymeric nanoparticles to control the differentiation of neural stem cells in the subventricular zone of the brain.* ACS Nano, 2012. **6**(12): p. 10463-74.

137. Leith, C., *Multidrug resistance in leukemia.* Curr Opin Hematol, 1998. **5**(4): p. 287-91.

138. Xia, C.Q. and P.G. Smith, *Drug efflux transporters and multidrug resistance in acute leukemia: therapeutic impact and novel approaches to mediation.* Mol Pharmacol, 2012. **82**(6): p. 1008-21.

139. Hu, C.M., S. Aryal, and L. Zhang, *Nanoparticle-assisted combination therapies for effective cancer treatment.* Ther Deliv, 2010. **1**(2): p. 323-34.

140. Drach, J., et al., *Induction of differentiation in myeloid leukemia cell lines and acute promyelocytic leukemia cells by liposomal all-trans-retinoic acid.* Cancer Res, 1993. **53**(9): p. 2100-4.

141. Ozpolat, B. and G. Lopez-Berestein, *Liposomal-all-trans-retinoic acid in treatment of acute promyelocytic leukemia.* Leuk Lymphoma, 2002. **43**(5): p. 933-41.

142. Agrawal, V., M.K. Paul, and A.K. Mukhopadhyay, *6-mercaptopurine and daunorubicin double drug liposomes-preparation, drug-drug interaction and characterization.* J Liposome Res, 2005. **15**(3-4): p. 141-55.

143. Li, X., et al., *Effect of stealthy liposomal topotecan plus amlodipine on the multidrug-resistant leukaemia cells in vitro and xenograft in mice.* Eur J Clin Invest, 2006. **36**(6): p. 409-18.

144. Wu, J., et al., *Reversal of multidrug resistance by transferrin-conjugated liposomes co-encapsulating doxorubicin and verapamil.* J Pharm Pharm Sci, 2007. **10**(3): p. 350-7.

145. Sharma, A.K., et al., *Prevention of MDR development in leukemia cells by micelle-forming polymeric surfactant.* J Control Release, 2008. **131**(3): p. 220-7.

146. Tiwari, M.D., et al., *All-trans retinoic acid loaded block copolymer nanoparticles efficiently induce cellular differentiation in HL-60 cells.* Eur J Pharm Sci, 2011. **44**(5): p. 643-52.

147. Yadav, K.S., et al., *Long circulating PEGylated PLGA nanoparticles of cytarabine for targeting leukemia.* J Microencapsul, 2011. **28**(8): p. 729-42.

148. Krishnan, V., et al., *Dexamethasone-loaded block copolymer nanoparticles induce leukemia cell death and enhance therapeutic efficacy: a novel application in pediatric nanomedicine.* Mol Pharm, 2013. **10**(6): p. 2199-210.

149. Mukherjee, P., et al., *Potential therapeutic application of gold nanoparticles in B-chronic lymphocytic leukemia (BCLL): enhancing apoptosis.* J Nanobiotechnology, 2007. **5**: p. 4.

150. Podsiadlo, P., et al., *Gold nanoparticles enhance the anti-leukemia action of a 6-mercaptopurine chemotherapeutic agent.* Langmuir, 2008. **24**(2): p. 568-74.

151. Guo, D., et al., *Synergistic cytotoxic effect of different sized ZnO nanoparticles and daunorubicin against leukemia cancer cells under UV irradiation.* J Photochem Photobiol B, 2008. **93**(3): p. 119-26.

152. Chen, B., et al., *Synergistic effect of magnetic nanoparticles of Fe(3)O(4) with gambogic acid on apoptosis of K562 leukemia cells.* Int J Nanomedicine, 2009. **4**: p. 251-9.

153. Zhang, G., et al., *Fe3O4 nanoparticles with daunorubicin induce apoptosis through caspase 8-PARP pathway and inhibit K562 leukemia cell-induced tumor growth in vivo.* Nanomedicine, 2011. **7**(5): p. 595-603.

154. Singh, A., F. Dilnawaz, and S.K. Sahoo, *Long circulating lectin conjugated paclitaxel loaded magnetic nanoparticles: a new theranostic avenue for leukemia therapy.* PLoS One, 2011. **6**(11): p. e26803.

155. Wang, J., et al., *Apoptotic mechanism of human leukemia K562/A02 cells induced by magnetic iron oxide nanoparticles co-loaded with daunorubicin and 5-bromotetrandrin.* Int J Nanomedicine, 2011. **6**: p. 1027-34.

156. Wang, J., et al., *Synthesis and antitumor efficacy of daunorubicin-loaded magnetic nanoparticles.* Int J Nanomedicine, 2011. **6**: p. 203-11.

157. Liopo, A.V., et al., *Laser nanothermolysis of human leukemia cells using functionalized plasmonic nanoparticles.* Nano Biomed Eng, 2012. **4**(2): p. 66-75.

158. Nobili, S., et al., *Pharmacological strategies for overcoming multidrug resistance.* Curr Drug Targets, 2006. **7**(7): p. 861-79.

159. Steinbach, D. and O. Legrand, *ABC transporters and drug resistance in leukemia: was P-gp nothing but the first head of the Hydra?* Leukemia, 2007. **21**(6): p. 1172-6.

160. Bellamy, W.T., *P-glycoproteins and multidrug resistance.* Annu Rev Pharmacol Toxicol, 1996. **36**: p. 161-83.

161. Tekade, R.K., et al., *Surface-engineered dendrimers for dual drug delivery: a receptor up-regulation and enhanced cancer targeting strategy.* J Drug Target, 2008. **16**(10): p. 758-72.

162. Tekade, R.K., et al., *Exploring dendrimer towards dual drug delivery: pH responsive simultaneous drug-release kinetics.* J Microencapsul, 2009. **26**(4): p. 287-96.

163. Ma, P., et al., *Development of idarubicin and doxorubicin solid lipid nanoparticles to overcome Pgp-mediated multiple drug resistance in leukemia.* J Biomed Nanotechnol, 2009. **5**(2): p. 151-61.

164. Reddy, L.H., et al., *A new nanomedicine of gemcitabine displays enhanced anticancer activity in sensitive and resistant leukemia types.* J Control Release, 2007. **124**(1-2): p. 20-7.

165. Reddy, L.H., et al., *Preclinical toxicology (subacute and acute) and efficacy of a new squalenoyl gemcitabine anticancer nanomedicine.* J Pharmacol Exp Ther, 2008. **325**(2): p. 484-90.

166. Li, R., et al., *P-glycoprotein antibody functionalized carbon nanotube overcomes the multidrug resistance of human leukemia cells.* ACS Nano, 2010. **4**(3): p. 1399-408.

167. Huang, Y.C., et al., *Pegylated gold nanoparticles induce apoptosis in human chronic myeloid leukemia cells.* Biomed Res Int, 2014. **2014**: p. 182353.

168. Avalos, A., et al., *Cytotoxicity and ROS production of manufactured silver nanoparticles of different sizes in hepatoma and leukemia cells.* J Appl Toxicol, 2014. **34**(4): p. 413-23.

169. Jingyuan Li, C.C., Xuemei Wang, Zhongze Gu, Baoan Chen, *Novel Strategy to Fabricate PLA/Au Nanocomposites as an Efficient Drug Carrier for Human Leukemia Cells in Vitro.* Nanoscale Res Lett, 2011. **6**(1): p. 29.

170. Guo, D., et al., *Anti-leukemia activity of PVP-coated silver nanoparticles via generation of reactive oxygen species and release of silver ions.* Biomaterials, 2013. **34**(32): p. 7884-94.

171. Fisher, G.A. and B.I. Sikic, *Clinical studies with modulators of multidrug resistance.* Hematol Oncol Clin North Am, 1995. **9**(2): p. 363-82.

172. Coley, H.M., *Overcoming multidrug resistance in cancer: clinical studies of p-glycoprotein inhibitors.* Methods Mol Biol, 2010. **596**: p. 341-58.

173. Ferrari, M., *Cancer nanotechnology: opportunities and challenges.* Nat Rev Cancer, 2005. **5**(3): p. 161-71.

174. Fomina, N., J. Sankaranarayanan, and A. Almutairi, *Photochemical mechanisms of light-triggered release from nanocarriers.* Adv Drug Deliv Rev, 2012. **64**(11): p. 1005-20.

175. Thanou, M. and W. Gedroyc, *MRI-Guided Focused Ultrasound as a New Method of Drug Delivery.* J Drug Deliv, 2013. **2013**: p. 616197.

176. Fomina, N., et al., *UV and near-IR triggered release from polymeric nanoparticles.* J Am Chem Soc, 2010. **132**(28): p. 9540-2.

177. Yan, B., et al., *Light-responsive block copolymer vesicles based on a photo-softening effect.* Soft Matter, 2011. **7**(21): p. 10001-10009.

178. Zhao, Y., *Light-Responsive Block Copolymer Micelles.* Macromolecules, 2012. **45**(9): p. 3647-3657.

179. Stanley, S.A., et al., *Radio-wave heating of iron oxide nanoparticles can regulate plasma glucose in mice.* Science, 2012. **336**(6081): p. 604-8.

180. Zhang, L., et al., *General route to multifunctional uniform yolk/mesoporous silica shell nanocapsules: a platform for simultaneous cancer-targeted imaging and magnetically guided drug delivery.* Chemistry, 2012. **18**(39): p. 12512-21.

181. Ganta, S., et al., *A review of stimuli-responsive nanocarriers for drug and gene delivery.* J Control Release, 2008. **126**(3): p. 187-204.

182. Mura, S., J. Nicolas, and P. Couvreur, *Stimuli-responsive nanocarriers for drug delivery.* Nat Mater, 2013. **12**(11): p. 991-1003.

183. Vladimir Iani, J.M., LiWei Ma. *Measurements of light penetration into human tissues in vivo*. in *Photochemotherapy: Photodynamic Therapy and Other Modalities*. 1996. Barcelona, Spain: Proc. SPIE.

184. Lucian Fodor, Y.U., Monica Elman, *Light Tissue Interactions*, in *Aesthetic Applications of Intense Pulsed Light*. 2011, Springer London. p. 11-20.

185. Brieke, C., et al., *Light-controlled tools.* Angew Chem Int Ed Engl, 2012. **51**(34): p. 8446-76.

186. Gohy, J.F. and Y. Zhao, *Photo-responsive block copolymer micelles: design and behavior.* Chem Soc Rev, 2013. **42**(17): p. 7117-29.

187. Alvarez-Lorenzo, C., L. Bromberg, and A. Concheiro, *Light-sensitive intelligent drug delivery systems.* Photochem Photobiol, 2009. **85**(4): p. 848-60.

188. Sevick-Muraca, E.M., *Translation of near-infrared fluorescence imaging technologies: emerging clinical applications.* Annu Rev Med, 2012. **63**: p. 217-31.

189. Karu, T., *The Science of Low Power Laser Therapy*. 1998, London: Gordon and Breach.

190. Desmet, K.D., et al., *Clinical and experimental applications of NIR-LED photobiomodulation.* Photomed Laser Surg, 2006. **24**(2): p. 121-8.

191. Weissleder, R., *A clearer vision for in vivo imaging.* Nat Biotechnol, 2001. **19**(4): p. 316-7.

192. Sordillo, L.A., et al., *Deep optical imaging of tissue using the second and third near-infrared spectral windows.* J Biomed Opt, 2014. **19**(5): p. 56004.

193. America, A.N.S.I.o., *American National Standard for Safe Use of Lasers in Research, Development or Testing.* Laser Institute of America, Orlando, FL, 2012.

194. Flusberg, B.A., et al., *Fiber-optic fluorescence imaging.* Nat Methods, 2005. **2**(12): p. 941-50.

195. Yelin, D., et al., *Three-dimensional miniature endoscopy.* Nature, 2006. **443**(7113): p. 765.

196. Mai, S., et al., *Mechanisms of the ultraviolet light response in mammalian cells.* J Cell Sci, 1989. **94 (Pt 4)**: p. 609-15.

197. de Gruijl, F.R., H.J. van Kranen, and L.H. Mullenders, *UV-induced DNA damage, repair, mutations and oncogenic pathways in skin cancer.* J Photochem Photobiol B, 2001. **63**(1-3): p. 19-27.

198. Gentile, M., L. Latonen, and M. Laiho, *Cell cycle arrest and apoptosis provoked by UV radiation-induced DNA damage are transcriptionally highly divergent responses.* Nucleic Acids Res, 2003. **31**(16): p. 4779-90.

199. Rastogi, R.P., et al., *Molecular mechanisms of ultraviolet radiation-induced DNA damage and repair.* J Nucleic Acids, 2010. **2010**: p. 592980.

200. Kramer, G.F. and B.N. Ames, *Oxidative mechanisms of toxicity of low-intensity near-UV light in Salmonella typhimurium.* J Bacteriol, 1987. **169**(5): p. 2259-66.

201. Sinha, R.P. and D.P. Hader, *UV-induced DNA damage and repair: a review.* Photochem Photobiol Sci, 2002. **1**(4): p. 225-36.

202. Avci, P., et al., *Low-level laser (light) therapy (LLLT) in skin: stimulating, healing, restoring.* Semin Cutan Med Surg, 2013. **32**(1): p. 41-52.

203. Meek, K.M. and S. Hayes, *Corneal cross-linking--a review.* Ophthalmic Physiol Opt, 2013. **33**(2): p. 78-93.

204. Thomas Johnson, B.B., *Health Physics and Radiological Health*. 2011: Wolters Klumer | Lippincott Williams & Wilkins.

205. Ellis-Davies, G.C., *Caged compounds: photorelease technology for control of cellular chemistry and physiology.* Nat Methods, 2007. **4**(8): p. 619-28.

206. Klan, P., et al., *Photoremovable protecting groups in chemistry and biology: reaction mechanisms and efficacy.* Chem Rev, 2013. **113**(1): p. 119-91.

207. Beharry, A.A. and G.A. Woolley, *Azobenzene photoswitches for biomolecules.* Chem Soc Rev, 2011. **40**(8): p. 4422-37.

208. Szymanski, W., et al., *Reversible photocontrol of biological systems by the incorporation of molecular photoswitches.* Chem Rev, 2013. **113**(8): p. 6114-78.

209. Pelliccioli, A.P. and J. Wirz, *Photoremovable protecting groups: reaction mechanisms and applications.* Photochem Photobiol Sci, 2002. **1**(7): p. 441-58.

210. Hui Zhao, E.S.S., E. Bryan Coughlin, Patrick Theato, *o-Nitrobenzyl Alcohol Derivatives: Opportunities in Polymer and Materials Science.* Macromolecules, 2012. **45**(4): p. 1723–1736.

211. Velema, W.A., W. Szymanski, and B.L. Feringa, *Photopharmacology: beyond proof of principle.* J Am Chem Soc, 2014. **136**(6): p. 2178-91.

212. Tong, R., et al., *Photoswitchable nanoparticles for triggered tissue penetration and drug delivery.* J Am Chem Soc, 2012. **134**(21): p. 8848-55.

213. Jiang, J., X. Tong, and Y. Zhao, *A new design for light-breakable polymer micelles.* J Am Chem Soc, 2005. **127**(23): p. 8290-1.

214. Jiang, J.Q., et al., *Toward photocontrolled release using light-dissociable block copolymer micelles.* Macromolecules, 2006. **39**(13): p. 4633-4640.

215. Fomina, N., et al., *Low power, biologically benign NIR light triggers polymer disassembly.* Macromolecules, 2011. **44**(21): p. 8590-8597.

216. Lv, C., et al., *Photodegradable polyurethane self-assembled nanoparticles for photocontrollable release.* Langmuir, 2012. **28**(25): p. 9387-94.

217. Luo, Y.L., Y.S. Shiao, and Y.F. Huang, *Release of photoactivatable drugs from plasmonic nanoparticles for targeted cancer therapy.* ACS Nano, 2011. **5**(10): p. 7796-804.

218. Zhang, Z., J. Wang, and C. Chen, *Near-infrared light-mediated nanoplatforms for cancer thermo-chemotherapy and optical imaging.* Adv Mater, 2013. **25**(28): p. 3869-80.

219. Singhana, B., et al., *Light-Activatable Gold Nanoshells for Drug Delivery Applications.* AAPS PharmSciTech, 2014.

220. Liu, J., et al., *NIR-triggered anticancer drug delivery by upconverting nanoparticles with integrated azobenzene-modified mesoporous silica.* Angew Chem Int Ed Engl, 2013. **52**(16): p. 4375-9.

221. Li, Y., et al., *Light-triggered concomitant enhancement of magnetic resonance imaging contrast performance and drug release rate of functionalized amphiphilic diblock copolymer micelles.* Biomacromolecules, 2012. **13**(11): p. 3877-86.

222. Song, J., et al., *Photolabile plasmonic vesicles assembled from amphiphilic gold nanoparticles for remote-controlled traceable drug delivery.* Nanoscale, 2013. **5**(13): p. 5816-24.

223. Sun, L., et al., *NIR-responsive and lectin-binding doxorubicin-loaded nanomedicine from Janus-type dendritic PAMAM amphiphiles.* Biomacromolecules, 2012. **13**(11): p. 3581-91.

224. Liu, G.Y., et al., *Near-infrared light-sensitive micelles for enhanced intracellular drug delivery.* Journal of Materials Chemistry, 2012. **22**(33): p. 16865-16871.

225. Son, S., E. Shin, and B.S. Kim, *Light-responsive micelles of spiropyran initiated hyperbranched polyglycerol for smart drug delivery.* Biomacromolecules, 2014. **15**(2): p. 628-34.

226. Lin, Q., et al., *Anticancer drug release from a mesoporous silica based nanophotocage regulated by either a one- or two-photon process.* J Am Chem Soc, 2010. **132**(31): p. 10645-7.

227. Ji, W.D., et al., *Coumarin-containing photo-responsive nanocomposites for NIR light-triggered controlled drug release via a two-photon process.* Journal of Materials Chemistry B, 2013. **1**(43): p. 5942-5949.

228. Park, T.H., et al., *Photoswitchable particles for on-demand degradation and triggered release.* Small, 2013. **9**(18): p. 3051-7.

229. Yang, Y., et al., *NIR photoresponsive crosslinked upconverting nanocarriers toward selective intracellular drug release.* Small, 2013. **9**(17): p. 2937-44.

230. Min, Y., et al., *Near-infrared light-mediated photoactivation of a platinum antitumor prodrug and simultaneous cellular apoptosis imaging by upconversion-luminescent nanoparticles.* Angew Chem Int Ed Engl, 2014. **53**(4): p. 1012-6.

231. Viger, M.L., et al., *Near-Infrared-Induced Heating of Confined Water in Polymeric Particles for Efficient Payload Release.* ACS Nano, 2014.

232. Yuan, Q., et al., *Photon-manipulated drug release from a mesoporous nanocontainer controlled by azobenzene-modified nucleic acid.* ACS Nano, 2012. **6**(7): p. 6337-44.

233. Croissant, J., et al., *Two-photon-triggered drug delivery in cancer cells using nanoimpellers.* Angew Chem Int Ed Engl, 2013. **52**(51): p. 13813-7.

234. Tong, R., H.H. Chiang, and D.S. Kohane, *Photoswitchable nanoparticles for in vivo cancer chemotherapy.* Proc Natl Acad Sci U S A, 2013. **110**(47): p. 19048-53.

235. Zhou, L., et al., *DNA-mediated Construction of Hollow Upconversion Nanoparticles for Protein Harvesting and Near-Infrared Light Triggered Release.* Adv Mater, 2014. **26**(15): p. 2424-30.

236. Dvir, T., et al., *Photo-targeted nanoparticles.* Nano Lett, 2010. **10**(1): p. 250-4.

237. Babin, J., et al., *A new two-photon-sensitive block copolymer nanocarrier.* Angew Chem Int Ed Engl, 2009. **48**(18): p. 3329-32.

238. Katz, J.S., et al., *Modular synthesis of biodegradable diblock copolymers for designing functional polymersomes.* J Am Chem Soc, 2010. **132**(11): p. 3654-5.

239. Schumers, J.M., J.F. Gohy, and C.A. Fustin, *A versatile strategy for the synthesis of block copolymers bearing a photocleavable junction.* Polymer Chemistry, 2010. **1**(2): p. 161-163.

240. Han, D.H., X. Tong, and Y. Zhao, *Fast Photodegradable Block Copolymer Micelles for Burst Release.* Macromolecules, 2011. **44**(3): p. 437-439.

241. Liu, G. and C.M. Dong, *Photoresponsive poly(S-(o-nitrobenzyl)-L-cysteine)-b-PEO from a L-cysteine N-carboxyanhydride monomer: synthesis, self-assembly, and phototriggered drug release.* Biomacromolecules, 2012. **13**(5): p. 1573-83.

242. Feng, W., C. Han, and F. Li, *Upconversion-nanophosphor-based functional nanocomposites.* Adv Mater, 2013. **25**(37): p. 5287-303.

243. Yan, B., et al., *Near-infrared light-triggered dissociation of block copolymer micelles using upconverting nanoparticles.* J Am Chem Soc, 2011. **133**(49): p. 19714-7.

244. Bachelder, E.M., et al., *Acetal-derivatized dextran: an acid-responsive biodegradable material for therapeutic applications.* J Am Chem Soc, 2008. **130**(32): p. 10494-5.

245. Guardado-Alvarez, T.M., et al., *Activation of snap-top capped mesoporous silica nanocontainers using two near-infrared photons.* J Am Chem Soc, 2013. **135**(38): p. 14000-3.

246. Jaemoon Yang, J.L., Jinyoung Kang, Seung Jae Oh, Hyun-Ju Ko, Joo-Hiuk Son, Kwangyeol Lee, Jin-Suck Suh, Yong-Min Huh, Seungjoo Haam, *Smart Drug-Loaded Polymer Gold Nanoshells for Systemic and Localized Therapy of Human Epithelial Cancer.* Advanced Materials, 2009. **21**(43): p. 4339-4342.

247. Lee, S.M., et al., *Multifunctional nanoparticles for targeted chemophotothermal treatment of cancer cells.* Angew Chem Int Ed Engl, 2011. **50**(33): p. 7581-6.

248. Ma, Y., et al., *Gold Nanoshell Nanomicelles for Potential Magnetic Resonance Imaging, Light-Triggered Drug Release, and Photothermal Therapy.* Advanced Functional Materials, 2013. **23**(7): p. 815-822.

249. Yavuz, M.S., et al., *Gold nanocages covered by smart polymers for controlled release with near-infrared light.* Nature Materials, 2009. **8**(12): p. 935-939.

250. Agarwal, A., et al., *Remote triggered release of doxorubicin in tumors by synergistic application of thermosensitive liposomes and gold nanorods.* ACS Nano, 2011. **5**(6): p. 4919-26.

251. Yang, X., et al., *Near-infrared light-triggered, targeted drug delivery to cancer cells by aptamer gated nanovehicles.* Adv Mater, 2012. **24**(21): p. 2890-5.

252. Yan, B., et al., *Near infrared light triggered release of biomacromolecules from hydrogels loaded with upconversion nanoparticles.* J Am Chem Soc, 2012. **134**(40): p. 16558-61.

253. Tao, X., J. Li, and H. Mohwald, *Self-assembly, optical behavior, and permeability of a novel capsule based on an azo dye and polyelectrolytes.* Chemistry, 2004. **10**(14): p. 3397-403.

254. Lee, H.I., et al., *Light-induced reversible formation of polymeric micelles.* Angew Chem Int Ed Engl, 2007. **46**(14): p. 2453-7.

255. Kano, K., et al., *Photoresponsive Membranes - Regulation of Membrane-Properties by Photoreversible Cis-Trans Isomerization of Azobenzenes.* Chemistry Letters, 1980(4): p. 421-424.

256. Zhao, Y., *Photocontrollable block copolymer micelles: what can we control?* Journal of Materials Chemistry, 2009. **19**(28): p. 4887-4895.

257. Mabrouk, E., et al., *Bursting of sensitive polymersomes induced by curling.* Proc Natl Acad Sci U S A, 2009. **106**(18): p. 7294-8.

258. Jin, Q.A., et al., *Photo-responsive supramolecular self-assembly and disassembly of an azobenzene-containing block copolymer.* Soft Matter, 2010. **6**(21): p. 5589-5595.

259. Bedard, M.F., et al., *Polymeric microcapsules with light responsive properties for encapsulation and release.* Adv Colloid Interface Sci, 2010. **158**(1-2): p. 2-14.

260. Kitano, H., T. Oehmichen, and N. Ise, *Photo-Degradable Polymer Microcapsules.* Makromolekulare Chemie-Macromolecular Chemistry and Physics, 1991. **192**(5): p. 1107-1114.

261. Mei, X., et al., *Light-triggered reversible assemblies of azobenzene-containing amphiphilic copolymer with beta-cyclodextrin-modified hollow mesoporous silica nanoparticles for controlled drug release.* Chem Commun (Camb), 2012. **48**(80): p. 10010-2.

262. Croissant, J., et al., *Two-Photon-Triggered Drug Delivery via Fluorescent Nanovalves.* Small, 2014. **10**(9): p. 1752-5.

263. Griffon-Etienne, G., et al., *Taxane-induced apoptosis decompresses blood vessels and lowers interstitial fluid pressure in solid tumors: clinical implications.* Cancer Res, 1999. **59**(15): p. 3776-82.

264. Honey Priya James, R.J., Anju Alex, Anoop K.R., *Smart polymers for the controlled delivery of drugs – a concise overview.* Acta Pharmaceutica Sinica B, 2014. **4**(2): p. 120-127.

265. Lammers, T., *Smart drug delivery systems: back to the future vs. clinical reality.* Int J Pharm, 2013. **454**(1): p. 527-9.

266. Timko, B.P. and D.S. Kohane, *Materials to clinical devices: technologies for remotely triggered drug delivery.* Clin Ther, 2012. **34**(11): p. S25-35.

267. De Botton, S., et al., *Incidence, clinical features, and outcome of all trans-retinoic acid syndrome in 413 cases of newly diagnosed acute promyelocytic leukemia. The European APL Group.* Blood, 1998. **92**(8): p. 2712-8.

268. Warrell, R.P., Jr., et al., *Differentiation therapy of acute promyelocytic leukemia with tretinoin (all-trans-retinoic acid).* N Engl J Med, 1991. **324**(20): p. 1385-93.

269. Russo, D., et al., *All-trans retinoic acid (ATRA) in patients with chronic myeloid leukemia in the chronic phase.* Leukemia, 1998. **12**(4): p. 449-54.

270. Si, J., L. Mueller, and S.J. Collins, *CaMKII regulates retinoic acid receptor transcriptional activity and the differentiation of myeloid leukemia cells.* J Clin Invest, 2007. **117**(5): p. 1412-21.

271. Montesinos, P., et al., *Differentiation syndrome in patients with acute promyelocytic leukemia treated with all-trans retinoic acid and anthracycline chemotherapy: characteristics, outcome, and prognostic factors.* Blood, 2009. **113**(4): p. 775-83.

272. Vasdekis, A.E., et al., *Precision Intracellular Delivery Based on Optofluidic Polymersome Rupture.* Acs Nano, 2012. **6**(9): p. 7850-7857.

273. Timko, B.P., T. Dvir, and D.S. Kohane, *Remotely triggerable drug delivery systems.* Adv Mater, 2010. **22**(44): p. 4925-43.

274. Tiyaboonchai, W., J. Woiszwillo, and C.R. Middaugh, *Formulation and characterization of amphotericin B-polyethylenimine-dextran sulfate nanoparticles.* J Pharm Sci, 2001. **90**(7): p. 902-14.

275. Jose, J. and K. Burgess, *Syntheses and properties of water-soluble Nile Red derivatives.* J Org Chem, 2006. **71**(20): p. 7835-9.

276. Bewersdorf, J., B.T. Bennett, and K.L. Knight, *H2AX chromatin structures and their response to DNA damage revealed by 4Pi microscopy.* Proc Natl Acad Sci U S A, 2006. **103**(48): p. 18137-42.

277. Mukherjee, S., R.N. Ghosh, and F.R. Maxfield, *Endocytosis.* Physiol Rev, 1997. **77**(3): p. 759-803.

278. Gilleron, J., et al., *Image-based analysis of lipid nanoparticle-mediated siRNA delivery, intracellular trafficking and endosomal escape.* Nat Biotechnol, 2013. **31**(7): p. 638-46.

279. Leith, C.P., et al., *Acute myeloid leukemia in the elderly: assessment of multidrug resistance (MDR1) and cytogenetics distinguishes biologic subgroups with remarkably distinct responses to standard chemotherapy. A Southwest Oncology Group study.* Blood, 1997. **89**(9): p. 3323-9.

280. Meng, H., et al., *Engineered design of mesoporous silica nanoparticles to deliver doxorubicin and P-glycoprotein siRNA to overcome drug resistance in a cancer cell line.* ACS Nano, 2010. **4**(8): p. 4539-50.

281. El-Sayed, A., S. Futaki, and H. Harashima, *Delivery of macromolecules using arginine-rich cell-penetrating peptides: ways to overcome endosomal entrapment.* AAPS J, 2009. **11**(1): p. 13-22.

282. Sahay, G., et al., *Efficiency of siRNA delivery by lipid nanoparticles is limited by endocytic recycling.* Nat Biotechnol, 2013. **31**(7): p. 653-8.

283. Cortesi, R., et al., *Human leukemic K562 cells treated with cytosine arabinoside: enhancement of erythroid differentiation by retinoic acid and retinol.* Eur J Haematol, 1998. **61**(5): p. 295-301.

284. Guidez, F., et al., *Poor response to all-trans retinoic acid therapy in a t(11;17) PLZF/RAR alpha patient.* Leukemia, 1994. **8**(2): p. 312-7.

285. Licht, J.D., et al., *Clinical and molecular characterization of a rare syndrome of acute promyelocytic leukemia associated with translocation (11;17).* Blood, 1995. **85**(4): p. 1083-94.

286. Ruthardt, M., et al., *Opposite effects of the acute promyelocytic leukemia PML-retinoic acid receptor alpha (RAR alpha) and PLZF-RAR alpha fusion proteins on retinoic acid signalling.* Mol Cell Biol, 1997. **17**(8): p. 4859-69.

287. Spicuglia, S., et al., *Characterisation of genome-wide PLZF/RARA target genes.* PLoS One, 2011. **6**(9): p. e24176.

288. Douer, D., et al., *Treatment of newly diagnosed and relapsed acute promyelocytic leukemia with intravenous liposomal all-trans retinoic acid.* Blood, 2001. **97**(1): p. 73-80.

289. Sakhtianchi, R., et al., *Exocytosis of nanoparticles from cells: role in cellular retention and toxicity.* Adv Colloid Interface Sci, 2013. **201-202**: p. 18-29.

290. Kizaki, M., et al., *Mechanisms of retinoid resistance in leukemic cells: possible role of cytochrome P450 and P-glycoprotein.* Blood, 1996. **87**(2): p. 725-33.

291. Ruthardt, M., et al., *Opposite effects of the acute promyelocytic leukemia PML-retinoic acid receptor alpha (RAR alpha) and PLZF-RAR alpha fusion proteins on retinoic acid signalling.* Mol Cell Biol, 1997. **17**(8): p. 4859-69.

292. Dong, X. and R.J. Mumper, *Nanomedicinal strategies to treat multidrug-resistant tumors: current progress.* Nanomedicine (Lond), 2010. **5**(4): p. 597-615.

293. Gelfert, A., *Nanotechnology as Ideology: Towards a Critical Theory of 'Converging Technologies'.* Science Technology and Society, 2012. **17**(1): p. 143-164.

294. Crawley T., K.P., Tolvas L., Marttila T., *Background Paper 2: Finance and Investor Models in Nanotechnology*, in *OECD/NNI International Symposium on Assessing the Economic Impact of Nanotechnology*, O.f.E.C.a.D. Working Party on Nanotechnology, Editor. 2012, Organization for Economic Cooperation and Development. p. 4.

295. Patel A., C.K., Agrahari V., Mitra A., *Ocular drug delivery systems: An overview.* World J Pharmacol., 2013. **2**(2): p. 47-64.

296. DeLouise, L.A., *Applications of nanotechnology in dermatology.* J Invest Dermatol, 2012. **132**(3 Pt 2): p. 964-75.

297. Chanda, B., et al., *Retinoic acid signaling is essential for embryonic hematopoietic stem cell development.* Cell, 2013. **155**(1): p. 215-27.

298. Sharp PA, C.C., Kastner MA, Lees J, Sasisekharan R, Yaffe MB, Bhatia SN, Jacks TE, Lauffenburger DA, Langer R, Hammond PT, Sur M., *The Third Revolution: Convergence of Life Sciences, Physical Sciences, and Engineering.* Massachusetts Institute of Technology, 2011.